Design, Modeling and Analysis of a Continuous Process for Hydrogenation of Diene based Polymers using a Static Mixer Reactor

by

Chandra Mouli R Madhuranthakam

A thesis
presented to the University of Waterloo
in fulfillment of the
thesis requirement for the degree of
Doctor of Philosophy
in
Chemical Engineering

Waterloo, Ontario, Canada, 2007

AUTHOR'S DECLARATION

I hereby declare that I am the sole author of this thesis. This is a true copy of the thesis, including any required final revisions, as accepted by my examiners.

I understand that my thesis may be made electronically available to the public.

Abstract

Hydrogenated nitrile butadiene rubber (HNBR) which is known for its excellent elastomeric properties and mechanical retention properties after long time exposure to heat, oil and air is produced by the catalytic hydrogenation of nitrile butadiene rubber (NBR). Hydrogenation of NBR is carried out preferably in solution via homogeneous catalysis. As yet, it is being commercially produced in a semi-batch process where gaseous hydrogen continuously flows into a batch of reactant polymer. Several catalysts have been exploited successfully for the hydrogenation of NBR in organic solvents, which include palladium, rhodium, ruthenium, iridium and osmium complexes. Owing to the drawbacks of batch production (such as time taken for charging and discharging the reactants/products, heating and cooling, reactor clean up), and the huge demand for HNBR, a continuous process is proposed where potential time saving is possible in addition to the high turn over of the product.

Numerical investigation of the HNBR production in a plug flow reactor and a continuous stirred tank reactor showed that a reactor with plug flow behavior would be economical and efficient. A static mixer (SM) reactor with open-curve blade internal geometry is designed based on the simulation and hydrodynamic results. The SM reactor was designed with 24 mixing elements, 3.81 cm ID and 90 cm length. The reactor has a jacket in which steam is used to heat the polymer solution. The hydrodynamics in the SM reactor (open-flat blade structure) with air-water system showed that plug flow could be achieved even under laminar flow conditions ($Re_h < 20$). For a constant mean residence time, the Peclet number was varying such that it is 4.7 times the number of mixing elements (n_e) used in the SM reactor. Empirical correlations were developed for gas hold up (ε_G) and overall mass transfer coefficient (K_La). The mass transfer experiments showed that high K_La, 4 to 6 times compared to that of the conventional reactors could be achieved in the SM reactor at particular operating conditions.

Very important information on the Peclet number, liquid hold were obtained from the hydrodynamic experiments conducted with the actual working fluids (hydrogen, polymer solutions) in the SM reactor. The superficial gas velocity had an adverse effect on both Peclet number and liquid hold up. The viscosity of the polymer solution also had a marginal negative effect on the Peclet number while a positive effect on the liquid hold up. The hydrogenation performance with the homogeneous catalyst $OsHCl(CO)(O_2)(PCy_3)_2$ was performed in the continuous process with SM

reactor. Complete hydrogenation of NBR was possible in a single pass. The effect of mean residence time, catalyst and polymer concentration on the final degree of hydrogenation was studied. The minimum catalyst required to achieve degree of hydrogenation over 97% was empirically found and an empirical correlation was developed for degree of hydrogenation as a function of operating conditions and parameters.

Hydrogenation in the SM reactor is modeled by using plug flow with axial dispersion model that is coupled with the concentrations of carbon-carbon double bond, hydrogen and osmium catalyst. The model involves coupled, non-linear partial differential equations with different dimensionless parameters. The proposed model was verified with the experimental results obtained from the hydrogenation and hydrodynamic experiments. The model could satisfactorily predict the degree of hydrogenation obtained from experimental results at various operating conditions. In general, the designed continuous process with SM reactor performed well and was an effective method of manufacturing HNBR on a continuous basis. The designed system is amicable to the industrial operating conditions and promises to be highly efficient and economic process for production of HNBR.

Acknowledgements

First of all, I would like to thank Prof.Garry L Rempel for his excellent guidance through out my research program. His simple yet most effective suggestions have helped me in numerous situations to get through the crunch situations.

Many thanks to Prof. Qinmin Pan for her academic guidance in my research work.

Special thanks to Dr.Neil T. McManus, a friend, philosopher and guide, who taught me experimental techniques and chemistry related to hydrogenation of diene polymers.

My heartiest thanks to Prof. A. Elkamel, who helped me in academic as well as personal issues. His profound knowledge yet striking simplicity and elegance in dealing with the students is awesome.

I cheerfully acknowledge the company of my labmates, Xingwang Lin, Guangwei He, Jianmin Liu, Jialong Wu, Lifeng Zhang, Zhenli Wei, Dongyu Fang, Oh, Pear, Nut, and Su.

I relish my close association with my heart winning friends Lokesh, Viral, Suresh, Edison, Niju, Mercy, Saraswathi, Naresh Bhai who made my stay in Waterloo a memorable and sprightly one.

This note goes unworthy without mentioning the blessings of my parents and success wishing sister and brother. Their abundant giving nature make me feel so secure that I try anything in this world with great abandon yet with sense of responsibility without fear of losing.

My special thanks to Revathy Madhuranthakam for sharing equally the joys and sorrows experienced over the course of this work.

Financial assistance from Natural Sciences and Engineering Research Council (NSERC) and Lanxess Inc., is gratefully acknowledged.

Dedication

To Lord Shiva and My Parents

Table of Contents

List of Figures

List of Tables

Chapter 1
Introduction

1.1 Background

Catalytic hydrogenation of nitrile butadiene rubber (NBR) is a post polymerization process which alters and optimizes the chemical and physical properties of the parent polymer (NBR). Hydrogenated nitrile butadiene rubber (HNBR) is widely known for its physical strength and retention properties after long time exposure to heat, oil and chemicals. The unique properties attributed to HNBR have resulted in wide adoption of HNBR in automotive, industrial and assorted, performance demanding applications. On a volume basis, the automotive industry is the largest consumer of HNBR using it for dynamic and static seals, hoses and belts. Also, significant use is in oil exploration and processing, as well as rolls for steel and paper mills.

The modification route has been used, as the copolymer cannot be synthesized by traditional approaches such as free radical or coordinative polymerization. Hydrogenation of NBR is carried out preferably via homogeneous catalysis. As yet, it is being produced in a semi-batch process accompanied with hydrogen transfer from gas to liquid phase. Several catalysts have been exploited successfully for the hydrogenation in organic solvents that include palladium, rhodium, ruthenium, iridium and osmium complexes. Ru- and Os- based catalytic processes are receiving more prominence due to their effectiveness and much cheaper catalyst cost than the Rh- based systems. Because of the huge demand for HNBR, the need for continuous production becomes important compared to the conventional batch production. Though batch processing is capable of achieving high olefin conversions, it is disadvantageous in terms of throughput. A batch process will be advantageous if a new product is to be produced. When the throughput has to be increased, a batch process can no longer be favorable in terms of auxiliary costs such as processing the raw material for the reactor time required to fill and empty the reactor which takes a significant fraction of production time. In addition to that, the heat produced in the continuous process can be integrated elsewhere in the process which is not possible with a batch process. In many aspects, a continuous process is always superior to a batch process.

Parent (1996) and Kehl (1998) proved that the continuous process is feasible through a plug flow reactor packed with non porous ceramic saddles. The length to diameter ratio of the packed reactor was very high and is not favorable for scale up and there are always chances of hot spots forming in

the reactor when high concentrations of polymer are used. Pan et al. (2002) have numerically investigated the potential configuration for the optimum design for the continuous hydrogenation of NBR. From their analysis, a plug flow reactor with an instant mixing component (CSTR) at the inlet would be an optimum configuration for the above said purpose.

1.2 Scope of the Research Work

The ultimate goal of this research work is to design a continuous process for economic and efficient production of hydrogenated nitrile butadiene rubber. The heart of the process is the reactor. The most common types of reactors used in the process industry are either a plug flow reactor (PFR) or a continuously stirred tank reactor (CSTR). Because of the extensive knowledge available on CSTR, several processes use it despite its many draw backs. The current research is focused on the studying the performance of the static mixer reactor with respect to hydrogenation of NBR using organometallic catalysts. This originates from the preliminary numerical analysis performed to study the performance of different flow reactors. In the current study, a Kenics KMX static mixer reactor is designed for accomplishing the goal of the project. A static mixer is a tubular device that has static elements arranged along the length of the reactor such that it would ensure perfect mixing, heat transfer and mass transfer. The hydrodynamics (residence time distribution, liquid hold up and mass transfer) in a static mixer reactor with 18 elements having open-flat blade structure (similar to a Sulzer SMX) is investigated with an air/water system to know whether the required reactor characteristics (such as plug flow behavior, good mass transfer) is achievable or not.

Further, numerical investigation was performed to estimate and analyze the effect of different operating parameters on the hydrogenation of NBR based on the flow behavior obtained from the hydrodynamic study. Though the hydrodynamic study in the open-blade structure was promising, yet with the actual working fluids and operating conditions, the reactor behavior can be different. Hence, some of the residence time distribution and liquid hold up experiments were conducted in the KMX static mixer reactor which has open-curve blade internal geometry.

In addition to the static mixer reactor, other process equipment such as pumps, preheater, heat exchanger, gas liquid separator are designed and the bench scale set up for conducting hydrogenation is constructed by connecting all equipment. The main focus is to study the performance of the designed static mixer reactor for hydrogenation (rather than studying the performance of other process equipment in the continuous process). The feasibility of the designed process, process

conditions, chemical parameters are studied by conducting hydrogenation experiments in the continuous process. Successful hydrogenation (hydrogenation degree over 97%) was achieved in the designed continuous process. The experimental results obtained from the continuous process are simulated by proposing a model that takes the coupled behavior of carbon-carbon double bond, hydrogen and catalyst concentration into account. The proposed model predicts the reactor performance to a greater extent. The results and findings are discussed in this dissertation. With the successful hydrogenation results and the model prediction, preliminary analysis of scale up to a pilot plant is explored towards the end of this work.

1.3 Thesis Outline

The thesis is organized according to the following structure. In Chapter 2, the literature related to hydrogenation of NBR, hydrogenation kinetics, previous work on a continuous process, gas liquid reactors, static mixers, hydrodynamics in static mixers and internal geometry selection is explained and reviewed. In Chapter 3, the hydrodynamic study in the static mixer reactor (open-flat blade geometry) with air-water system is discussed. This includes the study of the residence time distribution, liquid hold up and mass transfer in the static mixer reactor. In Chapter 4, the numerical investigation of the static mixer reactor with respect to hydrogenation is extensively discussed and the effect of different operating parameters and conditions are explored. In Chapter 5, the residence time distribution and liquid hold up experiments conducted in the actual Kenics KMX static mixer reactor (open-curve blade geometry) with hydrogen gas, polymer solutions as working fluids are discussed. The empirical modeling of the corresponding hydrodynamic parameters is also discussed. In Chapter 6, the design of the continuous set up, different process equipment, static mixer reactor sizing, experimental techniques, polymer and catalyst solution preparation, technique for estimation of hydrogenation degree are discussed. In Chapter 7, the hydrogenation of NBR results obtained in the continuous process using an osmium catalyst for different operating conditions (superficial gas liquid velocities, catalyst concentration and polymer concentration) are presented. In Chapter 8, modeling of the hydrogenation performance in the static mixer reactor is discussed followed by preliminary analysis on the scale up for the pilot plant design. Finally, the conclusions and recommendations regarding this research work are given in Chapter 9.

Chapter 2
Literature Review

2.1 HNBR Production

Nitrile-butadiene rubber is an oil resistant rubber extensively used in the automotive industry. It is produced through emulsion polymerization of butadiene (Bd) and acrylonitrile (ACN). The amount of ACN in NBR will vary from 18 to 50 % by weight, depending on the final application and the properties required. Increasing the ACN content the volume swell of the polymer decreases thereby improving the rubber's resistance to oil, heat and abrasion, but sacrifices its low temperature flexibility and compatibility with plasticizers. On the other hand, decreasing the ACN content the associated compound will have higher volume swell and improved low temperature resistance. A byproduct of the polymerization of Bd is a residual carbon-carbon double bond left in the final polymer. A cis or trans configuration of the polymer results when Bd polymerizes via 1,4-addition while a pendent vinyl bond is formed on a side chain if 1,2 addition occurs. The proportions of each of the configuration vary depending on the grade of NBR. For Krynac 38.50, the trans configuration makes up approximately 75% of the unsaturation, while the vinyl bond accounts 2% only. The remnant olefinic bond in the polymer back bone causes a greater susceptibility to physical breakdown when exposed to heat, light or ozone. By selectively hydrogenating these unsaturated bonds to form HNBR, the polymer's resistance to heat and ozone can be improved along with long durability when exposed to aggressive environments (Parent, 1996).

2.1.1 Hydrogenation Kinetics

Figure 2.1 shows the typical reaction scheme for hydrogenation of NBR. The first organometallic catalyst used for HNBR production was the Wilkinson's catalyst, $RhCl(PPh_3)_3$. It is still used commercially and is known for its good activity and consistency in assuring product quality. It does not hydrogenate the nitrile group, regardless of the process conditions. The disadvantage with this catalyst is that it requires cocatalyst in the form of excess triphenylphosphine to stabilize the catalyst at elevated temperatures and is only active in chlorinated solvents (McManus et al.,1995). The next organometallic catalyst that provides a promising alternate to Wilkinson's catalyst is $Ru(CH{=}CH_2Ph)Cl(CO)(PCy_3)_2$. The ruthenium analog is much cheaper than Wilkinson's catalyst and is stable in ketones thus avoiding the need for chlorinated solvents to dissolve the rubber (NBR).

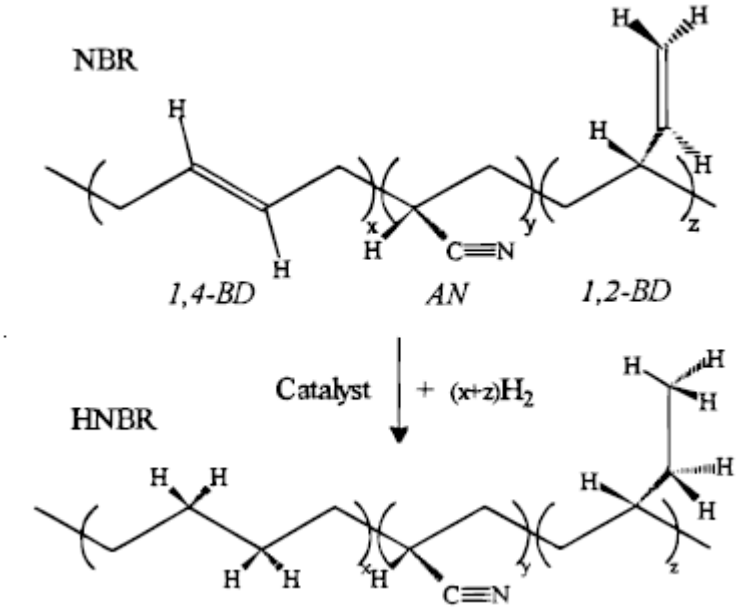

Figure 2.1 Scheme for hydrogenation of NBR (Parent et al., 1998)

Also, it does not need any cocatalyst. The disadvantages with the ruthenium based catalyst include, substantially lower activity compared to Wilkinson's catalyst and some crosslinking has been observed during the hydrogenation that would effect the processability of the rubber (Martin et al., 1997). The osmium based catalyst, $OsHCl(CO)(O_2)(PCy_3)_2$ was found to be the most active catalyst compared to the Wilkinson's and ruthenium based catalysts (Parent, 1996).These catalysts are not stable in ketones and hence chlorinated solvents are used. Also, these catalysts do not require a cocatalyst to boost the activity. The osmium catalysts are also prone to crosslinking but to a much lesser extent than the ruthenium catalysts.

Two significant differences were found among these catalysts with respect to hydrogenation of NBR. The first difference is the effect of hydrogen pressure on the reaction rate. With the Wilkinson's catalyst and the ruthenium catalyst, the reaction rate is generally first order with respect to the partial pressure of hydrogen. At high pressures and low polymer concentration, this shifts to zero order. While with the osmium catalysts, a second order dependence was observed up to very high pressures before it goes to zero order. Hence, with the osmium catalyst, an increase in the reaction pressure would have a strong impact compared to Wilkinson's or ruthenium catalysts. The second difference is related to the selectivity of the catalyst to hydrogenate certain olefin configurations. The Rh and Ru catalysts doesn't show any preference towards certain olefin

configurations, whether it be cis, trans or vinyl. However, with the osmium catalyst, rate of hydrogenation is very high during the first 25% of the reaction which is due to the facile hydrogenation of cis and vinyl olefin while the remaining reaction time is spent hydrogenating the trans-olefin at a much slower rate. However, all three catalysts behave similarly with respect to nitrile concentration. With increase in the nitrile concentration, the reaction rate would decrease which is due to the tendency of the nitrile group to coordinate with the catalyst thus competing with the olefin coordination. This is a big problem, as a process for higher scale of production, higher polymer concentrations are used and consequently high nitrile concentrations have to be handled.

2.1.2 Continuous Process for HNBR production

The only reported research regarding the continuous hydrogenation of NBR was carried out by S.Parent (1996), S.A.Kehl (1998), Pan et al., (2002). For the first time, Parent (1996) constructed a bench scale continuous setup and studied the feasibility of continuous hydrogenation of NBR. The setup used by Parent consisted of a tubular flow reactor packed with non-porous ceramic saddles. Later, S.A. Kehl (1998) assessed the hydrodynamic performance of the reactor with respect to liquid hold up, dispersion and also mass transfer limitations.

In his (S.A. Kehl, 1998) studies on continuous hydrogenation, the homogeneous catalyst $OsHCl(CO)(O_2)(PCy_3)_2$ was forced to have higher activity than the ruthenium analog $Ru(CH{=}CH_2Ph)Cl(CO)(PCy_2)_2$ though the former suffered from severely reduced activity because of the inability to adequately purge the reactor system of oxygen. It was found that the reaction was under complete kinetic control when the NBR solution presaturated with hydrogen was used. His studies didn't include heat transfer effects though there was a vital problem for fast reactions such as the inability to adequately remove the heat of reaction resulting from the hydrogenation of concentrated solutions. Overall, the packed bed reactor turned out to perform well and even proved to be amicable to the industrial conditions with the exceptions of scant studies on mass transfer limitations and heat transfer difficulties.

Pan et al. (2002) have numerically investigated the potential configuration or optimum design for the continuous hydrogenation of NBR. Using the intrinsic hydrogenation rate, they studied the hydrogenation performance in CSTR and PFR separately. Since any flow system can be expressed as a combination of CSTR and PFR, they studied the potential configuration that is optimal for the continuous hydrogenation of NBR. From their analysis, a plug flow reactor with an instant mixing

component (CSTR) at the inlet would be an optimum configuration for the production of HNBR using a continuous process.

2.2 Static Mixers as Gas Liquid Reactors

In the gas liquid reaction, the gas-phase reactant dissolves in a liquid to react with the liquid or other substances in the liquid. The dissolving of the gas in the liquid is a mass transfer step that can have slight or large effect on the rate of the reaction, depending upon the gas solubility, the mass transfer coefficient and the intrinsic kinetics of the reaction. The conventional gas liquid reactors used in the process industry include, bubble columns, tubular reactors, packed bed reactors, spray contactors, venturi reactors and more recently static mixer reactors. For a given reaction, the intrinsic rate of reaction is the same for all these reactors, but the mass transfer coefficients differ greatly, and the selection of reactor type and reaction conditions are strongly influenced by the mass transfer characteristics (Harriott, 2003). For a particular system, the gas liquid reactor is chosen based on the mass transfer coefficient and the mean residence time of the liquid phase, but also on the yield and selectivity with multiple reactions (Nagel et al. 1981). Since, static mixers are known to produce high interfacial area; most of the conventional gas liquid reactors are replaced by them. They are also used in several unit operations equipment. Rader et al. (1989) have reported many applications of static mixers used in unit operation equipment for both cocurrent and countercurrent flows. Distillation and other column operations are now using structured packings instead of the tray or random packing. When static mixers are used as gas liquid reactors, residence time distribution (RTD), liquid hold up, pressure drop, heat transfer phenomenon are also very important factors to be considered in addition to the mass transfer characteristics.

2.2.1 Geometry of the Internal Element

Static mixers are basically used to blend fluids of different densities and viscosities. They were principally used in the polymer industry for blending. Static mixers often referred as ‘motionless mixers’, have become standard continuous operation equipment in the process industries now-a-days. They are used for a wide variety of applications in the chemical process industries such as, in chlorination and oxidation, acid and base dilution, fast reactions, plug flow finishing reactors, thermal homogenization, reactant/catalyst blending, gasoline blending, water and waste treatment, pharmaceuticals (Thakur et al. 2003). Until the 1970s, the static mixers were not established in the process industry even though it was patented much earlier. An 1874 patent describes a single element,

multilayer motionless mixer used to mix air with a gaseous fuel. Furthermore, French patents were issued in the 1950's. More than 30 commercial models are currently available. Commercial static mixers have a wide variety of basic geometries and many adjustable parameters that can be optimized for specific applications.

Figure 2.2 shows some of the different commercial static mixers. The various types of static mixers behave quite differently, and classification schemes have been proposed to explain these differences based on the geometry of the mixing elements. The commercial static mixers can be divided into five main categories: namely open designs with helices (Figure 2.2a), open designs with blades (Figure 2.2b, g-j), corrugated-plates (Figure 2.2c), multi-layers designs (Figure 2.2d and e), and closed designs with channels or holes (Figure 2.2f). Deciding which type of mixer should be used for a certain process mainly depends on the task and the physical properties of the process fluids involved. Some are designed for laminar and some for turbulent flows. A Kenics mixer can be used for both types of flows (Thakur et al. 2003).

- SMX is used as a laminar flow static mixer for high viscosity liquids and liquids with extremely different viscosities.
- SMXL is used to enhance heat transfer in viscous fluids
- SMV, KVM are turbulent flow static mixers for low viscosity process fluids. The SMV mixer is used for gas-liquid contacting and liquid-liquid extraction.
- SMR is a heat exchanger and reactor designed for laminar radial mixing with high heat transfer capacity and low pressure drop.
- SMF (not shown in figure) is used for applications with plugging problems.

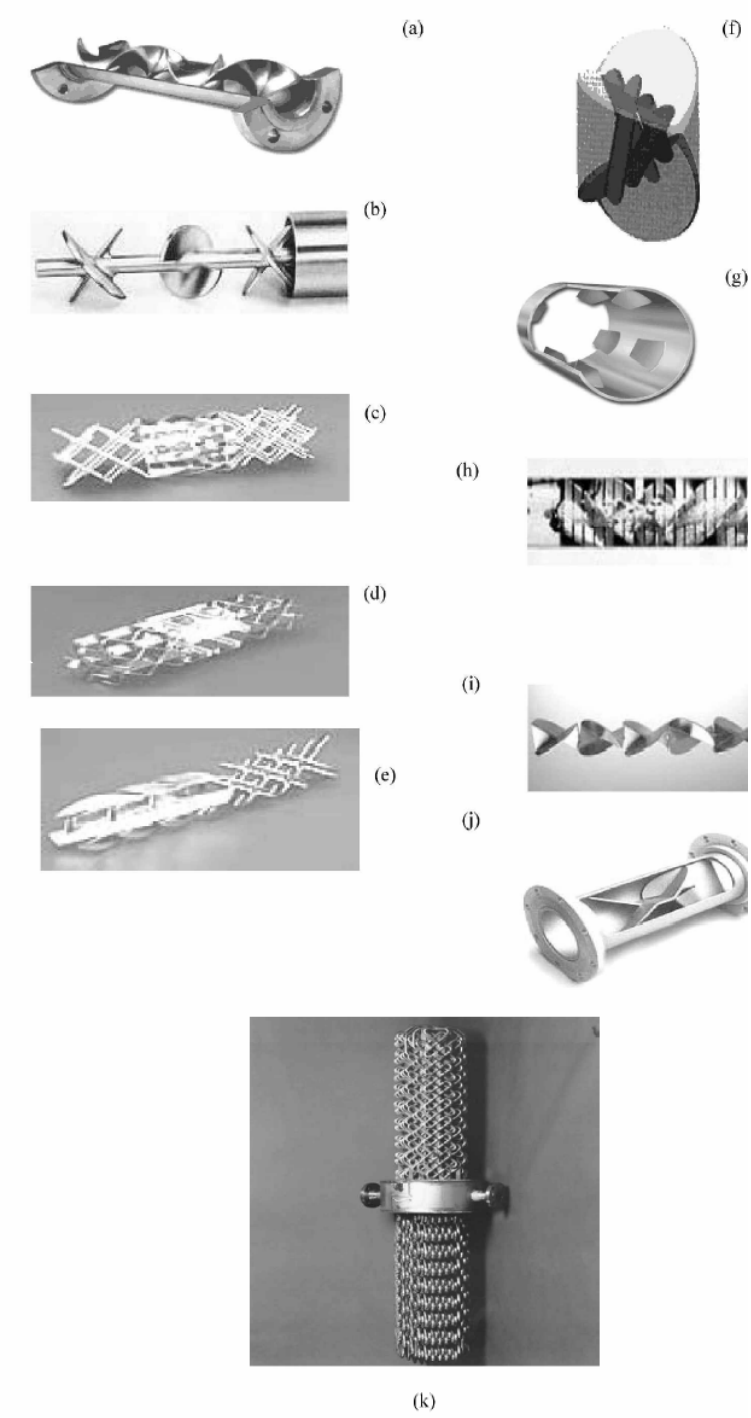

Figure 2.2 Elements of different commercial static mixers: (a) Kenics (Chemineer Inc.); (b) low pressure drop (Ross Engineering Inc.); (c) SMV (Koch-GlitschInc.); (d) SMX (Koch-Glitsch Inc.); (e) SMXL (Koch-Glitsch Inc.); (f) Interfacial Surface Generator-ISG (Ross Engineering Inc.); (g) HEV

(Chemineer Inc.);(h) Inliner series 50 (Lightnin Inc.); (i) Inliner series 45 (Lightnin Inc.); (j) Custody transfer mixer (Komax systems Inc.); (k) SMR (Koch-Glitsch, Inc.). (Thakur et al. 2003)

2.2.2 Residence Time Distribution

Knowledge about the residence-time distribution in static mixers is especially important when the mixer is used as a chemical reactor (Bayer et al. 2003). Figure 2.3 shows typical RTD for different continuous reactors.

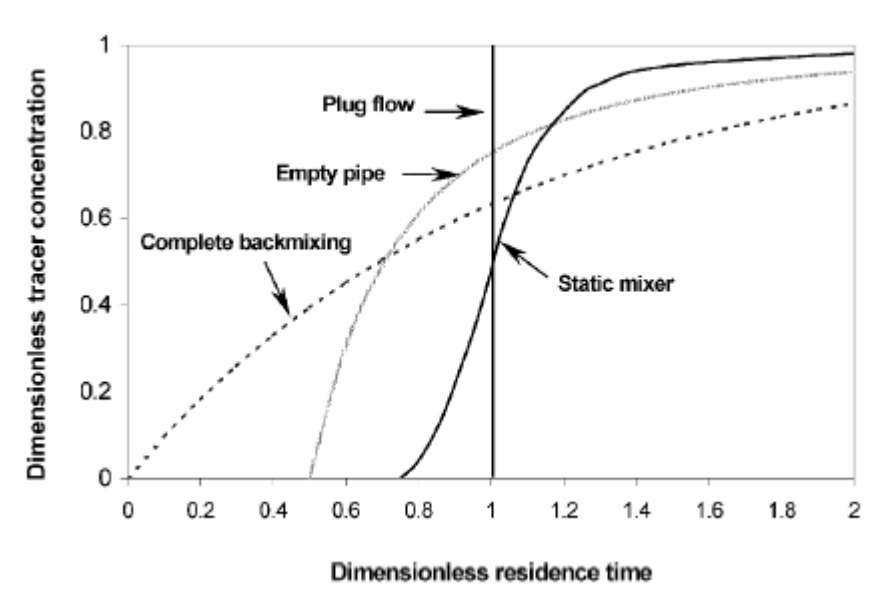

Figure 2.3 Residence time distribution for different flow reactors (Bayer et al. 2003).

The time the fluid spends inside a reactor (static mixer) will reflect the quality of the product, degree of mixing and chemical reaction yields. Residence time distribution (RTD) plays a vital role when a static mixer is used as a chemical reactor. RTD for various static mixers are quantified by the Peclet number ($Pe = uL/D_{ax}$) which is a measure of the width of RTD according to Danckwerts dispersion model (Danckwerts, 1953) . For an ideal continuous stirred tank reactor (CSTR) Pe = 0 while for an ideal plug flow reactor, $Pe = \infty$. The higher Pe is, the narrower the residence time distribution would be. The Pe value for static mixers in laminar flow depends on the number of mixing elements. For example, to achieve a Pe of 20, only five SMX elements are required. To achieve the same residence time distribution in continuously stirred tank reactors, a series of ten vessels ($N_c \approx Pe/2 = 10$) is required. Streiff et al (technical reviews, Sulzer company) also proved that the static mixers viz. Sulzer SMX, SMXL and SMV can be characterized with Pe value to describe their RTD. More over,

there are only very limited studies on the residence time distribution that have appeared in the literature. Most of them dealt with the flow in Kenics static mixer with helical internal elements. A first RTD model, proposed by Naumann (1982), considered Kenics static mixers as empty tubes having occasional planes of radial mixing. The experimental RTD data of Nigam and Vasudeva (1980) on Newtonian fluids were well fitted when four Kenics elements were made equivalent to one plane of complete radial mixing. Their results indicated that the RTD's are narrower than those for laminar flow in empty straight tubes but the deviation from plug flow was appreciable. Later, this model was extended to power law non-Newtonian fluids by Nigam and Naumann (1985). Different residence time distribution (RTD) models for static mixers with helical elements have been proposed for both Newtonian and non-Newtonian flow (Nigam and Naumann, (1985); Pustelnik, (1986); Hobbs and Muzzio, (1997)). Nguyen et al (1985) carried out RTD experiments in a Sulzer SMX mixer with 37 mixing elements, and used the model of plug flow with axial dispersion to fit their data. Huai et al (1998) carried out experiments with rheologically complex fluids in a Sulzer SMX mixer with different combinations of number of elements. They modeled their data with a two parameter RTD model based on each mixing element, the two parameters being functions of a generalized Reynolds number. Basically, this model consists of an association in parallel of, a part of plug flow components and a part of a continuous stirred tank reactor, repeated over the number of mixing elements. The RTD data for a pure liquid phase in SMX and KMX static mixers are compared by Heniche et al. (2005).

Very scant literature is available on the liquid side RTD when SM reactors are used for gas liquid operations. Literature on Peclet number as a function of Reynolds number in packed bed reactors operated in counter current fashion for gas liquid systems is given by Westerterp et al.(1984). Steigel and Shah (1977) proposed an empirical correlation for Peclet number (based on particle diameter) in packed beds with gas liquid flows operated in cocurrent upward flow. It is represented by equation (2.1)

$$\boldsymbol{Pe} = 0.128\,\mathrm{Re}_L^{0.245}\,\mathrm{Re}_G^{-0.16}(\boldsymbol{a}_p\boldsymbol{d}_p)^{0.53}$$

$$\textbf{where}, \quad \boldsymbol{Pe} = \frac{\boldsymbol{u}_L\boldsymbol{d}_p}{\boldsymbol{D}_a}, \mathrm{Re}_L = \frac{\boldsymbol{\rho u}_L\boldsymbol{d}_p}{\boldsymbol{\mu}_L}, \mathrm{Re}_G = \frac{\boldsymbol{\rho u}_G\boldsymbol{d}_p}{\boldsymbol{\mu}_G} \qquad \textbf{(2.1)}$$

Limited literature on the RTD in SM reactors with open blade internal structure in gas liquid systems led to the investigation of flow behavior which is discussed in Chapter 3 and Chapter 5.

2.2.3 Liquid Hold Up (ε_L)

Liquid hold up is an important hydrodynamic parameter that is needed for performance evaluation, scale up and design. Over the years, many correlations were proposed for estimating the gas hold up ($1-\varepsilon_L$) in packed bed reactors. When the gas-liquid flow in the SM reactor is in a homogeneous regime, the liquid hold up can be represented as the ratio of volumetric flow rate of liquid to the total(gas and liquid) flow rate (Heyouni et al. 2002). If they are not in the same regime, the liquid hold up depends on the individual flow rates, physical properties of the working fluids, gas distributor design, reactor internals and power consumption (Veera et al. 2001). A recent work by Behkish et al. (2006) illustrates the different correlations used for estimation of gas hold up in packed bed reactors for different working fluids. Less literature is available on the liquid hold up in static mixer reactors (especially with open blade internal structure) when a heterogeneous flow regime is maintained. New empirical correlations are derived by conducting experiments with different working fluids and are presented in Chapter 3 and Chapter 5.

2.2.4 Volumetric Mass Transfer Coefficient (K_La)

Gas liquid reactions limited by mass transfer can be improved by static mixers. They can be used in multiphase systems to decrease dispersed phase drop sizes and to increase interfacial mass transfer. In practice, mixer performance is typically characterized by a single parameter such as the mass transfer coefficient, K_La, or the Sauter mean diameter, d_{32}. The various processes taking place in a reactor as far as gas liquid reactions are concerned can be depicted as intermixing of the reactants, equalization of concentration by diffusion and the actual chemical reaction. In gas-liquid reactions the speed of the mass transfer process is the limiting factor which often determines the reaction rate. Static mixers offer large interfacial area for gas-liquid flows, resulting in enhanced heat and mass transfer. They provide not only high effective radial mixing but also feature a narrow residence time distribution. If immiscible components are contacted co-currently in static mixers, a swarm of droplets or bubbles (in case of gas-liquid contacting) and a large interfacial surface, which is continuously renewed, are formed. With a static mixer, the drop size distributions can be achieved which are narrower than with stirred systems or dynamic in-line devices. On the other hand, the performance of the static mixer also depends on the physical-chemical properties of the individual phases. The typical drop size is between 100 and 1000 μm; for drops smaller than 10 μm, separation becomes difficult. The mechanisms of breakage and coalescence of gas bubbles and drops are similar. However they exhibit three differences (Thakur et al. 2003):

1. Liquid drops can form smaller than bubbles-with minimum diameter around 10-100 μm for bubbles and 0.1-1 μm for drops.
2. The dispersed to continuous ratios of viscosity and density will be quite different for gas-liquid and liquid-liquid systems.
3. In gas-liquid systems it is generally easy to know whether gas is dispersed based on the gas and liquid flow rates, while in liquid-liquid systems phase inversion is possible.

Schneider (1988) has conducted many coalescing gas liquid reactions in various conventional reactors combined with different static mixers (of Sulzer type). He studied various reactor configurations such as, Sulzer mixers in in-line configuration, loop reactor with forced and natural circulation, bubble reactor with the inner tube filled with SMV mixer packings, cascade type bubble reactor and stirred vessel with static mixer. The conventional stirred vessel has high local energy dissipation adjacent to the stirrer, where fine bubbles (diameter less than 1 mm) are formed and thus a large interfacial area is produced. Since the residence time in this zone is very short, outside this zone, the bubbles coalesce (diameter 3 to 5 mm) and the mass transfer area decreases sharply. Thus the system is totally back mixed. The same is true in diaphragm-perforated plate. When Sulzer mixers are used in in-line configuration, the energy dissipation is uniform over the whole mixer volume and bubbles of equal size (diameter 1 to 2 mm) are uniformly distributed over the whole reactor volume. Schneider found out that the mass transfer coefficient (k_L) in Sulzer mixer to be 10 to 50 times greater than that of conventional systems. The Sauter mean diameter, d_S, of the dispersed drops can be calculated for the SMV according to the equation (Streiff et al. 1997):

$$d_s / d_h = 0.21 We^{-0.5} \mathrm{Re}_h^{0.15} \qquad \textbf{(2.2)}$$

For dissolving oxygen in water, the k_La value for SMV is calculated according to the relation:

$$k_L a = 7.2x10^{-3} \varphi_d^{0.8} d_h^{0.26} (P/V)^{0.69} \qquad \textbf{(2.3)}$$

Mass transfer is not only determined by the reactants physical properties, but also by the mass specific energy input ε. According to turbulence theory, changes in drop or bubble size are proportional to $d \sim \varepsilon^{-0.4}$ (Bayer et al. 2003). The specific mass-transfer area depends on the bubble size and on the dispersed phase ratio,φ_d. Also, the mass transfer coefficient, k_L, increases with increasing energy input. Liquid-liquid and gas-liquid systems are governed by the relationship (Bayer et al. 2003)

$$k_L a / \varphi_d = \varepsilon^{0.8} \qquad \textbf{(2.4)}$$

Many studies have been aimed at estimating the Sauter mean diameter in co-current, liquid-liquid systems using static mixers. The first contribution to the prediction was that of Middleman (1974) who studied Kenics static mixer (Thakur et al. 2003). He proposed the following relation:

$$\frac{d_{32}}{D} = A \cdot We^{a_1} \cdot \mathrm{Re}^{a_2} \qquad \textbf{(2.5)}$$

Since then, many other correlations have been published that include a variety of commercial static mixers. Most show an explicit dependence on the Weber number with an exponent that ranges from -0.74 to -0.4. The exponent on the Reynolds number is slightly positive. Lately, Strieff et.al (Technical reviews) developed a general equation for the drop size distribution in static mixers that was in agreement with the experimental values. The drop size distribution is given by

$$d(\varphi_d) = C_n (1 + k\varphi_d) \left(\frac{(1 + B \cdot Vi) We_c}{2} \right)^{0.6} \left(\frac{\sigma}{\rho_c} \right)^{0.6} \left(\frac{\rho_c}{\rho_d} \right)^{0.1} \varepsilon^{-0.4} \qquad \textbf{(2.6)}$$

where $d(\varphi_d)$is the calculated characteristic drop size of interest, i.e. d_{min}, d_{10}, d_{sv},d_{90} or d_{max}. B,C_n and We_c are constants. Also, from their tests and analysis for all mixer types and mixer lengths an average of $We_c = 1.8$ was found. C_n depends on the drop size category. The measured drop sizes for different mixer types and the calculated drop sizes according to the above equation were in close agreement.
The specific energy dissipation is a function of the geometry of the mixing elements and of the flow velocity. The mean value for liquid-liquid flow can be calculated from the flow rate and the pressure drop of the static mixer Strieff et.al (Technical reviews):

$$\varepsilon = \frac{\Delta p \cdot \dot{V}}{\rho \cdot V} = \frac{f \cdot v_s^3}{2\varepsilon_v^3 D_h} = \frac{Ne \cdot v_s^3}{\varepsilon_v D_t} \qquad \textbf{(2.7)}$$

For gas-liquid flow, the friction factor *f* or the Ne-number in the above equation must be multiplied by a factor $\phi_L^2(1-\varphi_d)$. The interfacial area for mass transfer is inversely proportional to the drop or bubble size. The specific mass transfer area, phase ratio and liquid side mass transfer coefficient was combined in one equation as a function of the specific energy dissipation based on penetration theory (Strieff et al.Technical reviews):

$$k_L a = K_M \left(\frac{\varepsilon_v{}^3 D_h}{f} \right)^{1/6} \varepsilon^{0.766} \left(\frac{\sigma(1 + B \cdot Vi)}{\rho_c} \right)^{0.9} \left(\frac{\rho_c}{\rho_d} \right)^{0.15} \sqrt{D_F} \frac{\varphi_d}{(1 + k\varphi_d)^{1.5}} \quad \textbf{(2.8)}$$

where Vi is the viscosity number defined as

$$\boldsymbol{Vi} = \left[\frac{\boldsymbol{\mu_d} (\boldsymbol{\varepsilon} \cdot \boldsymbol{d}_{\max})^{1/3}}{\boldsymbol{\sigma}} \right] \sqrt{\frac{\boldsymbol{\rho_c}}{\boldsymbol{\rho_d}}} \quad \textbf{(2.9)}$$

Hence, the mass transfer coefficient is mainly a function of the specific energy dissipation $k_La \sim \varepsilon^{0.766}$. The corrections for friction factor and energy dissipation should be applied as explained in calculation of ε. The value of K_M is reported to be 2.8 to 3.4 for gas-liquid and for liquid-liquid mass transfer. On the other hand, the effect of gas and liquid velocities on the mass transfer coefficient has been studied by several authors. They correlated the mass transfer coefficient (obtained from experiments) with superficial liquid velocity and gas velocity following the equation

$$k_L a = A U_L^{\alpha} U_g^{\beta} \quad \textbf{(2.10)}$$

where the values of A, α and β are determined from experimental results. Mass transfer coefficients increased with increasing liquid and gas velocities. Much higher k_La were obtained than with other gas liquid reactors (bubble columns, stirred vessels). This effect was mainly due to an ability of static mixers to develop large interfacial area in the system, thus giving rise to the high mass transfer. The gas velocity had more effect on mass transfer coefficient k_La than the liquid velocity.

2.2.5 Heat Transfer

High heat transfer coefficients are achieved in the static mixers compared to other conventional reactors. The heat transfer coefficient (h_i) in the static mixers is modeled using the Nusselt correlation represented by the following equation:

$$\boldsymbol{Nu} = \boldsymbol{C}_1 (\mathrm{Re}_{\boldsymbol{h}}\, \mathrm{Pr})^{\boldsymbol{C}_2} (\mathrm{Pr}/\, \mathrm{Pr}_{\boldsymbol{w}})^{0.1} \quad \textbf{(2.11)}$$

where Nu is the Nusselt number defined as h_iD_i/K, and the constants C_1 and C_2 unique for a particular type of reactor. Typical values for C_1 and C_2 for comparison of heat transfer coefficients is reported by Bayer et al. (2003). Table 2.1 shows the constants in the Nusselt correlation for different SM reactors and Figure 2.4 shows the corresponding comparison of the heat transfer performance. It

clearly shows that the SM reactor with open blade internal structure (Sulzer SMX or Kenics KMX) has a high heat transfer coefficient compared to other internal structures.

Table 2.1 Constants C_1 and C_2 for Nusselt correlation

Mixer Type	**C_1**	**C_2**
SMX	2.6	0.35
SMXL	0.98	0.38
Helical	1.5	0.33

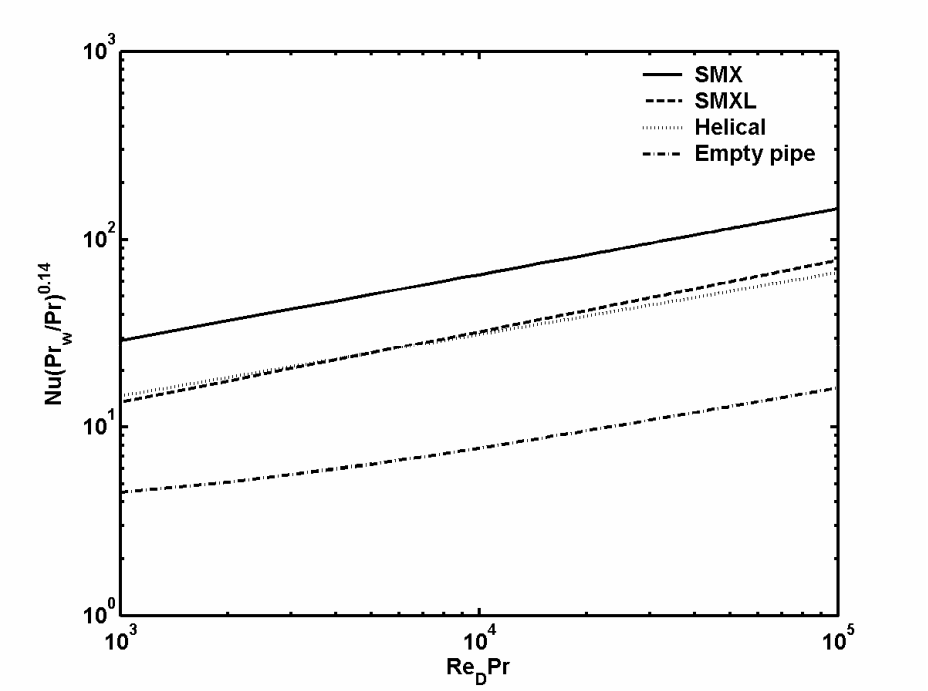

Figure 2.4 Comparison of heat transfer in static mixers (Bayer et al. 2003).

2.2.6 Pressure Drop in Gas-Liquid Flows

Pressure drop in static mixers is estimated by using the method proposed by Lockhart-Martinalle for multiphase flow. Shah and Kale (1992) and Chandra and Kale (1995) studied the pressure drop across static mixers involving gas-liquid flows and modeled the pressure drop that is similar to the Lockhart-Martinelli equation (Lockhart and Martinelli, 1949). The gas-liquid pressure drop in static mixers, $\Delta P_{G/L}$ is calculated from the individual pressure drops i.e. gas phase pressure drop and liquid phase pressure drop. The corresponding equation is given by:

$$\frac{\Delta P_{G/L}}{L} = \phi_L^2 . \frac{\Delta P_L}{L} = \phi_G^2 . \frac{\Delta P_G}{L} \qquad \textbf{(2.12)}$$

In equation (2.3), ϕ_L and ϕ_G are correction factors that can be found from the literature for various combinations of laminar and turbulent flow in the two phases (Cybulski and Werner, (1986)). The two correction factors are correlated to the ratio of the pressure drops of the two phases defined by:

$$\boldsymbol{X}^2 = \frac{\Delta \boldsymbol{P_L}}{\Delta \boldsymbol{P_G}} = \frac{\Delta \boldsymbol{P_L} / \boldsymbol{L}}{\Delta \boldsymbol{P_G} / \boldsymbol{L}}$$
$$\boldsymbol{\phi_L^2} = 1 + \frac{\boldsymbol{C}}{\boldsymbol{X}} + \frac{1}{\boldsymbol{X}^2} \qquad \textbf{(2.13)}$$

In empty pipes, C = 20 in turbulent-turbulent flows, C = 5 in laminar-laminar flows and C = 12 for laminar-turbulent flows. However, the C value is changed when using different static mixers. For SMX mixers, Kenics mixer and to Komax mixers, values of C in laminar range are given to be 2.6, 3.4, and 2.85 respectively (Streiff et al. (technical reviews), Shah and Kale (1992) and Chandra and Kale (1995)) . For power law fluids (non-Newtonian and viscoelastic liquid phases) the constant C is a function of flow index n:

$$C = \frac{n}{n+1} . C'' \qquad \textbf{(2.14)}$$

Since n = 1 for Newtonian fluid, C'' = 2C. Thus, Chandra and Kale (1995) report C" = 6.8, 5.6 and 5.2 for Kenics, Komax and SMX mixers respectively. For a viscoelastic solution, Chandra and Kale (1995) found that C" = 7.1, 6.0 and 6.2 for Kenics, Komax and SMX based mixers respectively.

2.3 Concluding Remarks

From the mass transfer and heat transfer point of view, the SM reactor with open blade internal structure is favorable for conducting hydrogenation in high viscosity systems such as nitrile butadiene solutions. The pressure drop will be more in the open blade geometry SM reactors which in turn means that the energy dissipation rate is also high. The effect of other vital parameters such as Peclet number (as function of gas-liquid flow rates) and liquid hold up with those structures are studied to evaluate the SM reactor performance for conducting the hydrogenation of NBR.

Chapter 3
Hydrodynamics in SM Reactor with Air/Water System

3.1 Introduction

Preliminary hydrodynamic experiments related to residence time distribution (RTD), gas hold up and mass transfer are conducted in a static mixer reactor using air and water as working fluids. The internal element used in this study has open-flat blade geometry. The RTD experiments are conducted in water alone and water/air system using sodium chloride solution as tracer. The experiments were conducted by varying the gas/liquid velocities and the number of mixing elements inside the reactor. The results obtained from the RTD experiments were modeled using plug flow with axial dispersion model. The model could fit well with the liquid alone (water) experimental results but deviated with the air/water system. The experiments were conducted to study the interdependence of the number of mixing elements used and the corresponding Peclet number in the water system. This information would give insight in studying and designing the actual reactor for hydrogenation of NBR. Also, the RTD experiments with the air/water system were designed to investigate the effect of gas flow rate on the dispersion (Peclet number) inside the SM reactor. The gas hold up and mass transfer experiments were designed in the SM reactor with the air/water system, so that the effect of gas and liquid flow rates on the gas hold up and over all mass transfer coefficient could be investigated. Though the physical properties of the air/water system are different from the actual working fluids in the actual hydrogenation system, these preliminary experiments were designed and performed to investigate the feasibility of using a SM reactor for hydrogenation of NBR.

3.2 Experimental

3.2.1 Experimental Set up

The experimental set up consists of a static mixer with eighteen elements and the internal structure of the element has an open blade geometry (same as Sulzer SMX). The reactor is configured vertically up, with the gas and liquid entering co-currently at the bottom and leaving at the top.

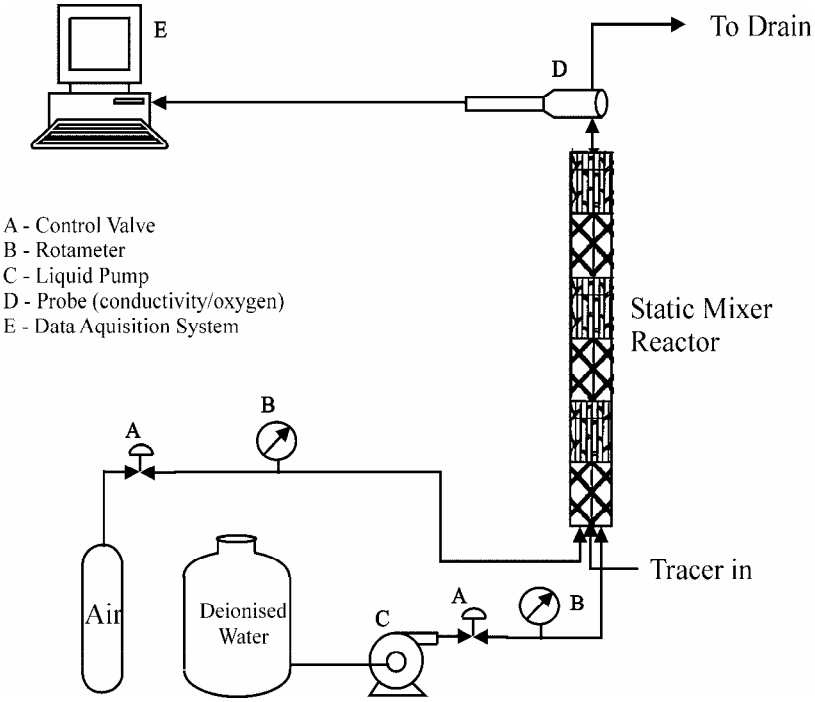

Figure 3.1 Reactor set up used for performing RTD, hold-up and mass transfer experiments.

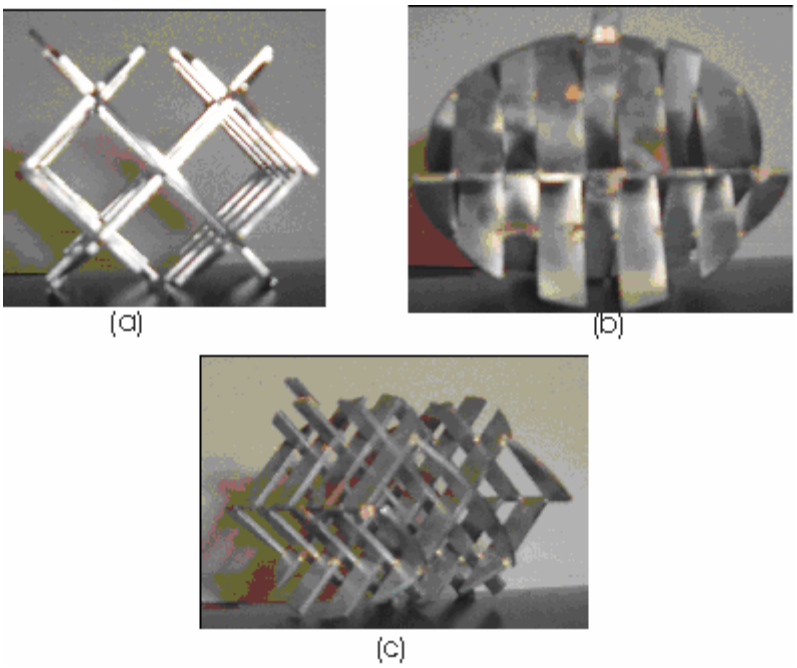

Figure 3.2 Geometry of the internal element. (a) Front view (b) Side view (90^o) (c) Side view (45^o)

Figure 3.1 shows the reactor set up used for studying the RTD, hold-up and mass transfer. The reactor is an acrylic pipe with a diameter of 6.3 cm and length of 90 cm. The geometry of the internal element is shown in Figure 3.2. The geometry of the internal element is same as that of the Sulzer SMX. The internal element is made from stainless steel circular discs of diameter 6.2 cm and thickness 1 mm. The circular discs are cut and welded together (in the Engineering Machine shop, University of Waterloo) to form an open blade structure as shown in Figure 3.2. These elements are arranged along the length of the reactor so that each element is at an angle 90^{o} with its neighboring element. In our system, the geometry of the element has open blade structure and is such that every alternate element does not completely cover the inside cross sectional area of the reactor but looks similar to that of an SMX element. The corresponding void fraction was found to be 0.95. The intricate net shaped internal structure splits a single flow into several partial flows and these partial flows in turn mix together after one complete rotation which is obtained for every four elements in this type of reactor. A direct coupled rotary vane pump (supplied by GE motors and Industrial Systems) is used to pump the liquid through the reactor while gas (air and oxygen free nitrogen supplied by Praxair) is delivered from corresponding compressed gas cylinders at the desired pressure. Liquid and gas flow rates are set using corresponding rotameters. At the exit of the reactor, a conductivity probe (which is in turn attached to a conductivity meter supplied by VWR) is connected to measure the liquid conductivity in RTD experiments. Similarly, an oxygen probe (supplied by Cole-Parmer) is connected to measure the dissolved oxygen concentration which is used to evaluate mass transfer coefficients for various gas liquid flow rates. These probes are in turn connected to a data acquisition system thus making the measurement online.

3.2.2 Experimental Methods

Residence time distribution is usually studied by injecting a tracer as an impulse input or step input and obtaining the outlet concentration of the tracer at the exit of the reactor. An impulse input (close to ideal impulse input because the time of injection is 1 second which is so small compared to the space time of the reactor which varied from 430 – 1380 seconds) of the tracer is introduced by arranging the tip of the needle exactly at the entrance of the reactor. A 0.25N sodium chloride (supplied by Fisher Scientific) solution is used as a tracer and deionized water is pumped through the reactor. The outlet concentration of the tracer is measured using a conductivity probe and read using a conductivity meter (supplied by VWR). The measured data is recorded online (at time intervals of 1 second) through the data acquisition system.

For determining gas hold-up, de-ionised water and air were used as working fluids in the static mixer. Deionised water is sent through the reactor at a particular flow rate. The initial height of the reactor is noted as (h_i). Air is also sent through the reactor from the bottom at a particular gas flow rate. Once the flow becomes steady, the valves at the entrance and exit are suddenly closed and the liquid is allowed to settle. Final height of the liquid in the reactor is noted as (h_f). The ratio of the difference in the liquid levels (h_i-h_f) to the original height (h_i) gives the gas hold-up (ε_G).). In the present study, a new model relating the liquid side Reynolds number, gas side Reynolds number and the number of elements (which is same as the L/D ratio) to the gas hold-up is proposed.

Mass transfer characteristics are studied in the static mixer reactor with eighteen elements by using water and air as working fluids. Initially, deionised water in a tank is completely purged off oxygen using oxygen free nitrogen for thirty minutes so that it becomes deficient of oxygen. Then, it is sent through the reactor at a particular flow rate. Once, the flow is steady, air is introduced at the entrance of the reactor at a particular flow rate. The oxygen from air is transferred to the oxygen deficient deionised water. The oxygen potential in the deionised water at the exit of the reactor is measured using an oxygen probe (Model 52, YSI) connected to a data acquisition system. The gas phase (in the form of bubbles) always had significant effect on the dispersion in the liquid phase which is the cause for the non-ideal flow in the reactor. A one dimensional plug flow with axial dispersion model (PFAD) superimposed with mass transfer rate is derived by applying a differential mass balance in the reactor. The differential mass balance on the oxygen concentration in the liquid phase is given by equation (3.1).

$$\frac{\partial C_{O_2}}{\partial t} = D_a \frac{\partial^2 C_{O_2}}{\partial z^2} - \overline{U} \frac{\partial C_{O_2}}{\partial z} + K_L a (C^*_{O_2} - C_{O_2}) \qquad \textbf{(3.1)}$$

where, D_a is the axial dispersion, $\overline{U}$ is the average liquid velocity, K_La is liquid side overall mass transfer coefficient, C_{O_2} and $C^*_{O_2}$ are the oxygen concentration in the deionized water at any time and equilibrium oxygen concentration respectively. Equation (3.1) is converted to dimensionless form by scaling the time with space time (τ), length with reactor length (L) and oxygen concentration with corresponding equilibrium value. The resulting dimensionless model for normalized oxygen concentration (ξ) is shown by equation (3.2).

$$\frac{\partial \xi}{\partial \theta} = \frac{1}{Pe}\frac{\partial^2 \xi}{\partial \lambda^2} - \frac{\partial \xi}{\partial \lambda} + \mathrm{St}\cdot(1-\xi)$$
$$\text{with } \xi = \frac{C_{O_2}}{C^*_{O_2}}, Pe = \frac{\bar{U}L}{D_a}, \lambda = \frac{z}{L}, \theta = \frac{t}{\tau}, \tau = \frac{L}{\bar{U}}, \mathrm{St} = K_L a \cdot \tau \qquad \textbf{(3.2)}$$

In equation (3.2), St is the Stanton number from which K_La is determined. The Peclet number for the flow conditions used in the mass transfer experiments is obtained from the RTD results which are discussed in the section 3.3.2. Open-open boundary conditions (described by equation (3.8) in section3.3.1 where ψ is replaced by ξ) are used for solving equation (3.2). Equation (3.2) is discretized in the space using central differences for the first and second derivates. Thus, the original partial differential equation is converted to ordinary differential equation. The discretization procedure is explained in Chapter 4 (section 4.2). The liquid side overall mass transfer coefficient (K_La) is estimated by nonlinear least square fitting obtained by minimizing the sum of squares of error (using MATLAB). The error corresponds to the difference between the experimental data and the data obtained from proposed model (given by equation (3.2)).

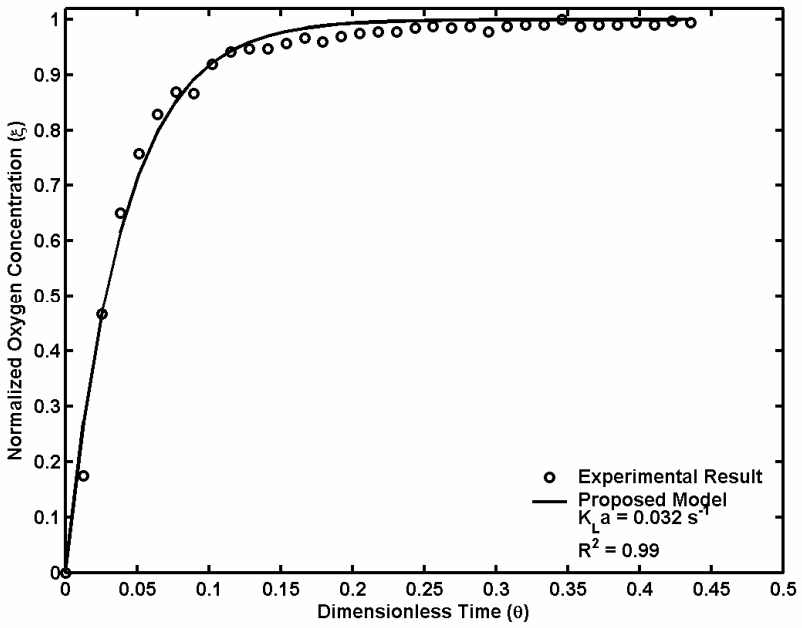

Figure 3.3 Comparison of the normalized oxygen concentration computed using the proposed model and experimental results (U_L=0.012 cm s^{-1}, U_G=0.166 cm s^{-1}, n_e = 18, Pe = 5.05).

Figure 3.3 shows the comparison of the normalized concentration computed using the proposed model and experimental data. It is clear that the experimental results could be satisfactorily fitted by using the proposed model with simultaneous estimation of $K_L a$.

3.3 Results and Discussion

Static mixers are designed for a particular process residence time when used for chemical reactions and mass transfer processes. Residence time distribution in static mixers greatly depends upon the geometry of the internal structure. Nigam & Vasudeva (1985) conducted experiments in a Kenics mixer (which has a helical type of internal structure) with water and a 70% diethylene glycol solution in water. They found that the RTD are narrower than those for laminar flow in empty straight tubes as well as those for low Reynolds number flow in helical coils. Later, Bayer et al., (2003) quantified the RTD in static mixers with any internal geometry with the Peclet number Pe, which is a measure of the width of residence time distribution according to the Danckwerts dispersion model (Danckwerts P.V., (1953)). The RTD data thus obtained from our reactor is analyzed by plotting the normalized exit age distribution. The experimental data are modeled using a plug flow with axial dispersion model with open boundary conditions (Froment & Bischoff, (1990)).

3.3.1 Plug Flow with Axial Dispersion (PFAD) Model

The plug flow with axial dispersion model is valid when there is flow where the radial dispersion is negligible and some dispersion occurs in the axial direction. This is the most widely used model for chemical reactors and other contacting devices. A balance on the molar flow rate, F_T, for the tracer, T, in the liquid at concentration, C_T, gives equation (3.3).

$$\frac{\partial C_T}{\partial t} = -\frac{1}{A}\frac{\partial F_T}{\partial z} \qquad \textbf{(3.3)}$$

where A is cross sectional area, z is the length of the reactor along the direction of flow. However, the molar flow rate F_T, accounting for both convection and dispersion is represented by equation (3.4).

$$F_T = -D_a A\frac{\partial C_T}{\partial z} + \overline{U} A C_T \qquad \textbf{(3.4)}$$

where D_a is the dispersion coefficient (m^2s^{-1}), and $\overline{U}$ is the average velocity of the liquid. Substituting equation (3.4) in equation (3.3) and simplifying one can obtain equation (3.5).

$$\frac{\partial C_T}{\partial t} = D_a \frac{\partial^2 C_T}{\partial z^2} - \bar{U} \frac{\partial C_T}{\partial z} \qquad \textbf{(3.5)}$$

Equation (3.5) can be made dimensionless by using appropriate scale factors and the resulting equation is represented by equation (3.6).

$$\frac{\partial \psi}{\partial \theta} = \frac{1}{Pe} \frac{\partial^2 \psi}{\partial \lambda^2} - \frac{\partial \psi}{\partial \lambda}$$
$$\text{with } \psi = \frac{C_T}{C_{TO}}, Pe = \frac{\bar{U} L}{D_a}, \lambda = \frac{z}{L}, \theta = \frac{t}{\tau}, \tau = \frac{L}{\bar{U}} \qquad \textbf{(3.6)}$$

The Peclet number defined as $\bar{U}$ L/D_a, is a measure of convection rate of transport to dispersion transport rate and is also referred to as Bodenstein number (especially in RTD experiments, because D_a can be replaced with the diffusion in mass transfer). The Peclet number is the one dimensionless parameter that represents the PFAD model. In determining the Peclet number from the actual measurements of the reactor dispersion, several combinations of the boundary conditions are used based on the flow conditions used in the real system. The two most important types of the boundary conditions usually encountered in a chemical processes are closed-closed boundary condition and open-open boundary condition. In the closed-closed system, the tracer before entering and after leaving the reactor will not have dispersion or diffusion and is assumed to have plug flow only. While, for the open-open system, the tracer at the entrance and the exit of the reactor has the same dispersion or diffusion as inside the reactor. These two boundary conditions are mathematically represented by the following equations (Froment and Bishoff (1990)):

For a closed-closed system,

$$\begin{aligned} &\textbf{At } \theta = 0 \ \textbf{ and } \ \lambda > 0 && \psi(0^+, 0) = 0 \\ &\textbf{At } \lambda = 0 && -\frac{1}{Pe} \frac{\partial \psi}{\partial \lambda} + \psi = \frac{C_{TO}}{C_T} = 1 \\ &\textbf{At } \lambda = 1 && \frac{\partial \psi}{\partial \lambda} = 0 \end{aligned} \qquad \textbf{(3.7)}$$

For a open-open system,

$$\textit{At } \theta = 0 \quad \textit{and} \quad \lambda > 0 \qquad \psi(0^+,0) = 0$$

$$\textit{At } \lambda = 0 \qquad \frac{1}{Pe}\frac{\partial \psi}{\partial \lambda}\Big|_{\lambda=0^-} + \psi(0^-,\theta) = \frac{1}{Pe}\frac{\partial \psi}{\partial \lambda}\Big|_{\lambda=0^+} + \psi(0^+,\theta)$$

$$\psi(0^-,\theta) = \psi(0^+,\theta) \qquad \textbf{(3.8)}$$

$$\textit{At } \lambda = 1 \qquad \frac{1}{Pe}\frac{\partial \psi}{\partial \lambda}\Big|_{\lambda=1^-} + \psi(1^-,\theta) = \frac{1}{Pe}\frac{\partial \psi}{\partial \lambda}\Big|_{\lambda=1^+} + \psi(1^+,\theta)$$

$$\psi(1^-,\theta) = \psi(1^+,\theta)$$

The Peclet number in these two types of systems can be evaluated from the mean residence time (t_m) and the variance (σ^2) of the experimental residence time distribution modeled by solving the equation (3.6) with appropriate boundary conditions. Table 3.1 shows the equations used to obtain the Peclet number for closed-closed and open-open systems. In the case of closed-closed systems, equation (3.6) has to be solved by using numerical methods while for the open-open systems an analytical solution is possible and is given by equation (3.9) (Fogler (1992)).

$$E(\theta) = \psi(1,\theta) = \frac{1}{2\sqrt{\pi\theta^3 / Pe}} \exp\left[\frac{-(1-\theta)^2}{4\theta / Pe}\right] \qquad \textbf{(3.9)}$$

Table 3.1 Mean residence time and Peclet number for closed-closed and open-open systems (Fogler,1992).

System	Mean Residence Time (t_m)	Equation for Peclet Number
Closed - Closed	τ	$\frac{\sigma^2}{t_m^2} = \frac{2}{Pe} - \frac{2}{Pe^2}(1 - e^{-Pe})$
Open - Open	$(1 + \frac{2}{Pe})\tau$	$\frac{\sigma^2}{t_m^2} = \frac{2}{Pe} + \frac{8}{Pe^2}$

Residence time distribution experiments are conducted by varying the liquid flow rate (which corresponds to N_{Re} varying from 44 to 213) and the number of elements (6 to 18 in increments of 6). The RTD experimental results are modeled using equation (3.9). Raines (Raines and Corrigan, 1967) suggested that in packed beds whose length to diameter ratio is more than 20, the closed-closed and open-open boundary conditions give the same performance while the difference is remarkable when the Peclet number is less than two.

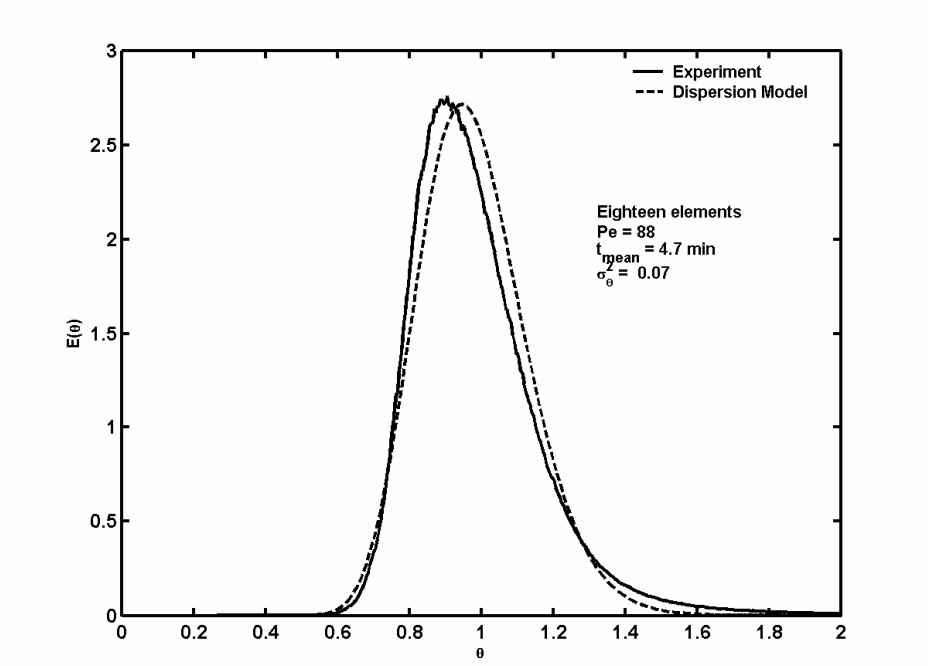

Figure 3.4 Residence time distribution in static mixer with 18 elements, Pe = 88, τ = 4.7 min, σ^2 = 0.07 (open blade internal structure)

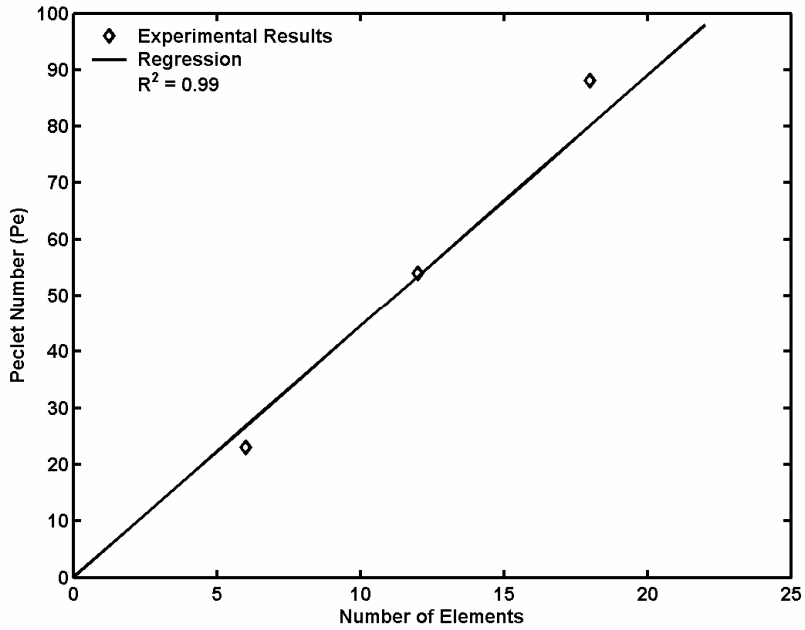

Figure 3.5 Peclet number vs. number of elements in the SM at laminar flow (t_{mean} = 4.7 min).

Figure 3.4 shows a comparison of RTD between the experimental data and model for a static mixer with 18 elements. For this case, Pe = 88, τ = 4.7 minutes and σ^2 = 0.07. Plug flow behavior can be achieved for higher values of Pe. For the same mean residence time, the variation of Pe with the number of elements was studied. Figure 3.5 shows the Peclet number as a function of the number of elements in the static mixer reactor for laminar flow.

The Peclet number in the reactor is approximately 4.7 times the number of elements. This is an important relation that is required to roughly design a reactor for a particular mean residence time. The significance of this relation is important even to compare the performances of different reactors. For example, to achieve a Peclet number of 100, a static mixer with 22 elements is required, while to achieve the same residence time distribution in continuously stirred tank reactors, a cascade of 50 ($N_C \sim Pe/2$) reactors in series is required.

3.3.2 RTD in Air/Water System

The RTD experiments with the air/water system were carried out with the same technique used for the water system alone. After the gas and liquid flows are set and becomes steady, the tracer is injected at the inlet of the reactor. The experiments were carried out with eighteen internal elements and the corresponding tracer concentration at the outlet was measured using the conductivity probe which is connected to a data acquisition system. The experimental results showed that the gas flow rate has a detrimental effect on the Peclet number. With the increase in the liquid flow rate, the Peclet number increased which is more obvious because the rate of convection would be more than the rate of dispersion. But, with the introduction of air, the reactor's flow behavior was approaching that of a CSTR.

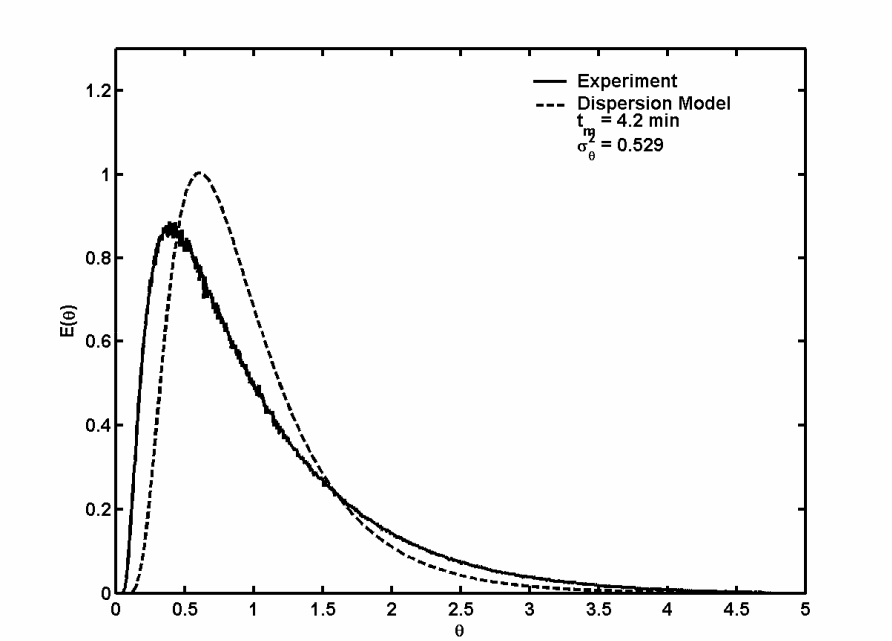

Figure 3.6 Comparison of the experimental RTD and the fitted dispersion model for air/water system with U_L = 0.315 cm s^{-1}, U_G = 0.535 cm s^{-1} and eighteen elements.

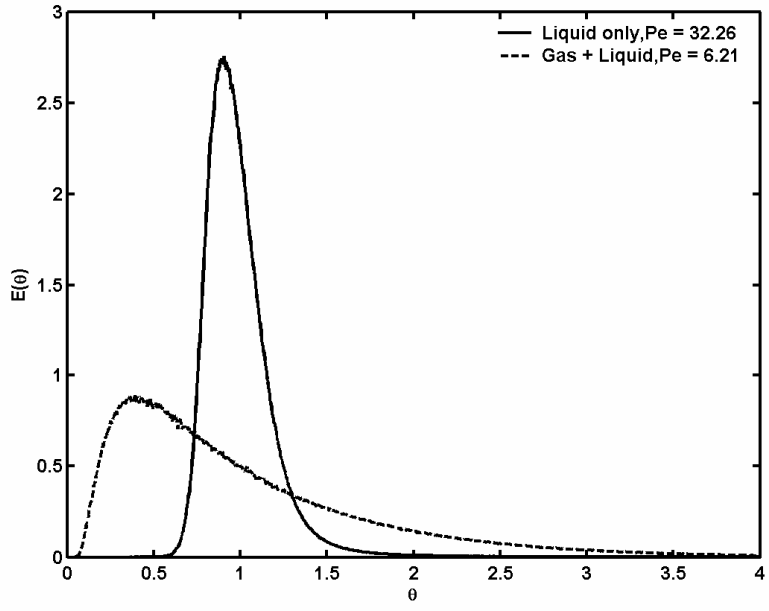

Figure 3.7 Comparison of RTD between liquid alone and gas/liquid system with U_L = 0.315 cm s^{-1}, U_G = 0.535 cm s^{-1} and eighteen elements.

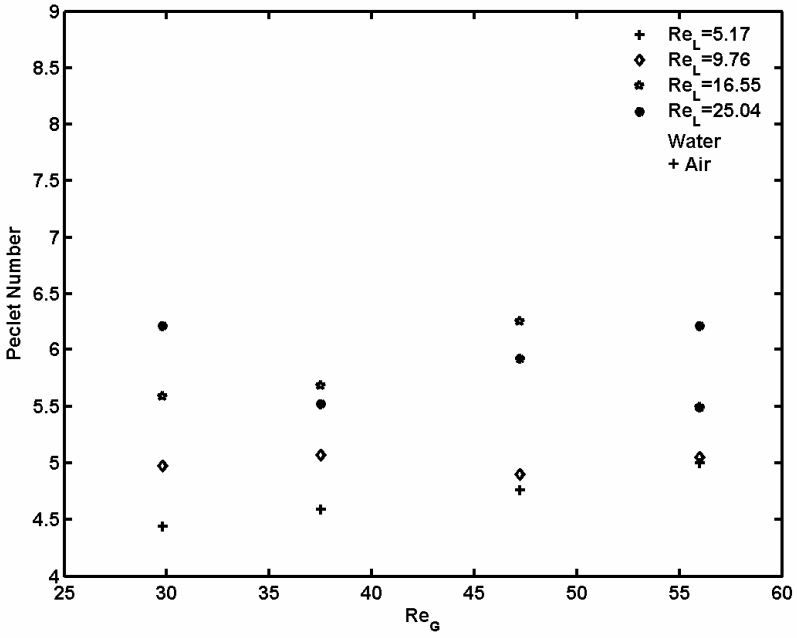

Figure 3.8 Effect of gas and liquid Reynolds numbers on Peclet number in air/water system

Figure 3.6 shows the typical RTD obtained and the fitted dispersion model for the air/water system. The model does not fit the experiment completely but could reflect the trajectory. This could be because of the experimental error also. The RTD curve is not smooth in some places because of the gas bubbles hitting the probe and then collapsing. To avoid this error, a discrete method of collecting samples could reduce the error. Figure 3.7 shows the harmful effect of air flow in the RTD experiment with an air/water system. In this figure, with the liquid alone for U_L = 0.315 cm s^{-1}, the Peclet number in the reactor was 32.26 while at the same liquid flow rate and U_G = 0.535 cm s^{-1}, the Peclet number was 6.21. For this typical case, the Peclet number in the air/water system decreased to five times that of water system alone. Figure 3.8 shows the effect of gas/liquid Reynolds numbers on the Peclet number. Because of the small range of the gas and liquid flow rates, a clear trend was not observed with respect to the effect of the gas side Reynolds numbers on the Peclet number. There was an increase in the Peclet number with the increase in the gas flow while in some cases it decreased also. An empirical correlation for Peclet number, as a function of the gas and liquid side Reynolds numbers is derived and the correlation is given by equation (3.10).

$$\boldsymbol{Pe} = \boldsymbol{\beta}_1 \, \mathrm{Re}_L^{\boldsymbol{\beta}_2} \, \mathrm{Re}_G^{\boldsymbol{\beta}_3} \qquad \textbf{(3.10)}$$

where β_1,β_2, and β_3 are constants, Re_L and Re_G are Reynolds numbers on the liquid and gas side respectively. The values of the parameters and the corresponding confidence intervals are shown in Table 3.2. The parameter corresponding to Re_G shows that with the increase in the gas flow rate the Peclet number increases but not as significant as the effect Re_L has on Peclet number. Further investigation at low liquid flow rates could be advantageous to study the effect of these individual phase flows on Peclet number.

Table 3.2 Parameter values and the confidence intervals corresponding to equation (3.10)

System	β_1	β_2	β_3	R^2	95% Confidence Interval on the Parameters	
Water + Air	2.9080	0.1636	0.0533	0.81	1.5973	4.2187
					0.1154	0.2118
					-0.0625	0.1691
Water	1.7852	0.8531	0	0.96	-1.8860	5.4565
					0.1890	1.5172

3.4 Gas Hold Up

Gas hold-up is an important design factor to be considered in designing a static mixer for two phase operation. The choice of the gas and liquid flow rates was based on specified space time and gas hold-up. Little data related to gas hold-up in static mixers is available in the literature. Couvert et al. (2002) did experiments in a static mixer with Sulzer SMX which has an open blade internal structure. In their experiments, gas was the continuous phase. They estimated the gas hold-up to be the ratio of gas flow rate to total flow rate. Heyouni et al (2002) also used the same method for the estimation of gas hold-up in Lightnin static mixers where liquid is the continuous phase. This method of estimating gas hold up involves usage of "no slip velocity" in a homogeneous flow regime where the relative velocity between the gas and the liquid phases (which is called the slip velocity) is zero. The same method of estimating the gas hold-up in our system led to large errors. The probable reason for that comes from the fact that the "no slip velocity" condition can't be used in a system where the gas and the liquid phases have large velocity differences. Experiments were carried out with the static mixer by varying gas and liquid flow rates and also the number of elements in the reactor. Gas hold-up data obtained from these types of reactors can be correlated using one of the two important types proposed in the

literature. The first type comprises correlating the gas hold-up directly to either the gas velocity or the liquid velocity (Thanos et al. (1996)). The second type correlates the gas hold-up with dimensionless numbers such as a gas side Reynolds number or a liquid side Reynolds number. Figure 3.9 shows the effect of the gas and liquid Reynolds numbers on gas hold-up in our system.

The experimental gas hold-up data obtained by varying gas and liquid flow rates and also the number of elements (6, 12 and 18) could be correlated by using equation (3.11).

$$\varepsilon_G = A N_{\mathrm{Re}_L}{}^{\alpha} N_{\mathrm{Re}_G}{}^{\beta} \exp(n\gamma) \qquad \textbf{(3.11)}$$

where *n* is the number of elements, N_{Re_L} and N_{Re_G} are Reynolds numbers based on liquid side and gas side respectively.

The parameters in the above equation are given by:

$A = 2.12\times10^{-5}$; $\alpha = -0.06$; $\beta = 1.18$; $\gamma = 0.01$

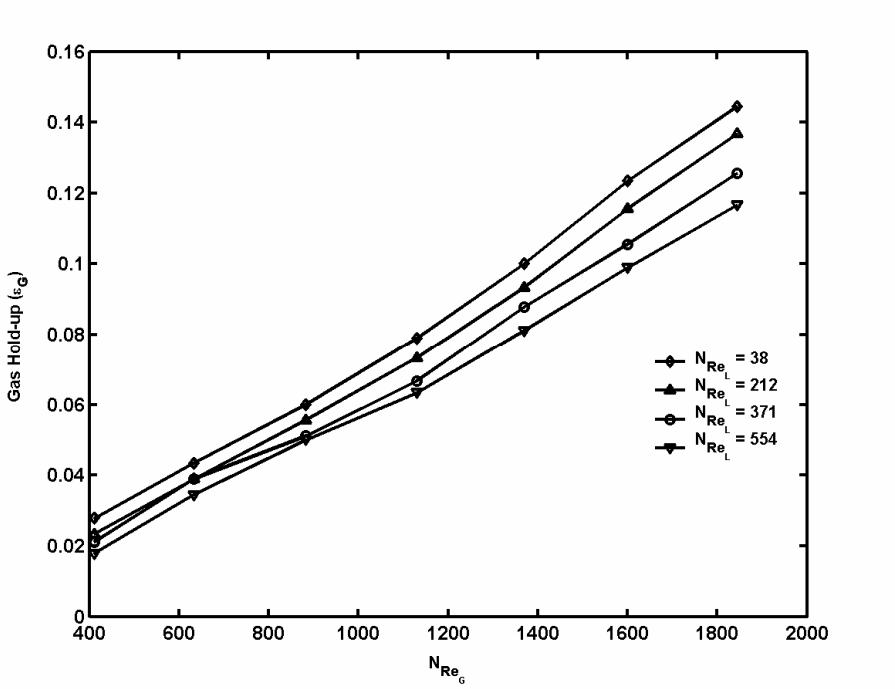

Figure 3.9 Gas hold-up vs. superficial gas Reynolds number for different liquid Reynolds number in a static mixer with eighteen elements.

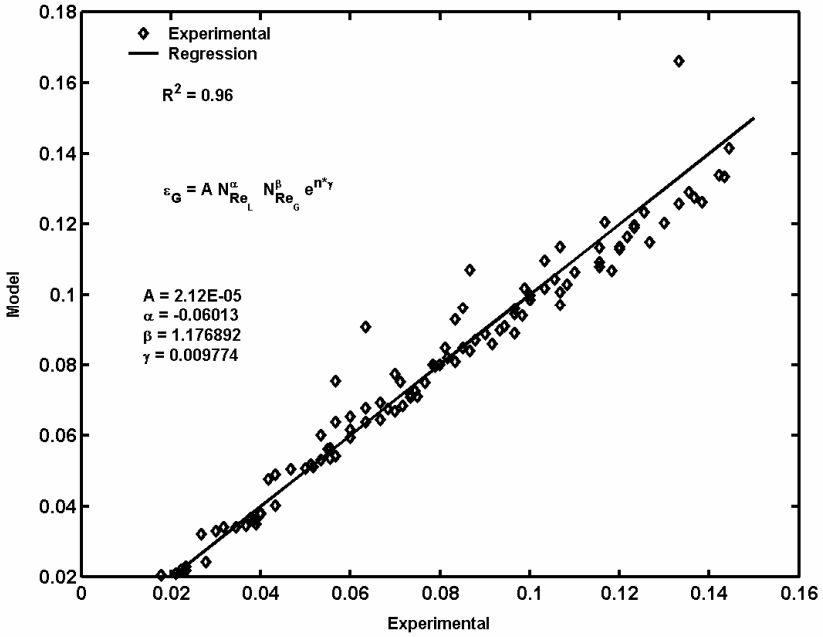

Figure 3.10 Gas hold-up data obtained from model (equation 3.11) vs. experimental hold-up

The negative power on the liquid side Reynolds number and the positive power on the gas side Reynolds number are in agreement with the fact that the gas hold-up decreases with the an increase in liquid flow rate and it increases with an increase in gas flow rate. It also indicates that the gas hold-up is more affected by the gas flow rate rather than by the liquid flow rate. The parameter γ also has the same effect as the parameter β, suggesting that with an increase in the number of elements, the gas hold up increases though it doesn't have stronger influence compared to the effect of parameter β. Figure 3.10 shows the validity of the model with respect to the experimental data.

3.5 Volumetric Mass Transfer Coefficient (K_La)

The liquid side mass transfer coefficient obtained from experiments for various gas and liquid flow rates is shown in Figure 3.11. The effect of gas and liquid flow rates on the mass transfer coefficient is correlated using the equation (3.12).

$$K_L a = A N_{RE_L}{}^{\alpha} N_{RE_G}{}^{\beta} \qquad \textbf{(3.12)}$$

the constants being A = 0.003 s^{-1}; α= 0.099; β = 0.307.

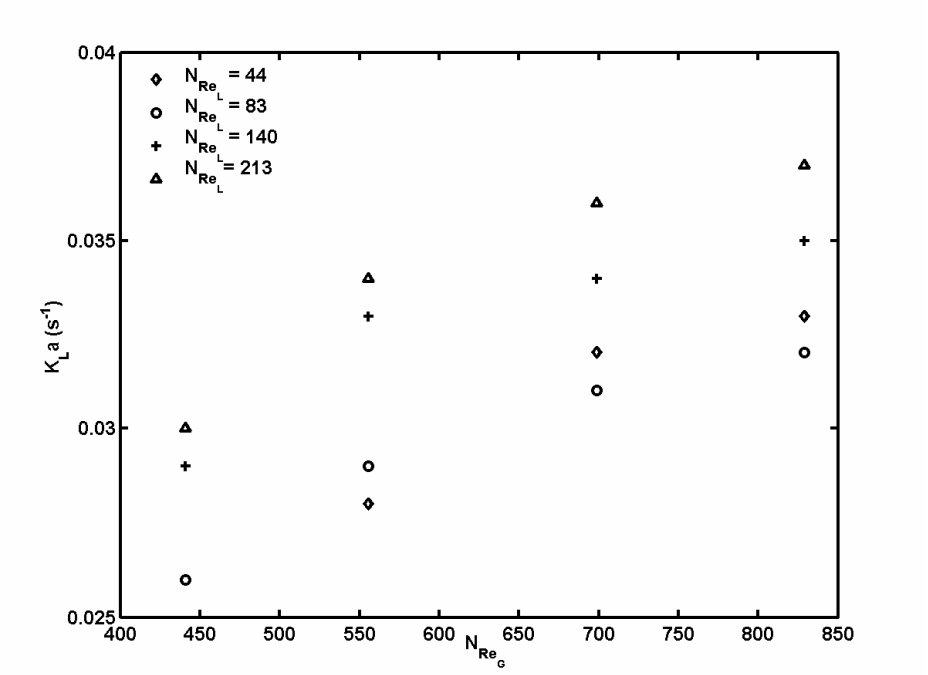

Figure 3.11 Effect of gas and liquid Reynolds numbers on K_La in a static mixer with 18 elements.

The parameters of equation (3.12) show that the gas side Reynolds number has more impact than the liquid Reynolds number. For a given liquid flow rate, an increase in the gas flow rate increases the interfacial area for mass transfer, thus increasing the mass transfer coefficient.

The coefficient A and the parameter α depend on the viscosity, surface tension, density and density difference of the working fluids. Experimental results shows that trend for the effect of mass transfer coefficient with respect to gas/liquid Reynolds numbers is similar to that obtained by Lakota et al. (2002) except that the geometry of the internal element is different and they have used a bubble column. Also, the coefficients in equation (3.12) depend on the regime in which gas and liquid flow rates are operated. Figure 3.12 shows the comparison between the model used to estimate K_La and experimental mass transfer coefficient. For higher gas flow rates and lower liquid flow rates, positive coefficients are reported when gas is used as the continuous phase (Couvert et al., 2002). Also, they obtained almost equal parameters for the gas and liquid side superficial velocities. Heyouni et al. (2002) reported high K_La values in a different geometry static mixer where they varied U_L from 70 – 130 cm s^{-1} and U_G from 1.6 - 43.7 cm s^{-1}.

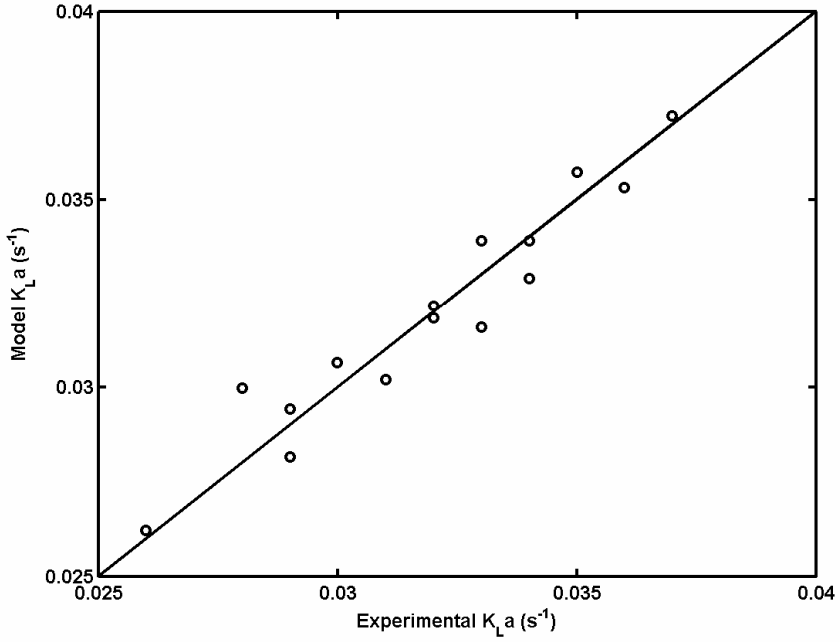

Figure 3.12 Comparison of the experimental volumetric mass transfer coefficient with the theoretical K_La estimated using equation (3.12) ($R^2 = 0.92$).

In this range (turbulent regime) of gas and liquid superficial velocities, they achieved K_La in the range of 0.1 - 2.4 s^{-1}. Also, in their case, a strong dependence of K_La on the liquid velocity was observed. Higher volumetric mass transfer coefficients are obtained in their case because of very high gas and liquid velocities. In the present study the mass transfer characteristics at high gas velocities and low liquid velocities were studied. The velocities, U_L were varied from 0.06 to 0.33 cm s^{-1} and U_G was varied from 0.56 to 1.047 cm s^{-1}. Despite the low liquid velocities, higher volumetric mass transfer coefficients (0.027 - 0.038 s^{-1}) are achieved. Owing to the negligible effect of U_L on the mass transfer, the K_La (in s^{-1}) is dimensionally correlated to U_G (in cm s^{-1}) alone according to the equation (3.12).

$$K_L a = A \cdot U_G^{\beta} \qquad \textbf{(3.13)}$$

where the constants, A = 0.737 and $\beta = 0.92$ with $R^2 = 0.9$

With a similar system (air/water), Lakota et al (2002) studied mass transfer characteristics in an empty column and a column packed with Sulzer SMV elements (U_L in the range of 0.3 – 5.4 cm s^{-1} and U_G in the range of 0.91 – 9 cm s^{-1}). They also found that the effect of superficial gas velocity on

K_La is high compared to the superficial liquid velocity. The coefficient A in their study was equal to 0.0184 and the parameter $\beta = 0.86$. The volumetric mass transfer coefficients obtained in our study are higher than those reported by Lakota et al. (2002) for the same system while the internal structure of the static mixer is different. The performance of the static mixer with open blade internal structure with respect to mass transfer is compared with dynamic mixers for same energy dissipation. For a typical dynamic mixer which has a Rushton turbine, with air-water system, the mass transfer coefficient is correlated with the superficial gas velocity and the power dissipated, which is represented by equation (3.14) (Moucha et al. (2003)).

$$K_L a = 2.148 \; x \; 10^{-3} \; (P_{tot} / V_L)^{1.13} U_g^{0.627} P_o^{0.287} \qquad \textbf{(3.14)}$$

where P_{tot} is the total energy consumption, P_o is the power number (for Rushton turbine $P_o = 5$).
The power dissipation ($\dot{\varepsilon}$) in the static mixer is calculated by using equation (3.15).

$$\dot{\varepsilon} = \Delta P_{G/L} \left(\frac{Q_L}{V_L} \right) \qquad \textbf{(3.15)}$$

where $\Delta P_{G/L}$ is the gas-liquid pressure drop, Q_L is the liquid volumetric flow rate and V_L is the volume of liquid. The gas-liquid pressure drop is estimated using the method proposed by Lockhart and Martinelli (1949) as discussed in section 2.2.6. The gas liquid pressure drop thus obtained is used to calculate the power dissipation using equation (3.14).

Figure 3.13 shows the comparison of mass transfer coefficients obtained in the static mixer with open blade internal structure with a column packed with SMV elements and a dynamic mixer with Rushton turbine for the same power dissipation and superficial gas velocity. It shows that, the mass transfer coefficients obtained in the static mixer are superior to the dynamic mixer and a column packed with SMV elements under identical operating conditions. Also, equation (3.12) predicts the volumetric mass transfer coefficient in the SM with open blade internal structure more accurately. The hydrodynamic data for the air/water system is tabulated in Appendix A.

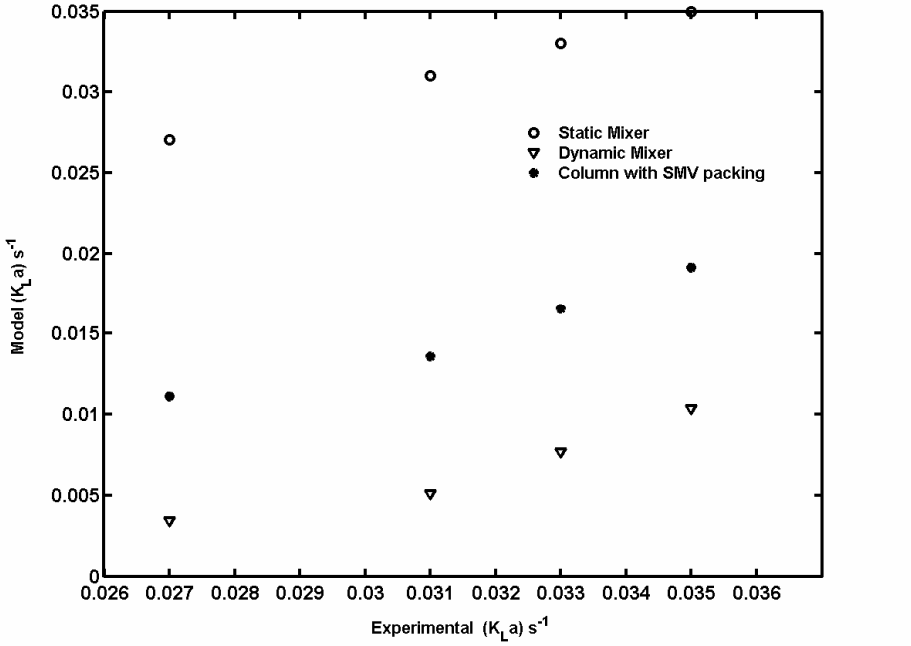

Figure 3.13 Comparison of the K_La values obtained from the model, packed column and dynamic mixer (equation 3.13) with the experimental K_La obtained in static mixer with open blade internal structure.

3.6 Concluding Remarks

The residence time distribution in static mixers with open blade internal structure (Sulzer SMX) is modeled using a PFAD model and shows that plug flow behavior can be obtained for an increased number of internal elements for a given mean residence time. A functional relationship is achieved between the Peclet number and the number of internal elements. The Peclet number for air/water system is studied for different operating conditions. An empirical correlation for Peclet number as a function of gas and liquid side Reynolds number was derived. An empirical model is derived for calculating the gas hold-up (air/water system) from the corresponding gas and liquid flow rates. Mass transfer coefficients were evaluated by fitting the PFAD model (superimposed with rate of mass transfer) to the experimental data. Empirical correlation for mass transfer coefficient (in static mixer with open blade internal structure) as a function of the gas/liquid side Reynolds numbers was derived. K_La values in the SM reactor are found to be high compared to other conventional reactors (packed column, dynamic mixer) under identical energy dissipation condition.

Chapter 4
Numerical Investigation of Performance of Static Mixer Reactor for Hydrogenation of NBR

4.1 Introduction

Residence time distribution experiments in Chapter 3 showed that the flow behavior in the static mixer reactor can be modeled using a plug flow with axial dispersion model. In addition to the flow behavior when a static mixer is used as a reactor other parameters such as reaction time, reactant properties, and mass transfer resistance are very important. Computation modeling is a very important tool for assessing the performance of a process before the actual process is built.

In this chapter, we will be focusing on the numerical investigation of dynamic analysis of a SM reactor with an open blade internal structure for hydrogenation of NBR. The dynamics of the SM reactor with respect to hydrogenation of NBR are derived starting from first principles. The resulting coupled PDE's are spatially discretized and solved in time dimensions. This is followed by the analysis of the model for different design parameters.

4.2 Dynamic Model Development and Synthesis

The preliminary residence time distribution experiments showed that the flow in the static mixer reactor can be modeled using a plug flow with axial dispersion model (PFAD). The well known PFAD model can be mathematically represented by equation (4.1) when applied to small section as shown in Figure 4.1:

$$\frac{\partial \boldsymbol{c}}{\partial \boldsymbol{t}} = \nabla \cdot (\boldsymbol{D}\ \nabla \boldsymbol{c}) - \overline{\boldsymbol{U}} \cdot \nabla \boldsymbol{c} + \boldsymbol{\phi}(\boldsymbol{c}) \qquad \textbf{(4.1)}$$

where c refers to the concentration of the reaction component and $\boldsymbol{\phi}$ (c) is the reaction rate or the source term. For isothermal, incompressible flow of polymer under constant flow rate and in a cylindrical reactor, equation (4.1) can be rewritten as:

$$\frac{\partial \boldsymbol{c}}{\partial \boldsymbol{t}} = \boldsymbol{D}_a \frac{\partial^2 \boldsymbol{c}}{\partial \boldsymbol{z}^2} + \boldsymbol{D}_r \left(\frac{\partial^2 \boldsymbol{c}}{\partial \boldsymbol{r}^2} + \frac{1}{\boldsymbol{r}} \frac{\partial \boldsymbol{c}}{\partial \boldsymbol{r}} \right) - \overline{\boldsymbol{U}} \frac{\partial \boldsymbol{c}}{\partial \boldsymbol{z}} + \boldsymbol{\phi}(\boldsymbol{c}) \qquad \textbf{(4.2)}$$

The following assumptions are made according to the flow in the static mixer reactor: (i) catalyst can be instantaneously well-mixed; (ii) the film model for mass transfer is valid and the extent of reaction in the liquid film is negligible ;(iii) the temperature and the pressure are steady and constant ;(iv) the mass transfer coefficient and the interfacial area are constant;(v) the radial dispersion coefficient is negligible compared to axial dispersion ($D_a >>> D_r$);(vi) the axial dispersion (D) is independent of concentration and position. For hydrogenation of NBR, the kinetic mechanism has been investigated by several authors (Parent (1996), Martin et al.(1997), McManus et al.(1995)) for a wide range of operating conditions for different catalysts such complexes of rhodium, ruthenium and osmium. From their investigation, the intrinsic reaction rate R_H, was found to be first order with respect to catalyst and [C=C] concentration and could vary from zero to second order with respect to hydrogen concentration. Hence, the source term i.e. R_H in terms of generalized kinetics is represented by the following equation:

$$\phi(c) = R_H = k'[catalyst][C=C][H_2]^{\alpha} = k[C=C][H_2]^{\alpha} \qquad \textbf{(4.3)}$$

where k' and k are kinetic constants and α is the order of the reaction with respect to hydrogen concentration. Since the effect of catalyst concentration is assumed to be constant, an apparent kinetic constant, *k* is used in the rate law. Thus, the differential molar balance (from equation (4.2) and equation(4.3)) for the C-C double bond ([C=C]) and hydrogen ($[H_2]$) concentrations in the static mixer reactor are represented by:

$$\frac{\partial[C=C]}{\partial t} = D_a \frac{\partial^2[C=C]}{\partial z^2} - \overline{U}\frac{\partial[C=C]}{\partial z} - R_H \qquad \textbf{(4.4)}$$

$$\frac{\partial[H_2]}{\partial t} = D_a \frac{\partial^2[H_2]}{\partial z^2} - \overline{U}\frac{\partial[H_2]}{\partial z} - R_H + K_L a([H_2^*] - [H_2]) \qquad \textbf{(4.5)}$$

where $[H_2]$ is the hydrogen concentration and $[H_2^*]$ is the equilibrium concentration of hydrogen. The equilibrium hydrogen concentration, $[H_2^*]$ can be estimated form the solubility data published by Parent et al. (1996). $K_L a$ is the overall mass transfer coefficient. Since the gas phase is pure hydrogen, the mass transfer in the gas phase and in the film are assumed to be negligible. Hence, the overall mass transfer is equal to the liquid side mass transfer coefficient which in turn depends on the geometry of the internal structure, properties of the reactants and operating conditions. To study the effect of different important factors that affect the model, the above equations are converted to dimensionless form by using dimensionless variables which are defined as follows:

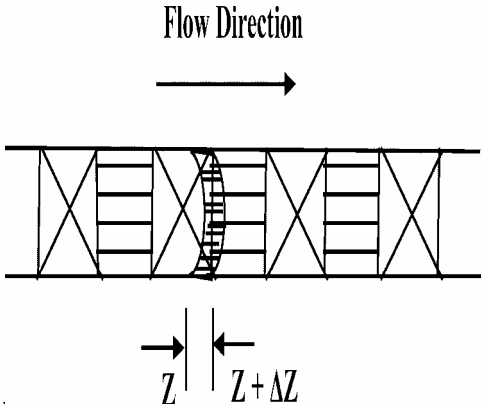

Figure 4.1 Rough sketch of a static mixer reactor, with a small control volume.

$$\lambda = \frac{z}{L} \qquad \textbf{(4.6)}$$

$$\theta = \frac{t}{\tau_R} \qquad \textbf{(4.7)}$$

$$\theta_\tau = \frac{\tau}{\tau_R} \qquad \textbf{(4.8)}$$

$$q = \frac{[C = C]_0}{[H_2^*]} \qquad \textbf{(4.9)}$$

$$\tau_R = \frac{1}{k[H_2^*]^\alpha} \qquad \textbf{(4.10)}$$

$$R = \frac{k[C = C]_0[H_2^*]^\alpha}{K_L a[H_2^*]} \qquad \textbf{(4.11)}$$

$$\boldsymbol{\tau} = \frac{\boldsymbol{L}}{\overline{\boldsymbol{U}}} \qquad \textbf{(4.12)}$$

$$x = 1 - \frac{[C = C]}{[C = C]_0} \qquad \textbf{(4.13)}$$

$$h = \frac{[H_2]}{[H_2^*]} \qquad \textbf{(4.14)}$$

The resultant dimensionless equations for the conversion x, and the normalized hydrogen concentration h, are given by:

$$\frac{\partial x}{\partial \theta} = \frac{1}{Pe} \cdot \frac{1}{\theta_\tau} \frac{\partial^2 x}{\partial \lambda^2} - \frac{1}{\theta_\tau} \frac{\partial x}{\partial \lambda} + (1 - x) h^\alpha \qquad \textbf{(4.15)}$$

$$\frac{\partial h}{\partial \theta} = \frac{1}{Pe} \cdot \frac{1}{\theta_\tau} \frac{\partial^2 h}{\partial \lambda^2} - \frac{1}{\theta_\tau} \frac{\partial h}{\partial \lambda} - q(1 - x) h^\alpha + \frac{q}{R}(1 - h) \qquad \textbf{(4.16)}$$

where Pe is the peclet number defined as $\boldsymbol{Pe} = \dfrac{\bar{\boldsymbol{U}}\boldsymbol{L}}{\boldsymbol{D_a}}$. The boundary conditions for the two equations are as follows:

$$\text{Initial Condition : At} \quad \boldsymbol{\theta} = 0; \quad \boldsymbol{x} = 0 \quad ; \quad \boldsymbol{h} = \boldsymbol{h}_0$$

$$\text{Boundary Condition 1 : } \boldsymbol{x}(0^+, \boldsymbol{\theta}) = \frac{1}{\boldsymbol{Pe}} \frac{\partial \boldsymbol{x}}{\partial \boldsymbol{\lambda}}\Big|_{\boldsymbol{\lambda}=0^+} \quad ; \quad \boldsymbol{h}_0 = \boldsymbol{h}(0^+, \boldsymbol{\theta}) - \frac{1}{\boldsymbol{Pe}} \frac{\partial \boldsymbol{h}}{\partial \boldsymbol{\lambda}}\Big|_{\boldsymbol{\lambda}=0^+}$$

$$\text{Boundary Condition 2 : At} \quad \boldsymbol{x} = 1; \quad \frac{\partial \boldsymbol{x}}{\partial \boldsymbol{\lambda}} = 0 \quad ; \quad \frac{\partial \boldsymbol{h}}{\partial \boldsymbol{\lambda}} = 0$$

In the above equations, the parameters q, R etc have unique physical meaning and h_0 refers to the initial normalized hydrogen concentration in the polymer solution (equal to 1 if NBR solution is presaturated with hydrogen or equal to zero if NBR solution is not presaturated with hydrogen). The parameter q stands for the loading of carbon-carbon double bonds; R is the ratio of maximal consumption rate of hydrogen in the hydrogenation reaction ($R_{H2\ max}$) to the maximum physical mass transfer rate of hydrogen from gas to liquid phase ($R_{MT\ max}$). In other words, R is the relative capacity of the intrinsic hydrogenation reaction over the mass transfer of the reactor (Pan et al. (2002)). The design equations thus obtained are coupled, non-linear partial differential equations. Since this is an IBVP (initial boundary value problem), method of lines (MOL) is conveniently used to solve for the

conversion and normalized hydrogen concentration. This is realized by a two step procedure. Firstly, the spatial derivatives on the right side of the equation are replaced by numerical approximation such as finite differences. The first and second derivatives are approximated using second order (three point) centered finite differences represented by the following formulae:

$$\left.\frac{\partial y}{\partial \lambda}\right|_{\lambda=i} = \frac{y(\lambda_{i+1}) - y(\lambda_{i-1})}{2(\Delta\lambda)} + O(\Delta\lambda^2) \qquad \textbf{(4.17)}$$

$$\left.\frac{\partial^2 \boldsymbol{y}}{\partial \boldsymbol{\lambda}^2}\right|_{\boldsymbol{\lambda=i}} = \frac{\boldsymbol{y(\lambda_{i+1}) - 2y(\lambda_i) + y(\lambda_{i-1})}}{(\Delta\boldsymbol{\lambda})^2} + \boldsymbol{O}(\Delta\boldsymbol{\lambda}^2) \qquad \textbf{(4.18)}$$

where i represents the grid point or node distributed in the spatial domain, y is an arbitrary independent variable (can be x , h) . $O(\Delta\lambda)$ and $O(\Delta\lambda^2)$ are corresponding orders of errors.

The resulting semi discrete (discrete in space and continuous in time) equations are:

$$\frac{dx_i}{d\theta} = x_{i+1}\left(\frac{1}{Pe\cdot\theta_\tau\cdot\Delta\lambda^2} - \frac{1}{2\cdot\theta_\tau\cdot\Delta\lambda}\right) - x_i\left(\frac{2}{Pe\cdot\theta_\tau\cdot\Delta\lambda^2} + h_i^\alpha\right) + x_{i-1}\left(\frac{1}{Pe\cdot\theta_\tau\cdot\Delta\lambda^2} + \frac{1}{2\cdot\theta_\tau\cdot\Delta\lambda}\right) + h_i^\alpha \qquad \textbf{(4.19)}$$

$$\frac{dh_i}{d\theta} = h_{i+1}\left(\frac{1}{Pe\cdot\theta_\tau\cdot\Delta\lambda^2} - \frac{1}{2\cdot\theta_\tau\cdot\Delta\lambda}\right) + h_i\left(-q(1-x_i)h_i^{\alpha-1} - \frac{2}{Pe\cdot\theta_\tau\cdot\Delta\lambda^2} - \frac{q}{R}\right) + h_{i-1}\left(\frac{1}{Pe\cdot\theta_\tau\cdot\Delta\lambda^2} + \frac{1}{2\cdot\theta_\tau\cdot\Delta\lambda}\right) + \frac{q}{R} \qquad \textbf{(4.20)}$$

Finally, the resulting ODE equations are efficiently solved using the ODE solvers of MATLAB.

4.3 Computational Results and Analysis

4.3.1 Reaction Trajectories

Adequate information on dynamic characterization can be obtained from the reaction trajectories in the SM reactor. In reactors like packed bed, bubble columns, SM reactors (where the outlet concentration/conversion is very important and behaves as a PFR) the equilibrium point is the

extreme terminal point. The equilibrium point is (x_{final},h_{final}) and is usually independent of the operating conditions. Figure 4.2 reflects the similar trend and shows the reaction trajectories (x vs. h) for different starting conditions and different residence times. It clearly shows that the reaction trajectories though starting from different operating conditions, follow a unique path to reach the equilibrium point (x_{final},h_{final}). The initial condition for normalized hydrogen concentration, h_0 is equal to zero when the NBR solution doesn't have any soluble hydrogen initially while h_0 is equal to unity when the NBR solution is completely saturated with hydrogen. Figure 4.3 shows the three dimensional reaction trajectories with x-h-θ as co-ordinates at the starting period with different residence time conditions. The solid lines correspond to $h_0 = 0$ and the dashed lines correspond to $h_0 = 1$ for different residence times. These three dimensional curves are projected onto two dimensional planes x- θ to study the effect of different initial conditions. Figure 4.4 (corresponding two dimensional plots of x- θ) shows the time required to reach the stationary points and the level of stationary points. Figure 4.5 shows the effect of inlet hydrogen concentration on conversion when the mass transfer resistance is varied from a low to a high value. It is evident that the conversion obtained in the case of $h_{in} = 1$ is higher than that of the case where $h_{in} = 0$ when there is high mass transfer resistance.

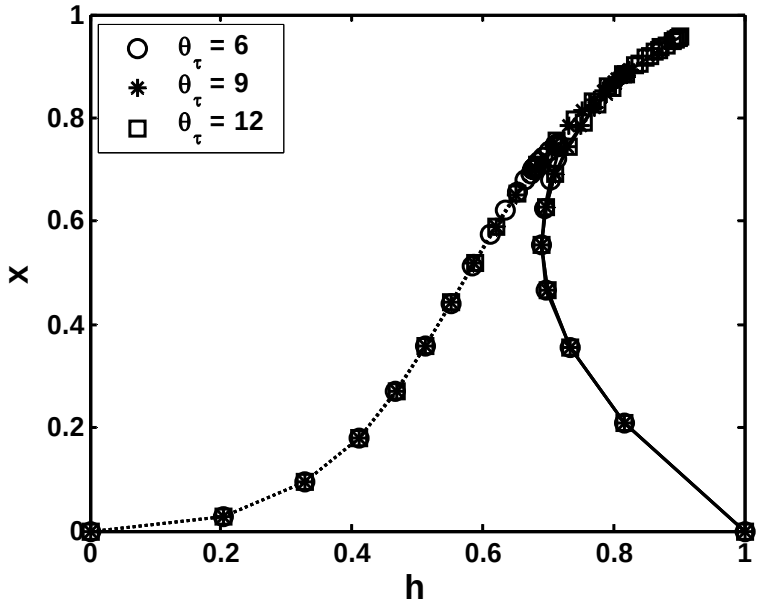

Figure 4.2 Reaction trajectory in the static mixer for Pe = 100, q = 1, $x_0 = 0$, α = 1 and R = 1(dotted line starting point $(x_0,h_0) = (0,0)$, solid line starting point $(x_0,h_0) = (0,1)$)

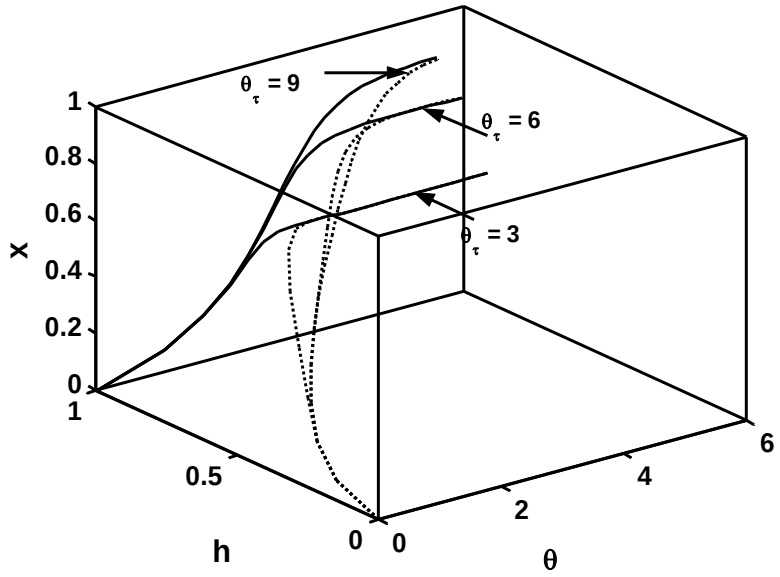

Figure 4.3 Three dimensional reaction trajectories in the static mixer (Pe = 100, q = 1 , x_0 = 0 and R = 1, dotted line starting point (x_0,h_0) = (0,0),solid line starting point (x_0,h_0) = (0,1))

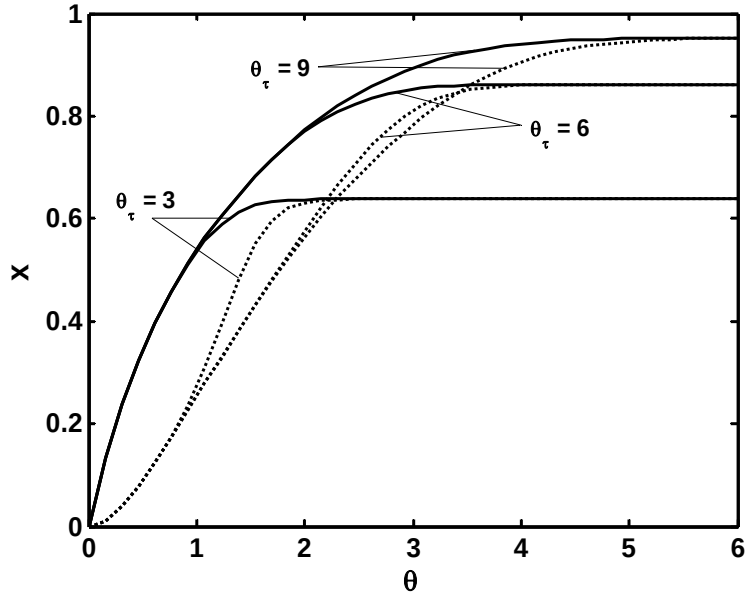

Figure 4.4 Projection of x – θ curves (Pe = 100, q = 1, x_0 = 0 and R = 1,dotted line starting point (x_0,h_0) = (0,0), solid line starting point (x_0,h_0) = (0,1))

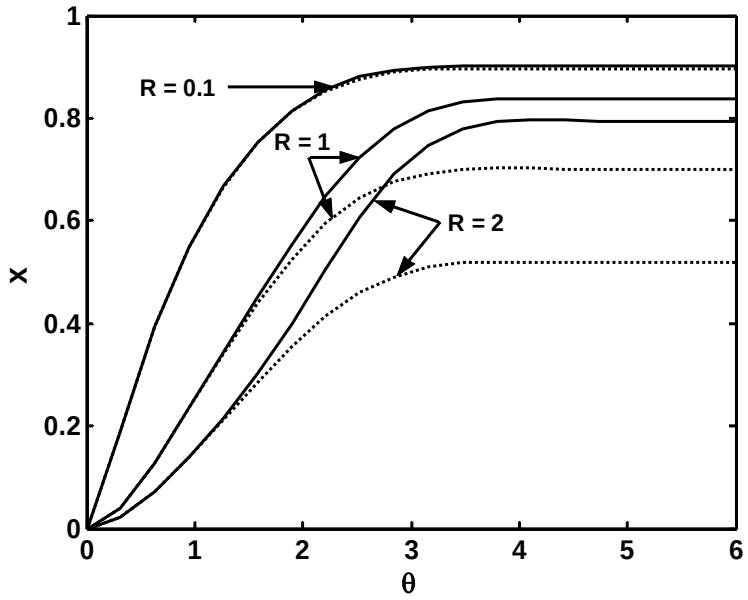

Figure 4.5 Conversion vs. θ curves for different mass transfer resistances (Pe = 100, q = 1, x_0 = 0 and R = 0.1, solid line h_{in} = 1, dotted line h_{in} = 0)

Higher solubility of hydrogen in NBR solution can be obtained if and only if the mass transfer characteristics of the internal structure in the SM are superior. This way, in addition to obtaining a higher conversion, formation of unfavorable products can be avoided. Later, it is shown that by manipulating the θ_τ value, the SM can assure higher conversion of NBR.

4.3.2 Effect of Mean Residence Time on Hydrogenation of NBR

Figure 4.6 shows the effect of residence time on hydrogenation for different carbon-carbon double bond loading (q) and mass transfer resistance (R) for h_0 =0. Since θ_τ is the ratio of the reactor residence time to reaction time, its value determines the volume of the reactor required for a particular turn over rate. From Figure 4.6, we can observe that higher θ_τ values give higher conversion when the q and R values are high. Also, when the double bond loading and and the mass transfer resistance is not very high, with lower θ_τ values, 100 % conversion can be achieved. This would entail us to go for a smaller volume reactor (which is economical) rather than going for a very big reactor. The trend obtained here for a SM reactor is similar to that obtained by Pan et al.(2002) for hydrogenation of NBR in a CSTR and PFR.

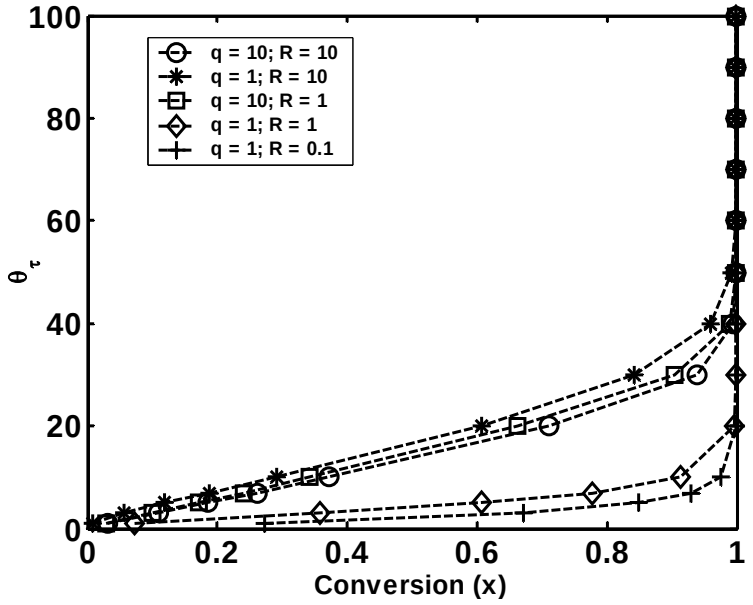

Figure 4.6 Effect of residence time on hydrogenation (Pe = 100,α = 1, x_0 = 0 and h_0 =0)

4.3.3 Effect of Peclet Number on Hydrogenation of NBR

Out of all the design parameters in the model equations, the Peclet number and the R are the most important parameters that have strong impact on the dimensions and geometry of the static mixer reactor. A lower Peclet number corresponds to CSTR behavior while a higher Peclet number will give plug flow behavior. Figure 4.7 and Figure 4.8 show the effect of Peclet number on hydrogenation for different inlet hydrogen concentration with first order kinetics with higher mass transfer resistance. It clearly shows that with lower Peclet number the conversion obtained is very low. Also, for a particular mass transfer resistance there exists a critical Peclet number ($Pe_{critical}$) above which an increase of Pe has the least increment in conversion. The critical Peclet number varies in each case and mostly depends on the value of R. An increase in the Peclet number will have a strong impact on the number of elements which was evident from the RTD experiments discussed in Chapter 3. This in turn governs the cost and maintenance (higher pressure drop) of the reactor also. To overcome this problem, the Peclet number is not increased above its critical value.

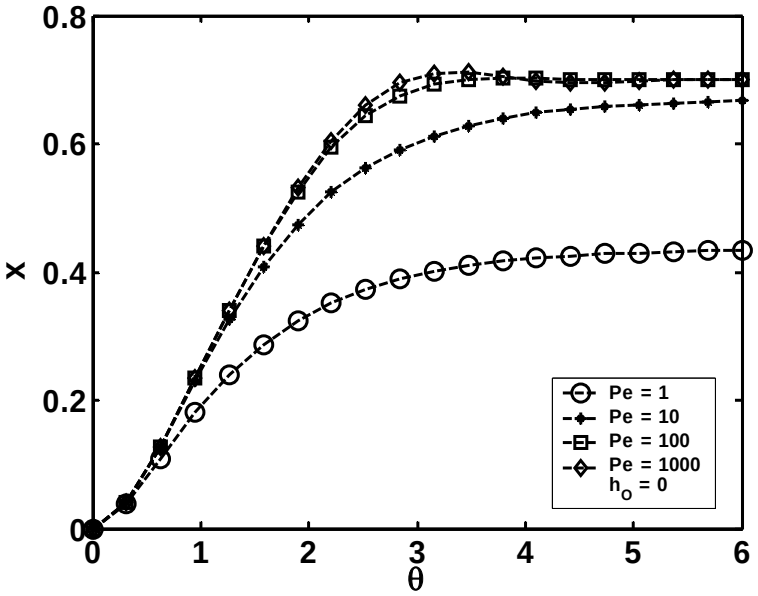

Figure 4.7 Effect of Peclet number on conversion for R = 1; q = 1; $\theta_\tau = 6$;$\alpha = 1$

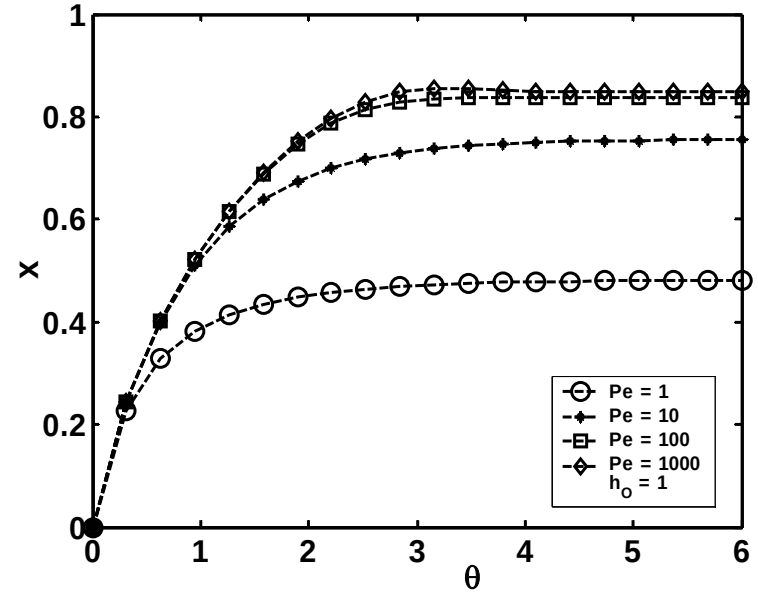

Figure 4.8 Effect of Peclet number on conversion for R = 1; q = 1; $\theta_\tau = 6$;$\alpha = 1$; $h_0 = 1$

The critical Peclet number is defined based on the following equations.

$$\frac{x(\mathrm{Pe}_{\mathrm{critical}})}{x(\mathrm{Pe}_{\mathrm{maximum}})} = 0.95 \qquad \textbf{(4.21)}$$

$$\frac{x(\mathrm{Pe}_{\mathrm{critical}})}{x(\mathrm{Pe}_{\mathrm{maximum}})} = 0.99 \qquad \textbf{(4.22)}$$

where $Pe_{maximum}$ = 1000. The simulations were done with maximum Peclet number ($Pe_{maximum}$) set to 1000 because the increase in the conversion (Δx = orders of 10^{-3}) for a further increase in Peclet number was very negligible. Figure 4.9 shows the profiles for the critical Peclet number obtained using equation (21) and equation (22) for different R values.

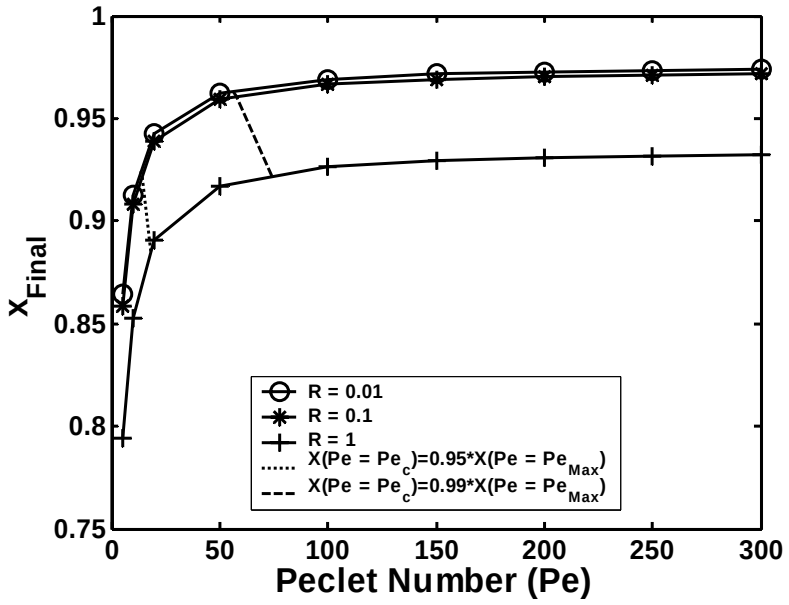

Figure 4.9 Profile of critical Peclet number needed for efficient hydrogenation (q = 1; θ_τ = 6;α =1; h_0 = 1)

4.3.4 Effect of the Number of Elements on Hydrogenation

Figure 4.10 shows the effect of the number of the mixing elements on the final conversion (x_{final}) for different order kinetics obtained for a typical condition where q = 1; θ_τ = 6;R =0.1; h_0 = 1. From the results obtained in the hydrodynamic study in Chapter 3, the linear relation between the number of

elements and the corresponding Peclet number is given as Pe = 4.7 x n_e where n_e is the number of mixing elements. In a Sulzer SMX static mixer Himmer (1994) reported that, Pe = 4 x n_e. The number of mixing elements has a strong impact on not only the size of the reactor but also on maintenance costs such as cost of pumps to overcome high pressure drops. The pressure drop in the SM with open blade internal structure almost varies linearly with the number of mixing elements (Rauline et. al. 2000). Figure 4.10 clearly shows that for all reaction orders, there exists an optimum value for the number of elements above which the increase in final conversion is almost negligible. From the simulations, the $n_{optimum}$ is found to be 20 and with a design safety factor of 20 % an SM reactor with 24 mixing elements would be most efficient with respect to assuring high final conversion.

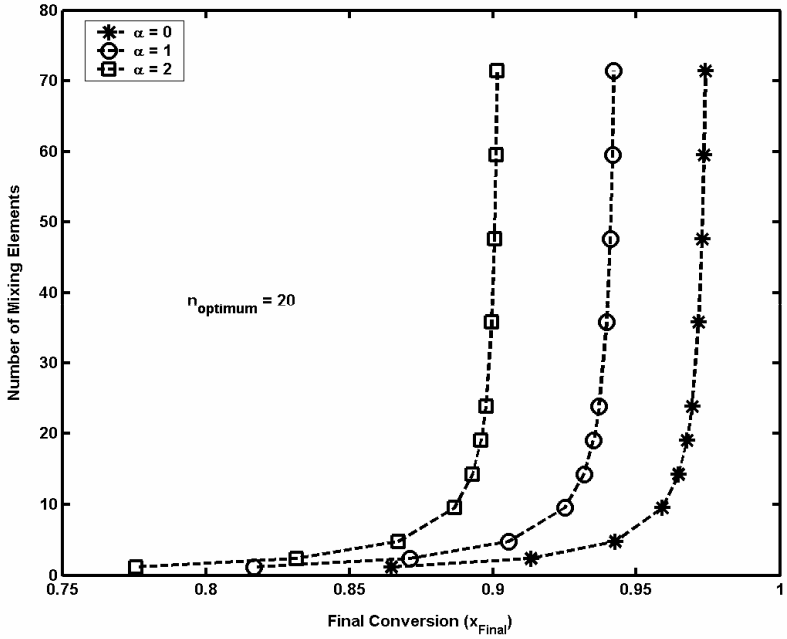

Figure 4.10 Effect of number of static mixer elements on hydrogenation (q = 1; θ_τ = 6;R =0.1; h_0 = 1)

4.3.5 Effect of R on Hydrogenation

R is a very important factor that plays a key role in hydrogenation of NBR in a SM. A low value of R is preferred for higher conversions. The effect of R is negligible at low values of q as shown in Figure 4.11. This would support our proposal that the reactor with high mass transfer characteristics (low R) would give the same higher conversions in spite of the higher double bond loading. However, the effect of the R value is less when it is less than a critical value. This critical value is defined by the equations similar to those used to find the critical Peclet number and are defined as:

$$\frac{x(\mathrm{R}_{\mathrm{critical}})}{x(\mathrm{R}=0)} = 0.95 \qquad \textbf{(4.23)}$$

$$\frac{x(\mathrm{R}_{\mathrm{critical}})}{x(\mathrm{R}=0)} = 0.99 \qquad \textbf{(4.24)}$$

The profiles for the critical R are shown in Figure 4.12. A small decrement further from $R = R_c$ would increase the operation cost of the SM reactor. For an increase in residence time (θ_τ) $R_{critical}$ also increases. But, an increase in residence time after a certain point would nullify the effect of R. Hence, there is always a trade off between these two design parameters.

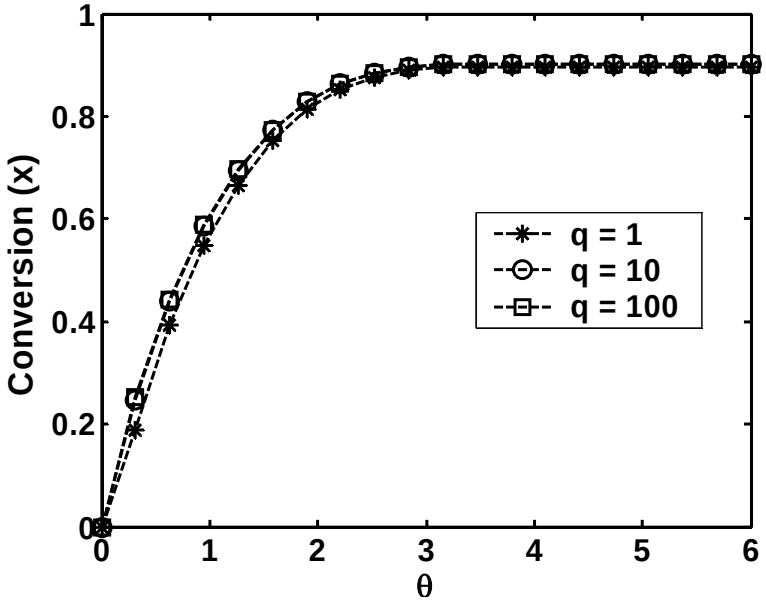

Figure 4.11 Effect of q at R = 0.1, Pe = 100, $\theta_\tau = 6$, $h_0 = 1$, $\alpha = 1$)

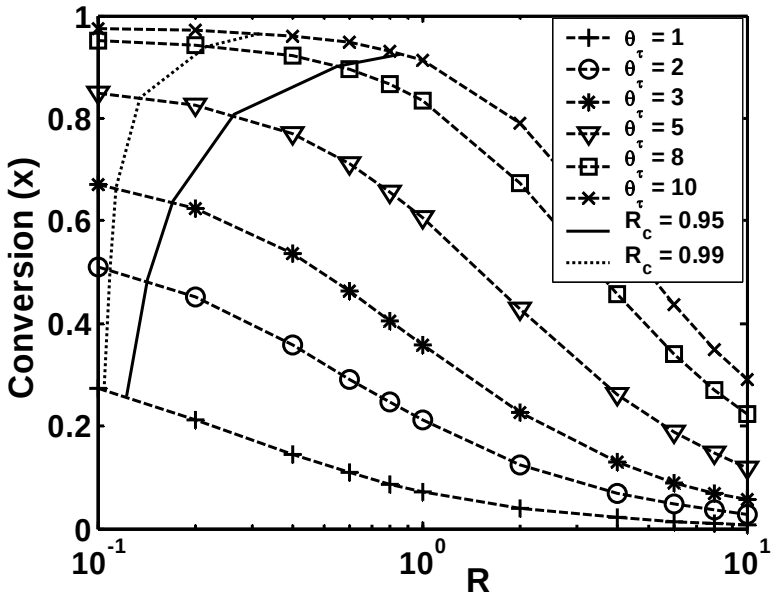

Figure 4.12 Effect of R on conversion (Pe = 100, q = 1, $x_0 = 0$ and $\alpha = 1$)

4.3.6 Effect of q on Hydrogenation

The effect of q is different at higher values of R. As discussed in the previous section, at lower values of R, the effect of double bond loading is not significant. Figure 4.13 shows the effect of q at R = 1 for two different initial hydrogen concentrations. For $h_0 = 0$, the conversion increases with an increase in q while for $h_0 = 1$, the conversion decreases with an increase in q. This effect will eventually disappear after q = 10. The difference between the conversion profiles is attributed to the effect of h_0 on the reaction. When $h_0 = 1$, the reaction will fast because of the abundant hydrogen that is already present in the NBR solution and hence, the reaction rate would be high that would lead to higher conversion. While in the case of $h_0 = 0$, initially the hydrogen has to get transferred from gas phase to polymer solution and then react. Hence in this case both reaction and mass transfer would be occurring simultaneously and this would lead to lower reaction rate or lower conversion. This trend is similar to the results obtained (in PFR and CSTR models) by Pan et al. (2002).

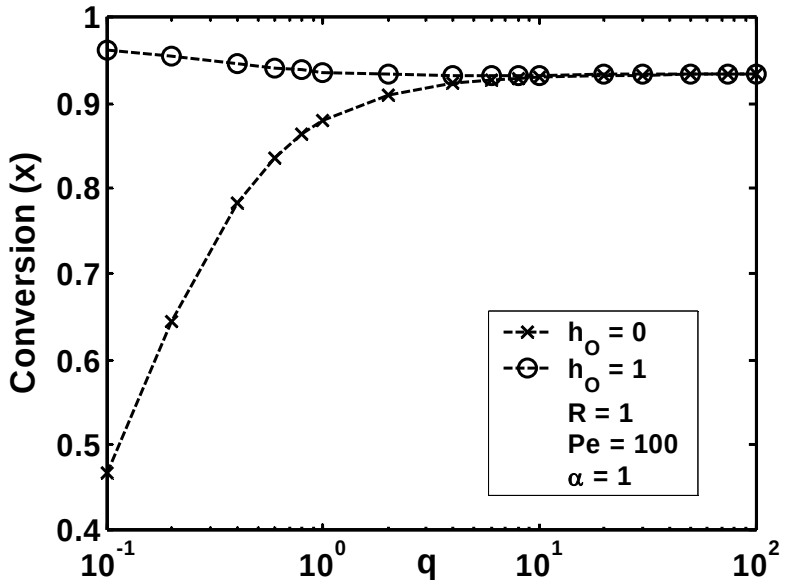

Figure 4.13 Effect of q on conversion ($\theta_\tau = 6$)

4.3.7 Effect of the Order of Reaction (α) on Hydrogenation

The effect of reaction kinetics is studied by varying the reaction order α. In the simulations, the values for the different design parameters are kept constant and the reaction order is varied. Figure 4.14 shows the conversion obtained in a SM with 24 elements for different values of α with R = 1. It shows that higher conversions can be obtained in all the three cases when R is low. But, the value of R cannot be constant for all the three cases as the reaction resistance varies though the mass transfer resistance can be the same. From equation (4.11) it can be easily seen that, R(α=1) = H_2^* R(α=0) and R(α=2) = $[H_2^*]^2$ R(α=0). Likewise, θ_τ also has to be varied since it also involves different kinetic constants as can be seen from equation (4.8). Hence, with the same reactor configurations higher conversions can be obtained for the same double bond loading when the mass transfer resistance is low and by adjusting the residence time parameter (θ_τ).

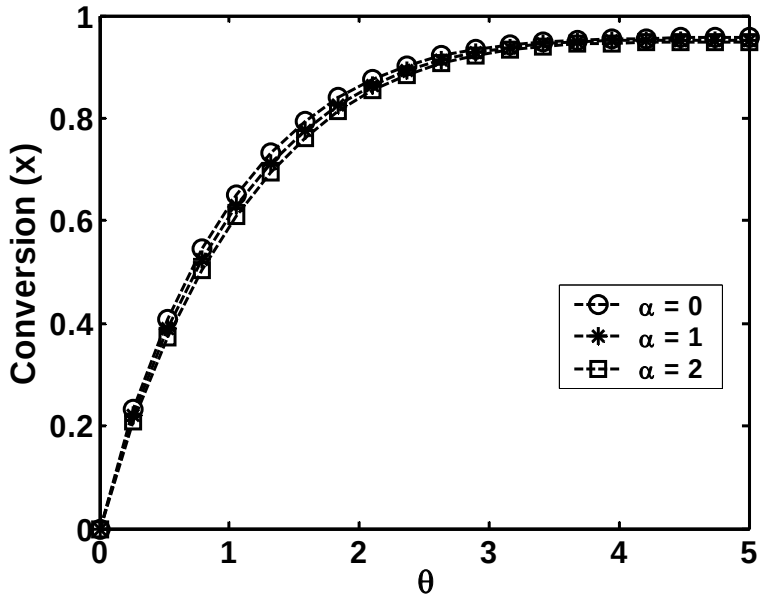

Figure 4.14 Effect of reaction order on hydrogenation of NBR (Pe = 100, $\theta_\tau = 8$, $h_0 = 1$, q = 1)

4.4 Comparison of SM Reactor Performance with Ideal PFR and CSTR

The performance of the static mixer with 24 elements for hydrogenation of NBR is compared to those of an ideal plug flow reactor (PFR) and a continuously stirred tank reactor (CSTR). The corresponding design equations for a PFR and CSTR are given below:

PFR

$$\frac{dx}{d\theta} = (1-x)h^{\alpha} \qquad \textbf{(4.25)}$$

$$\frac{dh}{d\theta} = \frac{q}{R}(1-h) - q(1-x)h^{\alpha} \qquad \textbf{(4.26)}$$

CSTR

$$\frac{dx}{d\theta} = (1-x)h^{\alpha} + \frac{x_0 - x}{\theta_\tau} \qquad \textbf{(4.27)}$$

$$\frac{dh}{d\theta} = \frac{q}{R}(1-h) - q(1-x)h^{\alpha} + \frac{h_0 - h}{\theta_{\tau}} \qquad \textbf{(4.28)}$$

with initial conditions at θ = 0, x = 0 and h = h_0 (can vary from 0 to 1)

Figure 4.15 shows the comparison of the performance of the SM with the conventional PFR and CSTR models. An interesting phenomenon observed in the simulation results is that, the static mixer reactor gives conversions that are amid CSTR and PFR after a critical residence time (θ_{τ}). For θ_{τ} less than or equal to 4, the conversions obtained in the SM reactor are lower than for PFR and CSTR. Hence, for θ_{τ} greater than $\theta_{\tau\text{-Critcal}}$ the conversion in a SM reactor eventually approaches to that of a PFR which provides the highest theoretically possible conversion.

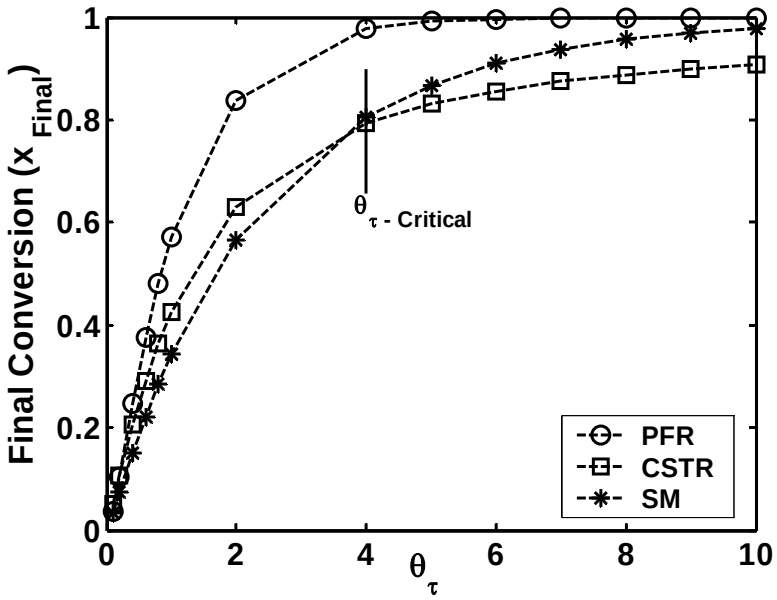

Figure 4.15 Comparison of the performance of SM with PFR and CSTR (R = 0.1, q = 1, α = 1, h_0 = 0)

4.5 Concluding Remarks

Dynamic modeling of a SM reactor with open blade internal structure with respect to a homogeneous gas/liquid reaction is established. The SM reactor is proposed to be used in a continuous process for the production of hydrogenated NBR using different catalysts. Its performance is realized theoretically by solving the models obtained by coupling reaction and mass transfer. From the

numerical simulations, it is observed that the performance of the SM reactor is mostly controlled and dominated by the design parameters viz., the relative capacity of intrinsic hydrogenation over the mass transfer of the reactor(R), Peclet number (Pe) (which also determines the number of mixing elements) that characterizes the reactor dispersion, C=C loading level (q), the ratio of the mean residence time to the pure reaction time (θ_τ). The SM reactor would perform efficiently at low R and high Pe. But, there is a critical value for both R and Pe. When $R<R_{critical}$, the increase in the conversion is relatively low and when $Pe > Pe_{critical}$, the same phenomenon is observed. Likewise, for different reaction orders, an optimum number of mixing elements is found from simulation. The $n_{optimum}$, was found to be 20. With a safety design factor of 20 %, 24 elements would promise efficient performance of the SM reactor for hydrogenation. It is also observed that with different catalysts, the same reactor configuration would give almost the same high conversions when R and θ_τ are adjusted. Finally, the performance of the SM reactor is compared with the ideal PFR and CSTR models. The SM reactor should be designed for $\theta_{\tau\text{-Critial}} > 4$ to get higher conversions approaching the performance of a PFR.

Chapter 5
Hydrodynamic Studies in SM Reactor with Hydrogen/Polymer Solution System

5.1 Introduction

The hydrodynamic experiments conducted in the static mixer reactor with open-flat blade structure (Chapter 3) were useful to assess the flow behavior, hold up and mass transfer characteristics. The information obtained from those experiments was useful to numerically investigate the performance of the static mixer reactor with respect to hydrogenation of nitrile butadiene rubber (Chapter 4). In the real system, with the properties of the working fluids and operating conditions being different, the hydrodynamic information can always be different from the earlier studies. In order to investigate the flow behavior in the actual reactor that has open-curve blade structure, residence time distribution (RTD) experiments were conducted with the actual polymer solution and hydrogen gas as working fluids. In addition to that, liquid hold up experiments were also conducted with the similar working fluids. Very scant literature is available for estimating the Peclet number in the KMX static mixer reactor, especially when it is used for gas/liquid operation. The Peclet number and the liquid hold up data obtained from the experiments were then used in the model prediction of the degree of hydrogenation which will be discussed in the Chapter 8.

RTD experiments were carried out with 2.5% (w/w) and 5.0% (w/w) hydrogenated polymer solution with and without using hydrogen gas. There are very few organic tracers that are compatible with this system. Unlike the sodium chloride or potassium chloride (which is a strong salt for aqueous system), the organic salts are very weak and often their concentration may not vary linearly with the conductance. A salt solution of n-butlyamineacetate, which is dissolvable in the polymer solution, is used as a tracer. The RTD is modeled using the plug flow with axial dispersion model with open-open boundary condition. The Peclet numbers obtained from the RTD experiments were modeled as function of liquid side and gas side hydraulic Reynolds numbers.

Liquid hold up experiments were carried out with monochlorobenzene, 2.5% (w/w), 5.0% (w/w) polymer solutions and hydrogen gas. The liquid hold up is modeled as a function of the gas/liquid superficial velocities and corresponding physical properties.

5.2 Experimental

5.2.1 Experimental Set up

The experimental set up used in the hydrodynamic study is shown in Figure 6.6. A separate line is connected between the polymer pump and the SM reactor (bypassing the preheater). The dimensions of the SM reactor, the geometry and size of the internal structure are discussed in section 6.1.1. The HNBR solutions obtained from the hydrogenation experiments (will be discussed in Chapter 7) are used in the hydrodynamic experiments. The polymer solutions are homogeneously premixed in a 20 L carboy using a multi agitator (that has a Rushton turbine geometry). Then, the solution is transferred to the feed tank. To enhance the homogeneity of the polymer solution, it is further degassed with nitrogen gas for half an hour before the experiment is conducted. The tracer (n-butylamine acetate) is taken in a properly sealed 500 ml glass bottle and is connected to the suction line of the catalyst pump. The out let of the reactor is also bypassed to the collection tank instead of allowing the solutions to pass through other parts of the equipment. Hydrogen gas (supplied by Praxair) is supplied from a compressed cylinder and the flow is controlled using a mass flow controller.

5.2.2 Experimental Approach and Operating Conditions

The pumps were primed before pumping the polymer solution and tracer into the reactor. The required flow rates are set by adjusting the pump settings. The liquid hold up is measured by using the conventional method of volumetry technique. The desired gas and liquid flow rates are set at the desired settings and run for at least two residence times till steady flow is assured. The pumps and the gas flow are suddenly turned off and simultaneously the valves at the top and bottom of the reactor are closed. Using the three way valve at the bottom of the reactor the polymer solution in the reactor is drained for at least one hour and the volume of the drained solution is measured. The ratio of the volume of the polymer solution drained to the volume of drained solution when there is no gas flow gives the liquid hold up (ε_L). RTD experiments were performed with and without gas flow. A salt solution of nbutylamineacetate (CH_3COOBu) was prepared by titrating acetic acid (supplied by Fisher Scientific) with tributyl amine (nBu_3N, supplied by Fisher Scientific). Initially, 343 ml of nBu_3N is mixed with 50 ml of monochlorobenzene (analytical grade supplied by Fisher Scientific) and bubbling with nitrogen. Then 83 ml of acetic acid is added drop by drop with simultaneous agitation, as the reaction is exothermic. The solution volume is topped up to 500 ml by adding MCB

and mixed until the nBu_3N is completely dissolved into the solution which is indicated by the presence of only one phase.

The reactor is operated for at least two times of the residence time untill the flow becomes steady. Discrete samples are collected at the sampling ports present at the first and twenty fourth element. A continuous measurement of the conductivity was not possible because, the gas bubbles in the gas/polymer mixture caused a saw tooth concentration profile. The conductivity of the samples is measured using a conductivity cell (probe, supplied by Sensorex). In contrast to the pulse input used in the hydrodynamic study in the SM reactor with the open-flat blade (Chapter 3), a step input in the tracer is used in the RTD experiments with the SM reactor with open-curve blade. As mentioned in the earlier section, because of the low concentration of the organic salt (tracer), experiments with pulse input were found to be not fruitful. Hence, a step input is used in the RTD experiments. The advantage with the step input over the pulse input is that there is no need to know about the total amount of tracer used in the polymer solution over the experimental time period. The major disadvantages with the step input are that the computation of the exit age distribution involves differentiation of the data (that can lead to large errors) and a large amount of tracer is required for each experiment. Mathematically, the step input is represented by equation (5.1).

$$\begin{aligned} C_{TO}(t) &= 0 && t < 0 \\ C_{TO}(t) &= \text{constant} && t \geq 0 \end{aligned} \qquad \textbf{(5.1)}$$

where, C_{TO} is the concentration of the tracer. The RTD function E(t) is calculated using equation (5.2).

$$E(t) = \frac{d}{dt}\left[\frac{C(t)}{C_o}\right]_{step} = \frac{dF}{dt} \qquad \textbf{(5.2)}$$

where C is the concentration of the tracer at any time t, C_o is the inlet concentration and F represents the cumulative distribution. From equation (5.2), it is evident that the calculation of E depends on the time step used in the differentiation. In the RTD experiments, the time step was varied from 1 to 5 minutes. Since the time steps were large, the RTD response at the inlet and outlet are modeled using the corresponding cumulative distribution, F which is given by equation (5.3).

$$F(t) = \frac{1}{2}\left(1 + erf\left(\frac{t - t_m}{\sigma\sqrt{2}}\right)\right) \qquad \textbf{(5.3)}$$

In equation (5.3), t_m is the mean and σ is the standard deviation of the distribution. The error function erf is defined by the equation (5.4).

$$\text{erf } y = \int_0^y e^{-a^2} da \qquad \textbf{(5.4)}$$

$$\text{with } \text{erf}(\pm\infty) = \pm 1 \quad \text{and} \quad \text{erf}(0) = 0$$

In the SM reactor system studied, the measurement of conductivity of the tracer, right at the inlet was not possible. Hence, samples were collected at the port present at the first element. The mean residence time and the variance for the distributions at the first element and twenty fourth element were evaluated and the Peclet number is derived by solving the equation for an open-open system given in Table 3.1. Since, the conductivity measurements at the inlet and exit of the reactor are used, the corresponding differences in the mean residence time and variance is used in the equation given in Table 3.1 i.e. t_m and σ^2 are replaced by Δt_m and $\Delta\sigma^2$ respectively where Δ represents the difference between exit and inlet values (for example $\Delta\sigma^2 = \sigma^2_{outlet} - \sigma^2_{inlet}$). The Peclet number thus obtained is used in equation (3.9) to model the RTD obtained for various gas/liquid flow rates.

All RTD experiments and liquid hold up experiments were carried out at room temperature and ambient pressure. The polymer flow rate is varied from 23 – 186 ml/min while the hydrogen flow rate is varied from 23 to 5580 ml/min in the hold up experiments. In the RTD experiments the hydrogen gas flow rate is varied from 46 ml/min to 564 ml/min and the liquid flow rates are varied from 23 ml/min to 98 ml/ min.

5.3 Results

5.3.1 Data Analysis for RTD Experiments

A typical residence time distribution profile (F curve) for both the inlet and outlet of the SM reactor is shown in Figure 5.1. As shown in the figure, the experimental data profiles for both inlet and outlet are not perfectly smooth. The operating conditions used in this experiment are 5% (w/w) polymer solution, the superficial liquid velocity is 0.034 cm/s and there is no gas flow. Also, it can be seen that the inlet profile did not show a sharp step change in conductivity and hence the parameters were estimated by using the differences in the mean residence time and variance as discussed in the previous section. From the individual mean time and variances of the input and outlet experimental

data, using equation (5.3), F curves are fitted to the experimental data and are used to generate the E(t) and E(θ) curves. The E(θ) is calculated from the E(t) according to the equation (5.5).

$$E(\theta) = t_m E(t) \qquad \textbf{(5.5)}$$

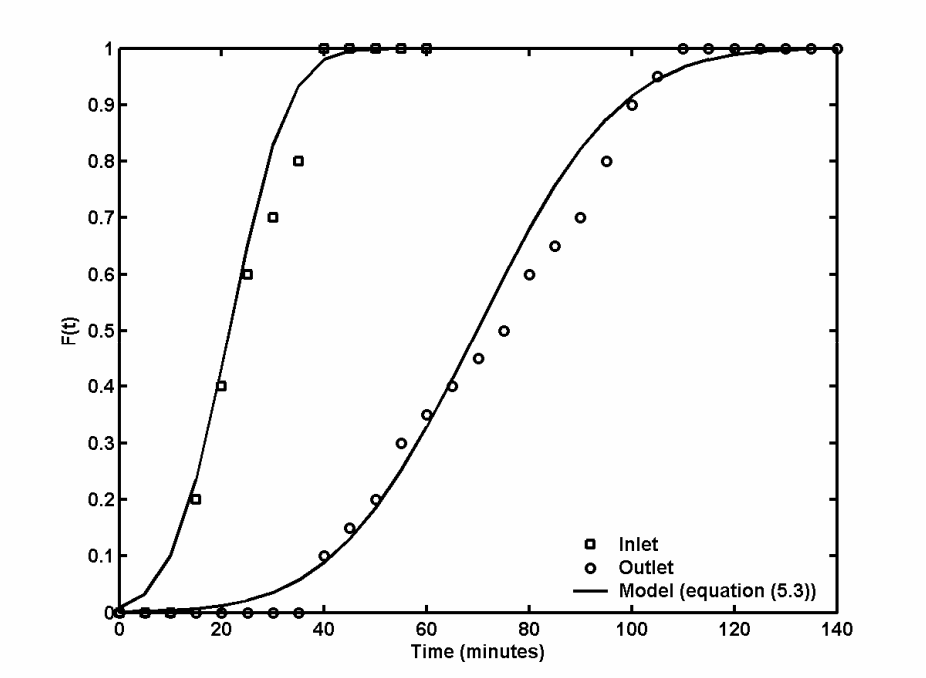

Figure 5.1 The normalized inlet and outlet concentration and the corresponding F curve (equation (5.3)) with U_L = 0.034 cm s^{-1}, U_G = 0 and 5% (w/w) polymer.

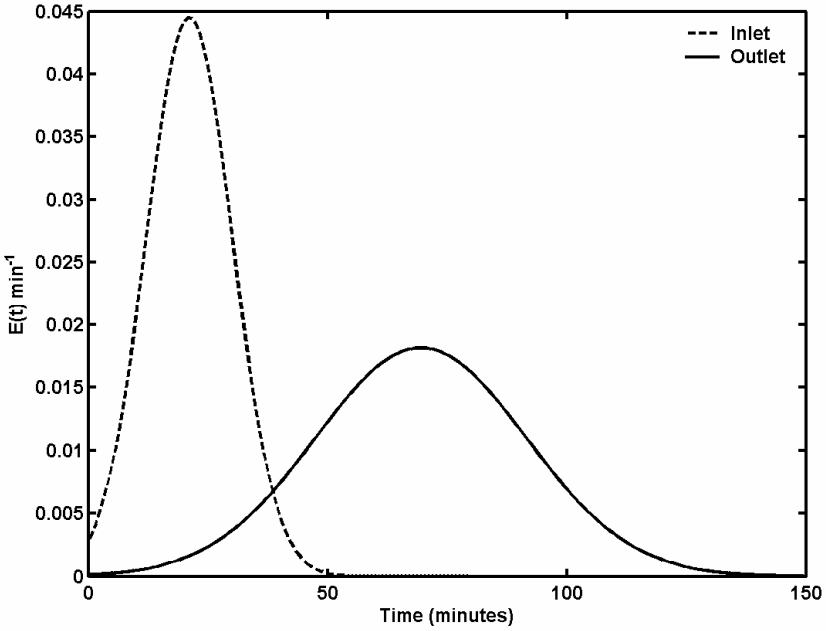

Figure 5.2 E(t) vs. time for the inlet and outlet with U_L = 0.034 cm s^{-1}, U_G = 0 and 5% (w/w) polymer.

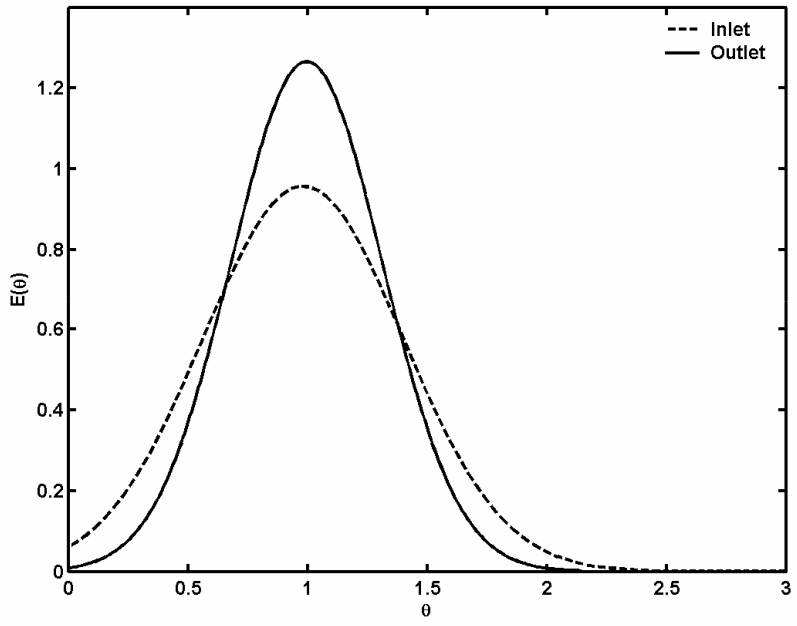

Figure 5.3 E(θ) vs. θ for the inlet and outlet with U_L = 0.034 cm s^{-1}, U_G = 0 and 5% (w/w) polymer.

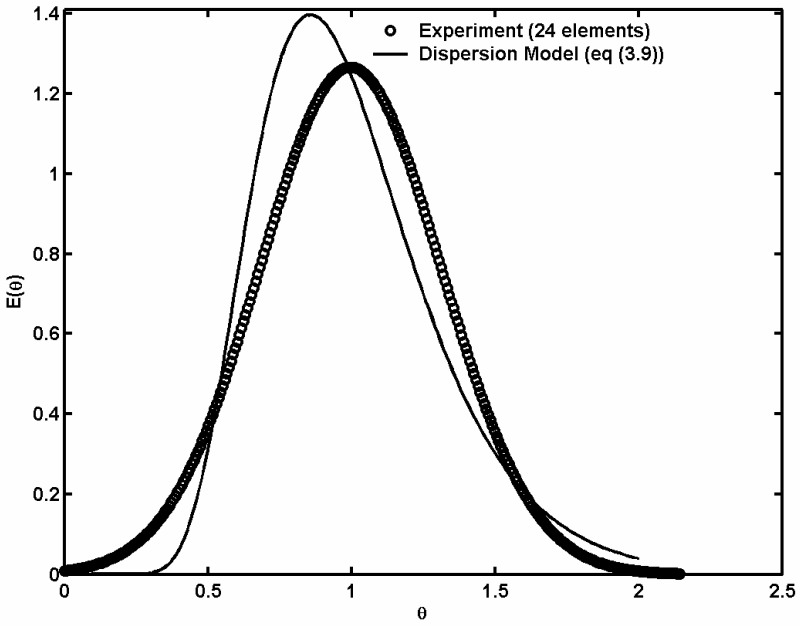

Figure 5.4 RTD Experimental vs. dispersion model with U_L = 0.034 cm s^{-1}, U_G = 0, 5% (w/w) polymer and Pe = 19.7.

Figure 5.2 shows the corresponding E(t) curves obtained by differentiating the F curves with respect to time which is represented by equation (5.2). The differentiation of F curves usually transforms a step response to a pulse response. The space time corresponding to the results shown in Figure 5.2, τ is equal to 44.11 minutes and the mean residence time obtained from the experiment, t_m is 48.25 min. This adds to the fact that mean residence time obtained in an open-open vessel is always greater than the actual space time (see the equation for mean residence time in Table 3.1). The Peclet number calculated from the variance and mean residence time for this experiment was found to be 19.7.

Figure 5.3 shows the normalized E(θ) versus θ curves for the inlet and outlet RTD curves corresponding to the E-curves in Figure 5.2. The E(θ) curves shows that the inlet and outlet distributions are symmetric with respect to θ = 1 which emphasizes the fact that all fluid elements have uniform time history. Also, there are no long tails or double peaks suggesting that there are no stagnant zones or channeling respectively. Figure 5.4 shows the comparison of the experimental RTD and the PFAD model with open-open conditions (refer to equation (3.9)).

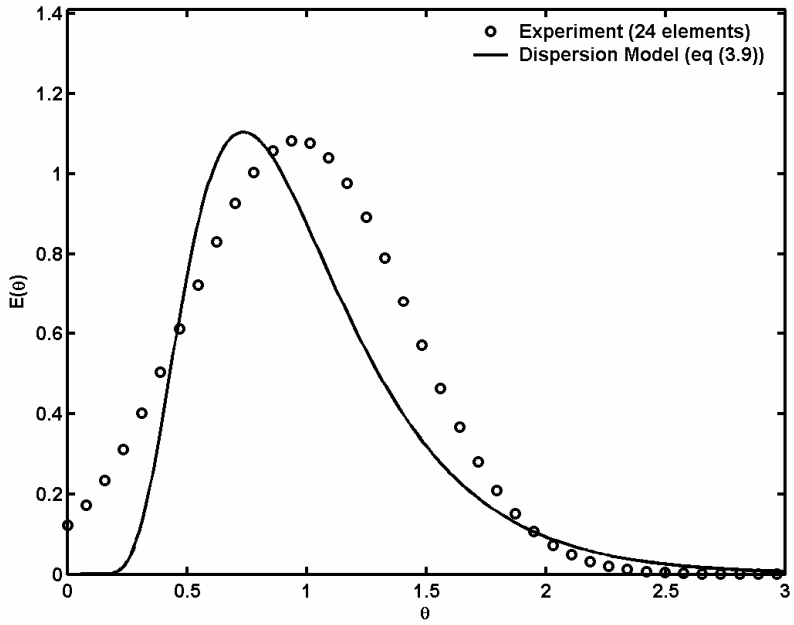

Figure 5.5 RTD Experimental vs. dispersion model with U_L = 0.072 cm s^{-1}, U_G = 0.22 cm s^{-1}, 2.5% (w/w) polymer and Pe = 9.62.

The discrimination between the experiment and the model is not far from negligible. The model follows the similar trend as that of experimental results. Similar results are obtained when there is gas flow in addition to the polymer flow. The deviation of the experimental RTD from the model can be due to many reasons. Firstly, the conductance of the tracer was not found to be linear with its concentration some times. The difference between the steady state conductivity of the tracer at inlet and outlet were always different. Similar phenomenon observed by Kehl (Kehl, 1998) in the RTD experiments performed in the packed bed reactor with identical working fluids. Also, the measurement technique used is a conventional one yet it is prone to a lot of errors. Discrete samples are collected at the sampling ports after draining little fluid left when the previous sampling was done. This may even cause error in the conductivity of the actual fluid inside the reactor. Also, the reciprocating pumps used to pump the polymer and the tracer at ambient conditions, used to deliver the flow periodically rather than in a continuous fashion. This problem can be overcome in the high pressure and high temperature conditions by throttling the valve present at the outlet of the pump. The last but very important reason for the deviation of the model and experiment is the analysis part. Since, the sampling time varied from 1 to 5 minutes, the derivative of the F curve with respect to

these large time steps to calculate E(t) is always prone to large errors. In addition to the above reasons, one has to count for the experimental error as well.

Figure 5.5 shows the experimental RTD and dispersion model for the polymer system with U_L = 0.072 cm s^{-1}, U_G = 0.22 cm s^{-1}, 2.5% (w/w) polymer and Pe = 9.62. The model could almost follow the trend of the experimental RTD as is evident form the figure. Figure 5.6 (a) and (b) shows the effect of gas and liquid side hydraulic Reynolds number on the Peclet numbers. With the introduction of gas into the reactor, one of the most important aspects observed is that the gas caused more dispersion and eventually made the SM reactor to behave like a CSTR. This could be because the gas flow would reduce the liquid hold up in the reactor and less liquid would result in low Peclet numbers. On the other hand, at high gas flow rates the average velocity of the liquid would be more and hence the Peclet number should increase with an increase in the gas velocity. These two phenomena are competitive and the results are analyzed based on the trend in Peclet numbers with respect to gas and liquid superficial velocities. Another important reason to study this effect is the operating regime. The operating conditions are chosen such that they are similar to those used in the actual hydrogenation experiments. This led to the polymer Reynolds numbers to be in the laminar regime and the gas side Reynolds numbers to be in the transition and turbulent regime. So, a heterogeneous regime might have formed with the specified operating conditions. Experiments within homogeneous regime where the gas and liquid Reynolds numbers are in laminar regime might help which can be useful for future investigation.

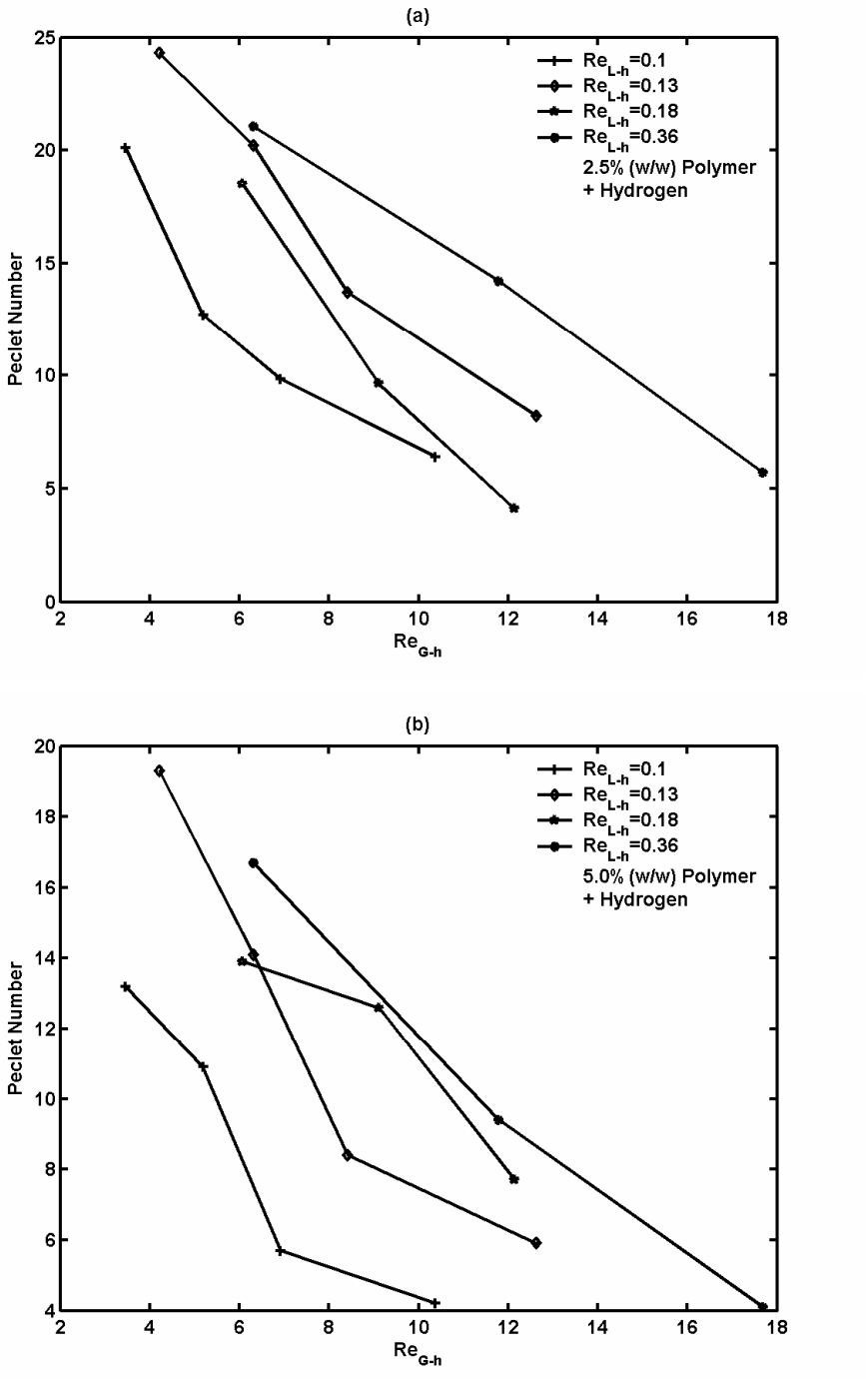

Figure 5.6 (a) Peclet number versus gas side hydraulic Reynolds number for 2.5% (w/w) polymer and hydrogen (b) Peclet number versus gas side hydraulic Reynolds number for 5.0% (w/w) polymer and hydrogen

The viscosity of the polymer solution had a negative effect on the Peclet numbers, with the Peclet numbers decreasing as the viscosity is increased. Figure 5.7 shows the effect of viscosity on the Peclet number in the two different polymer solutions for different liquid side hydraulic Reynolds numbers.

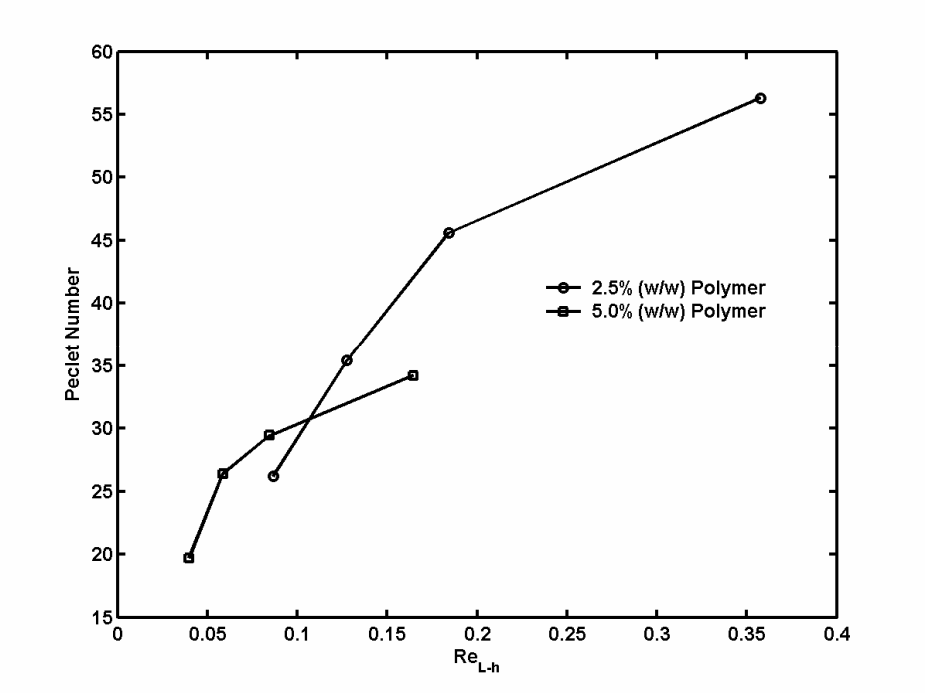

Figure 5.7 Peclet number versus liquid side Reynolds number for polymer solutions without gas

In both 2.5% (w/w) and 5.0% (w/w) polymer solutions, with an increase in the gas velocity, the Peclet number decreased drastically. There is very little literature on the effect of gas and liquid flow rates on the Peclet number in a SM reactor with the open-curve blade geometry. Some of the literature can be obtained related to the packed beds which are also used in most of the chemical processes. Steigel and Shah (1977) proposed an empirical correlation for the Peclet number on the liquid side as function of the gas and liquid side Reynolds numbers using an air/water system in packed columns operated in the cocurrent fashion. They also observed similar phenomenon where the Peclet number decreased with an increase in the gas flow rate and increased with an increase in liquid flow rate.

Empirical correlations for the liquid side Peclet numbers as a function of liquid and gas side Reynolds number based on the hydraulic diameter are developed for the 2.5% (w/w) and the 5.0% (w/w) independently for both with and without gas flow. The correlation is of the form as shown in equation (5.6).

$$\boldsymbol{Pe} = \boldsymbol{\beta}_1 \, \mathrm{Re}_{\boldsymbol{L-h}}^{\boldsymbol{\beta}_2} \, \mathrm{Re}_{\boldsymbol{G-h}}^{\boldsymbol{\beta}_3} \qquad \textbf{(5.6)}$$

where β_1,β_2, and β_3 are constants, $Re_{L\text{-}h}$ and $Re_{G\text{-}h}$ are Reynolds numbers defined based on the hydraulic mean diameter (D_H) of the SM reactor.

Table 5.1 Parameters for the correlation represented by equation (5.6)

System	β_1	β_2	β_3	R^2	95% Confidence Interval on the Parameters	
2.5% (w/w) + Hydrogen	225.3	0.45	-1.00	0.91	-34.2	484.7
					0.12	0.79
					-1.40	-0.61
5.0% (w/w) + Hydrogen	228.2	0.48	-0.92	0.90	-87.6	544.1
					0.15	0.82
					-1.32	-0.52
2.5% (w/w)	95.3	0.49	0	0.91	42.7	147.8
					0.15	0.83
5.0% (w/w)	64.3	0.34	0	0.91	14.4	114.2
					0.02	0.65

The parameters β_1, β_2, and β_3 in the equation (5.6) and their confidence level (for 95%) for the different systems are shown in Table 5.1. The comparison of the experimental Peclet numbers and the predicted Peclet numbers from the model (equation 5.6) is shown in Figure 5.8.

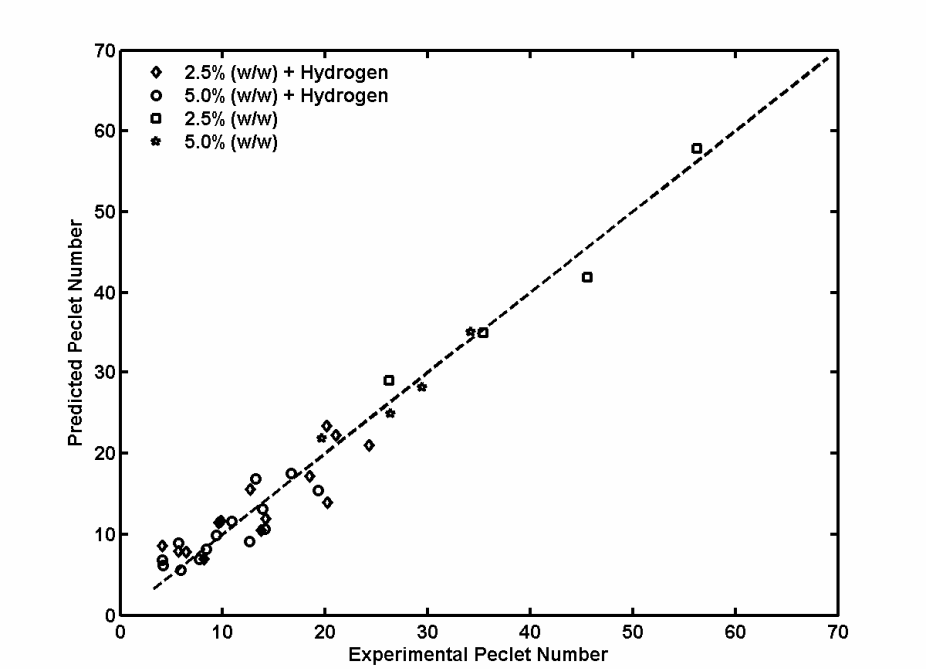

Figure 5.8 Comparison of the experimental Peclet number and the predicted Peclet number (equation (5.6)) for different systems.

5.3.2 Data Analysis for Hold up Experiments

Liquid hold up (ε_L) is measured by conducting experiments with the hydrogen, solvent (MCB), 2.5% (w/w) and 5.0% (w/w) polymer solutions. The liquid hold up is a dynamic property rather than a fixed quantity and depends most often on the gas/liquid flow rates. Other factors that would affect liquid hold up are the physical properties of the working fluids. The properties of the working fluid are shown in Table 5.2. The density and viscosity are estimated from the correlations proposed by Pan and Rempel (2004) while the surface tension is measured.

Table 5.2 Physical properties of the working fluids used in liquid hold up experiments

Property	MCB	2.5% (w/w) Polymer	5.0% (w/w) Polymer	Hydrogen Gas
Density, ρ (kg m^{-3})	1106	1163	1166	2.901
Viscosity, μ (Pa s)	0.004	0.0739	0.1613	11.185 x 10^{-6}
Surface Tension, σ (N m^{-1})	0.02926	0.02826	0.02781	-

The objective of this experimental study was to understand and develop a correlation for dynamic liquid hold up in the SM reactor with the operating conditions and working fluids similar to those used in hydrogenation of NBR. In SM reactors when the flow is homogeneous i.e. when the gas liquid flow rates are in the laminar regime ($Re_{L\text{-}h} < 20$), then the liquid hold up at ambient conditions is usually equal to the ratio of liquid flow rate to the sum of gas and liquid flow rate. But, if the flow regime is not laminar then the liquid hold up depends mostly on the superficial gas/liquid velocities and other physical properties. When a gas sparger is used, then the liquid hold up can depend on the geometry, number of holes and size of the holes. Since, only one sparger is tested in the current investigation, the effect of the sparger on the liquid hold up was not taken in account.

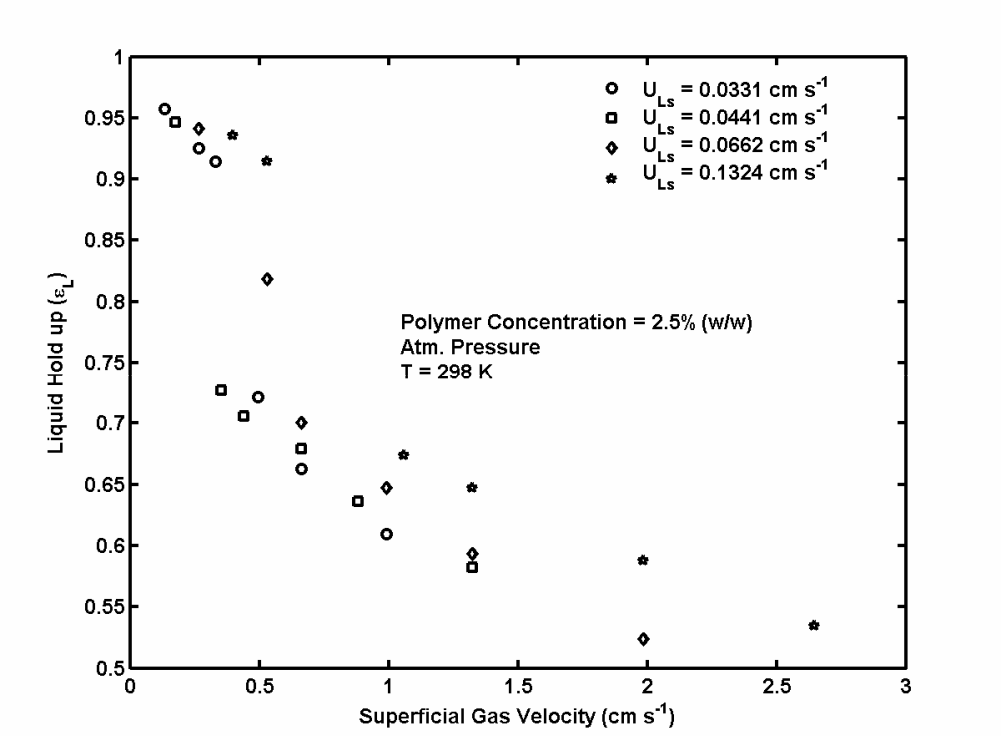

Figure 5.9 Effect of superficial gas and liquid velocities on liquid hold up for 2.5% (w/w) polymer and hydrogen system. (operating conditions mentioned on the figure)

Figure 5.9 shows the effect of superficial gas and liquid velocities on the liquid hold up for 2.5% (w/w) polymer and hydrogen gas. From the figure it is evident that the superficial gas velocity has a strong negative effect on the liquid hold up. The superficial liquid velocity has a positive effect on the liquid hold up, with increasing liquid velocity the liquid hold up increases, nevertheless the degree of the effect is less compared to the effect of gas velocity. Another notable feature observed in these

results is, when the superficial gas and liquid velocities are very low then the change in the liquid hold up is very low (refer to Figure 5.9 left hand side top corner). This is because the hydraulic Reynolds numbers for both the gas and liquid are in the same range and below 20, which is in the laminar regime. However, after that, the liquid side hydraulic Reynolds number increases steadily up to $Re_{L\text{-}h}$ = 15, while the gas side hydraulic Reynolds numbers varies from 2110 to 10570 where the flow is heterogeneous. Hence, very low liquid hold ups are obtained at very high superficial gas velocities.

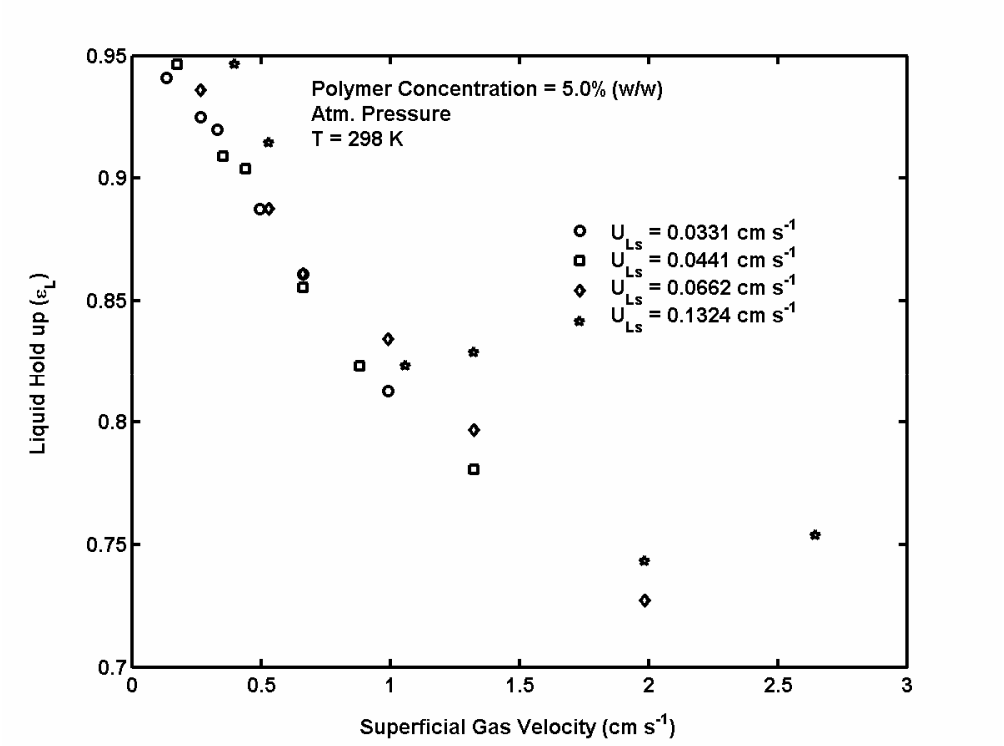

Figure 5.10 Effect of superficial gas and liquid velocities on liquid hold up for 5.0% (w/w) polymer solution and hydrogen system.(operating conditions mentioned on the figure)

However, the same phenomenon was not seen in the case of 5.0% (w/w) polymer solution and hydrogen gas or the MCB and hydrogen gas systems. The liquid hold up profiles were smooth even in the transition regime as shown in Figure 5.10 (for 5.0% (w/w) polymer and hydrogen gas) and Figure 5.11 (solvent and hydrogen gas). One possible reason is that the bubble break up and coalescence in the 2.5% (w/w) polymer solution would be high compared to that of the 5.0% (w/w) polymer system due to the viscosity and surface tension of the working fluids. Very scant literature is available on the liquid hold up in the static mixer reactors operated in the heterogeneous regime. Another interesting

phenomenon observed is that for a given superficial liquid velocity the liquid hold up in the 2.5% (w/w) polymer system was lower compared to the 5.0% (w/w) polymer system and MCB systems as the superficial gas velocity is increased. Figure 5.12 and Figure 5.13 shows the comparison of the liquid hold up in three systems for superficial liquid velocity, U_{Ls} = 0.0331 cm s^{-1} and U_{Ls} = 0.1324cm s^{-1} respectively.

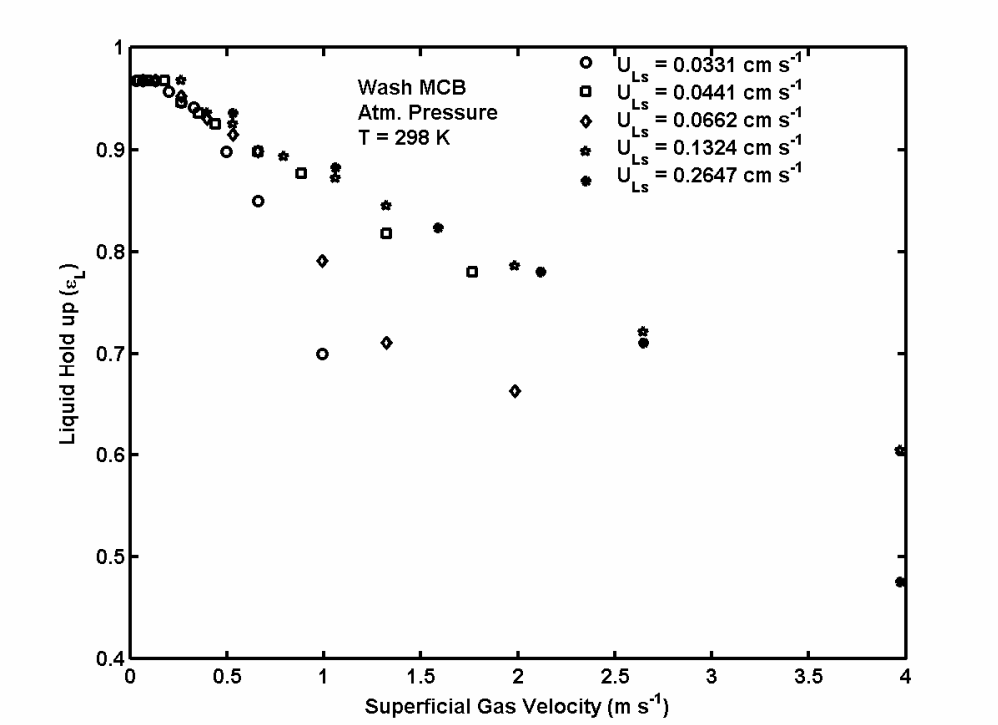

Figure 5.11 Effect of superficial gas and liquid velocities on liquid hold up for solvent (MCB) and hydrogen system.(operating conditions mentioned on the figure)

This phenomenon could be not only due to the surface tension but also the viscosity effects. Since the viscosity of the 5% (w/w) polymer solution is more than twice the viscosity of the 2.5% (w/w) polymer solution, the coalescence and break up of the gas bubbles in the 5% (w/w) polymer solution may be less than that occurs in the 2.5% (w/w) polymer solution. The difference in the surface tension of the three working fluids is not far from negligible. To verify this, further experiments with higher polymer concentration might be useful. Owing to the fact that the superficial gas and liquid velocities, physical properties has a strong effect on the liquid hold up, an empirical correlation for liquid hold up which takes all these parameters into account is derived and is represented by equation (5. 7).

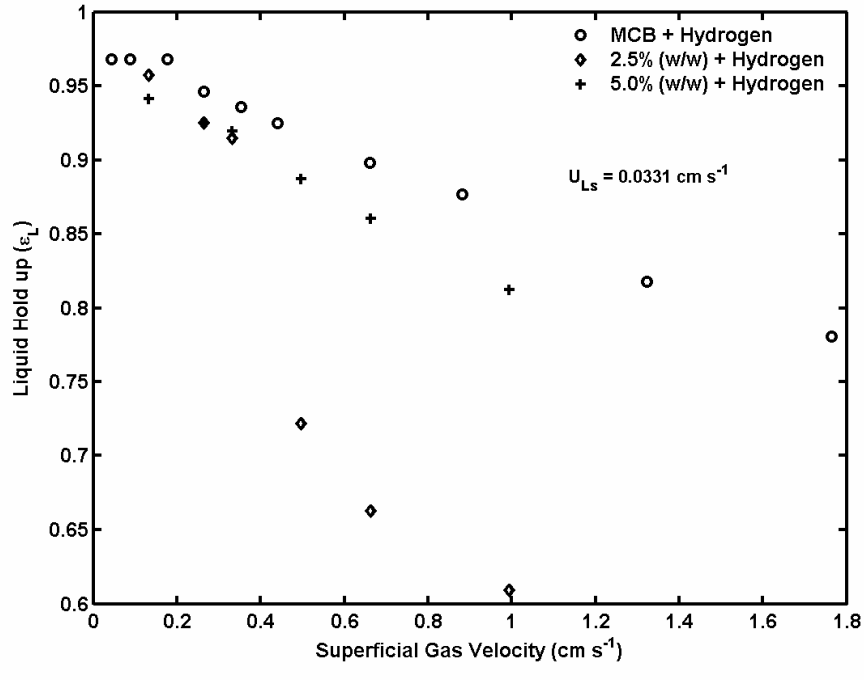

Figure 5.12 Comparison of ε_L versus U_{Gs} in different systems for U_{Ls} = 0.0331 cm s^{-1}.

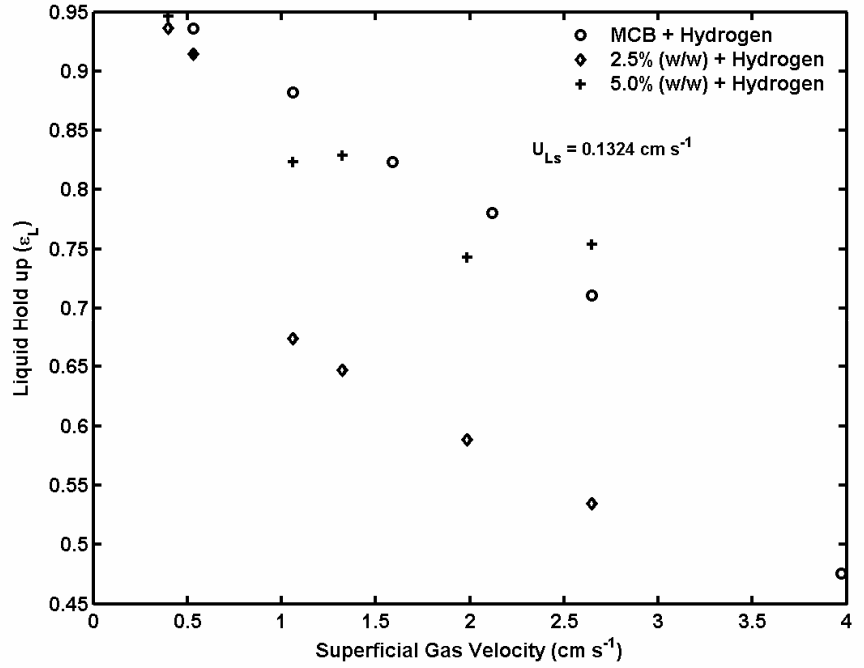

Figure 5.13 Comparison of ε_L versus U_{Gs} in different systems for U_{Ls} = 0.1324 cm s^{-1}.

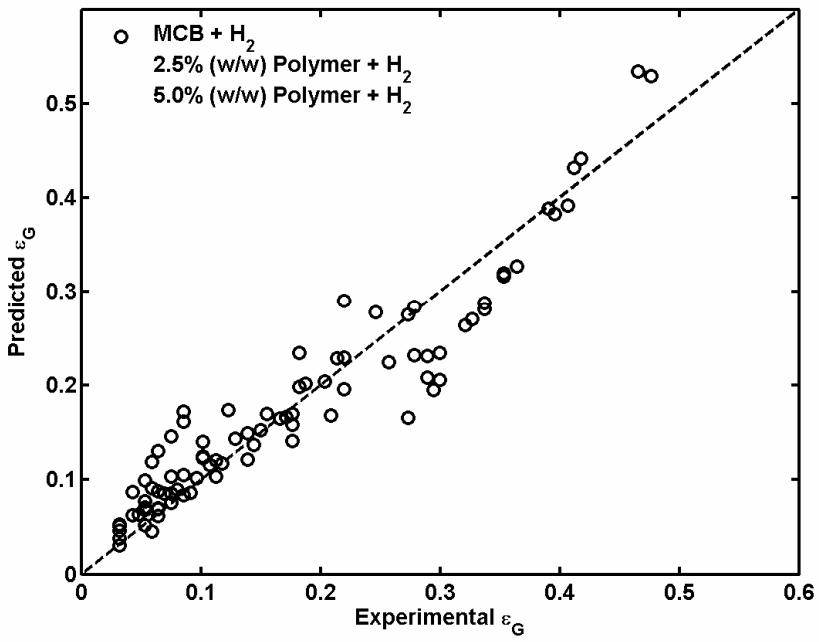

Figure 5.14 Model prediction vs. experimental values for the correlation described in equation (5.7).

The parameters for all the three systems show that with an increase in the hydrogen flow rate the gas hold up increases while it decreases with increase in the hydraulic Reynolds number on liquid side. The parameters β_4 and β_5 corresponding to the density ratio and viscosity ratio respectively shows that the gas hold up could be significantly effected by the physical properties also in addition to the flow conditions. The density ratio and viscosity ratio could have a strong importance in the bubble break up and coalescence which would in turn affect the gas hold up in the reactor. The correlation proposed for gas hold up as function of various operating conditions and physical properties would closely predict the experimental results as is evident from the high R^2 shown in Table 5.3 and Figure 5.14.

$$\varepsilon_G = 1 - \varepsilon_L = \frac{\beta_1 \left(\frac{U_{Gs} \mu_L}{\sigma_L} \right)^{\beta_2} \cdot \mathrm{Re}_{L-h}^{\beta_3}}{1 + \left(\frac{\rho_G}{\rho_L} \right)^{\beta_4} \cdot \left(\frac{\mu_G}{\mu_L} \right)^{\beta_5}} \qquad \textbf{(5.7)}$$

where β_1, β_2, β_3, β_4, and β_5 are parameters, the subscript G refers to gas (hydrogen) and L refers to the liquid (MCB, 2.5% (w/w) polymer solution and 5.0% (w/w) polymer solution). The values of the

parameters and their confidence interval (95%) for all the three systems studied are shown in Table 5.3. The hydrodynamic data for the hydrogen/polymer system is tabulated in Appendix B.

Table 5.3 Parameters and their confidence intervals for equation (5.7)

System	β_1	β_2	β_3	β_4	β_5	R^2	95% Confidence Interval	
I*	32.2	0.74	-0.3	2.53	-1.99	0.90	13.5	50.9
							0.66	0.82
II**							-0.39	-0.21
III***							2.27	2.78
							-2.18	-1.79

* MCB + H_2 ; ** 2.5% (w/w) polymer solution + H_2; *** 5.0% (w/w) polymer solution + H_2

5.4 Concluding Remarks

The RTD and liquid hold up experiments were conducted in the SM reactor (open-curve blade internal) with the same working fluids that are used in the actual hydrogenation experiments. The experimental results from the RTD experiments are conveniently modeled using a plug flow with axial dispersion (PFAD) model. The RTD experiments showed that with polymer flow only (without gas), as the liquid velocity is increased the Peclet numbers also increased. On the other hand the viscosity had a negative effect, with an increase in viscosity, the Peclet numbers decreased for the same liquid velocity. From the RTD experiments with polymer flow and gas flow, the Peclet numbers decreased with increasing gas flow in the current systems studied. The Peclet number in the polymer plus the hydrogen systems are modeled as functions of gas side and liquid side hydraulic Reynolds numbers. The liquid hold up experiments showed that liquid hold up is a strong function of the

superficial gas and liquid velocities in addition to the physical properties of the working fluids. The liquid hold up in 2.5% (w/w) polymer system was found to be lower than the 5.0% (w/w) polymer system at same operating conditions. An empirical correlation for liquid hold up is developed which is a function of the superficial gas/liquid velocities and physical properties (such as the density, viscosity and surface tension) of the working fluids.

Chapter 6
Static Mixer Reactor

The reactor set up used for hydrogenation of NBR consists of several pieces of equipment where unit operations and unit processes occur. This chapter provides the complete details of the different equipment design, experimental methods and analysis techniques used in the context of hydrogenation of NBR and the hydrodynamic study. Since, the gas to be dissolved in the polymer is pure hydrogen and with the dissolved hydrogen an irreversible chemical reaction occurs, and owing to the fact that in cocurrent up flow of gas/liquid systems, the mass transfer characteristics are superior to any other configuration, a vertical configuration of the static mixer (SM) reactor was chosen. The simplicity of construction, ability to achieve complete hydrogenation in one pass through the reactor bolsters the above proposed configuration.

The reactor lay out is shown in Figure 6.1. The unsaturated polymer solution to be hydrogenated is prepared by using the procedure outlined in section 6.2.1 and transferred to a 12 L polyethylene carboy (1- in Figure 6.1). The solution is purged by bubbling oxygen free nitrogen for four hours before pumping it to the preheater. Both the pumps on the polymer side and catalyst side are primed before pumping to the SM reactor as otherwise no solution would be drawn by the pumps. The pumps are designed so that they can deliver polymer solutions up to 20% (wt/wt) concentration and one hour mean residence time in the reactor. The priming procedure and the calibration of the pumps are detailed in section 6.1.3. A 2 L Parr reactor is used as a preheater and heats the solution to approximately 20^{o} C above the desired reaction temperature. Before the preheater is filled with the unsaturated polymer solution, it is degassed with oxygen free hydrogen for half an hour. Depending on the concentration of the polymer, the time taken to heat the unsaturated polymer solution varied from four to five hours.

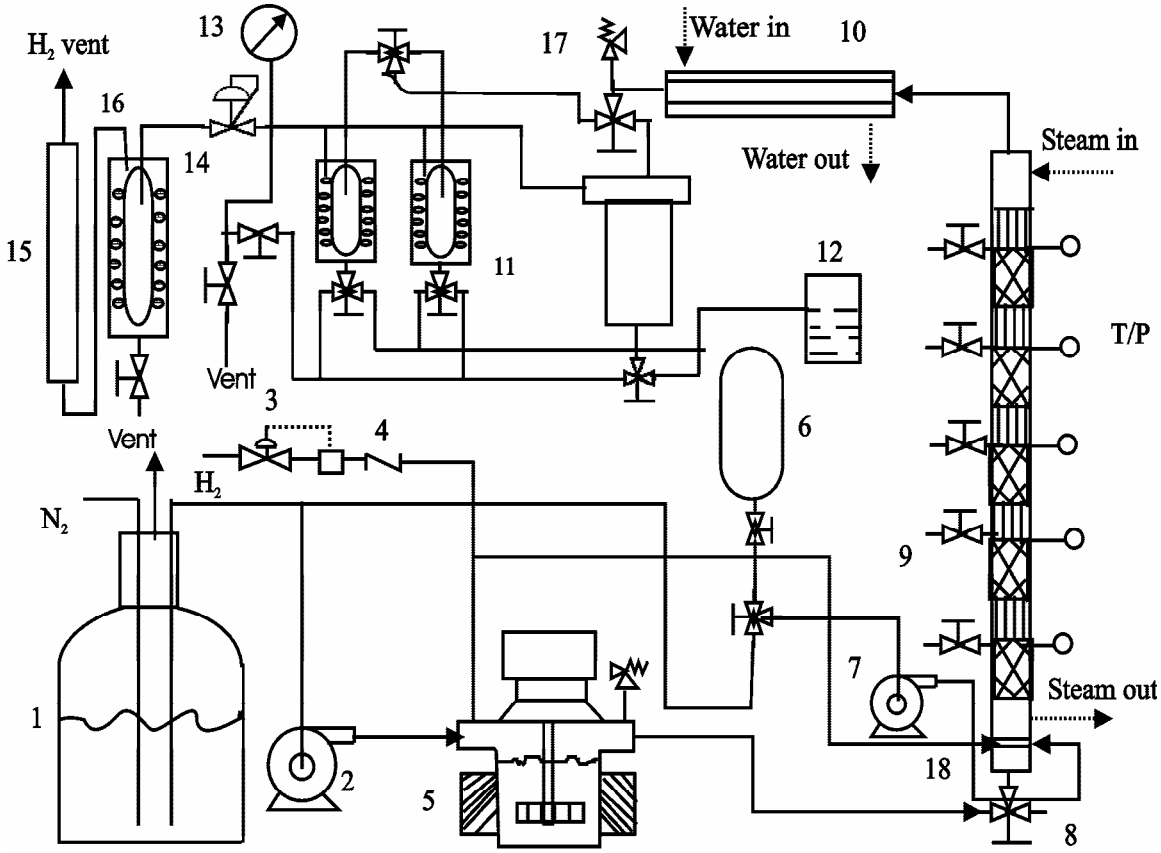

Figure 6.1 Schematic of the static mixer reactor set up used for hydrogenation of NBR

Oxygen free hydrogen is supplied from a compressed high pressure cylinder and a Brooks mass flow controller is used to control/set the required flow of hydrogen. The maximum flow rate that can be obtained through the mass flow controller is 6 L/min (at STP) and a by-pass line across the mass flow controller is used whenever flow rates greater than 6 L/min are required. A distributing valve located after the mass flow controller and by-pass line is used to direct the flow either to the preheater or the SM reactor or both depending on the required reactor operation conditions. The preheated unsaturated polymer solution and hydrogen gas mixture from the preheater enters the reactor through the three way distribution valve located at the bottom of the SM reactor. The distribution valve allows the reactor to be isolated from the transfer line and is also used to drain the reactor if necessary. The transfer line from the preheater to the reactor is insulated with fiber glass ribbon to avoid heat loss.

Pure hydrogen gas enters the reactor through a gas sparger located exactly opposite to the point where catalyst enters the reactor. The gas sparger has fifteen holes of 1 mm diameter facing upwards.

The catalyst solution preparation procedure is discussed in section 6.2.2. The catalyst solution thus prepared is transferred to a 1 L stainless steel bomb as shown in Figure 6.1. The bomb is pressurized to the operating pressure of the reactor. This would ensure two advantages; there will not be any vacuum formation as the catalyst solution is drawn when the reaction starts and the higher head on the upstream would ensure perfect control of flow on downstream of the pump. The catalyst solution is pumped into the reactor using the catalyst side pump at a predetermined flow rate. A three way valve is located at the bottom of the catalyst bomb which is used to purge the catalyst line to the reactor and priming purposes in addition to pumping the catalyst solution.

The hydrogen gas from the gas sparger and the catalyst stream enter the reactor in opposite directions and this ensures even distribution of catalyst in the unsaturated polymer solution at the entrance of the reactor. The SM reactor is 48.5 inches long with 1.5 inch internal diameter (ID). The housing is made of 316L stainless steel 80 schedule with 0.2 inches nominal wall thickness. The SM reactor has 24 KMX mixing elements arranged such that the angle between neighboring elements is 90^{o}. The reactor is surrounded with a 2.5 inch ID jacket through which steam flows. Since the reaction is exothermic, most of the heat is released within the first half of the reactor while relatively less heat is released in the later section of the reactor. Hence, the steam flow is operated in a countercurrent fashion with respect to the polymer flow in the reactor. The details of the reactor design and specifications are discussed in section 6.1.1. The reactor jacket is wrapped with ¾ inch fiber glass insulation to avoid heat loss to the environment.

The reacted polymer and the gas mixture from the reactor exits at the top and passes through a water cooled double pipe heat exchanger operated in a counter current fashion. The design of the heat exchanger for conveniently cooling the product mixture is discussed in section 6.1.2. A three way valve sequentially distributes the cooled gas/liquid mixture between a 2 L gas/liquid separator and two sight glasses connected in parallel. The gas liquid separation occurs by gravity, with the liquid settling at the bottom of the separator. The sight glasses are rated for 1500 psi and the 2 L separator is rated for 2000 psi. While one of the separators is being filled with the reacted polymer solution, the other separator can be drained into a 12 L collection tank via a three valve located at the bottom of

each of the separators. Hydrogen gas exits at the top of the gas/liquid separators through an annular fitting and passes through a one way check valve that isolates the separators while they are draining. A gas return line connected to the three way valves at the bottom of the gas/liquid separators allows them to be repressurized after they have been drained of liquid. A Bourdon gauge located after the check valves is used to measure the system pressure. The system pressure is controlled by using a back pressure regulator rated to 1500 psig. A secondary sight glass is located after the regulator to collect any residual liquid that might have been carried through as a result of a process upset. Finally, the exhaust hydrogen gas passes through a rotameter and vented to a stack.

6.1 Equipment Design and Calibration

6.1.1 SM Reactor Specifications and Sizing

From the physical/chemical properties of the reactants and hydrodynamic study, a SM reactor with KMX internal geometry is chosen for achieving complete hydrogenation in one pass. From Chapter 2 it is evident that the open blade (flat) internal structure is superior to other structures in terms of mass transfer, heat transfer and mixing. Further, the design of convex blade is more applicable for higher viscosity systems assuring plug flow behavior, superior mass and heat transfer with the sacrifice of higher pressure drop (Heneche et al.(2005)). From the simulation results discussed in Chapter 4, the optimum number of mixing elements required for successful hydrogenation is 20 but with a 20% design factor, 24 mixing elements are used in the SM reactor. Since, the process considered for design is at bench scale level; with 1 L reactor volume the diameter is calculated to be 1.42". But the standard diameter available is 1.5". Hence the reactor with 1.5" ID 80S, 24 elements is designed for efficient hydrogenation of nitrile butadiene rubber (NBR). The total length of the reactor is 48.5" with the length of the reactor zone being 36.76". The reactor, internal elements and the jacket are made up of 316L stainless steel. The reactor is rated to 2270 psi at 300^{o} F while the jacket is rated to 455 psi at 300^{o} F. The jacket is 2.5" ID 40S with a steam inlet located at the top and outlet at the bottom. Figure 6.2 shows the schematic of the reactor with the specification details (length, geometry of the element, location of gas sparger). The internal element has open blade geometry with the blades being concavely curved and the flow should be in the direction facing the concave side. All dimensions in the Figure 6.2 are inches. The jacket is designed by studying the temperature profiles obtained from simulations. Rugged design of the jacket is made by solving the steady state equations for carbon-

carbon double bond concentration (C=C) and temperature. For simplicity, the hydrogen concentration is assumed to be excess and constant; a first order reaction rate is considered. The detailed calculations are shown in Appendix C.

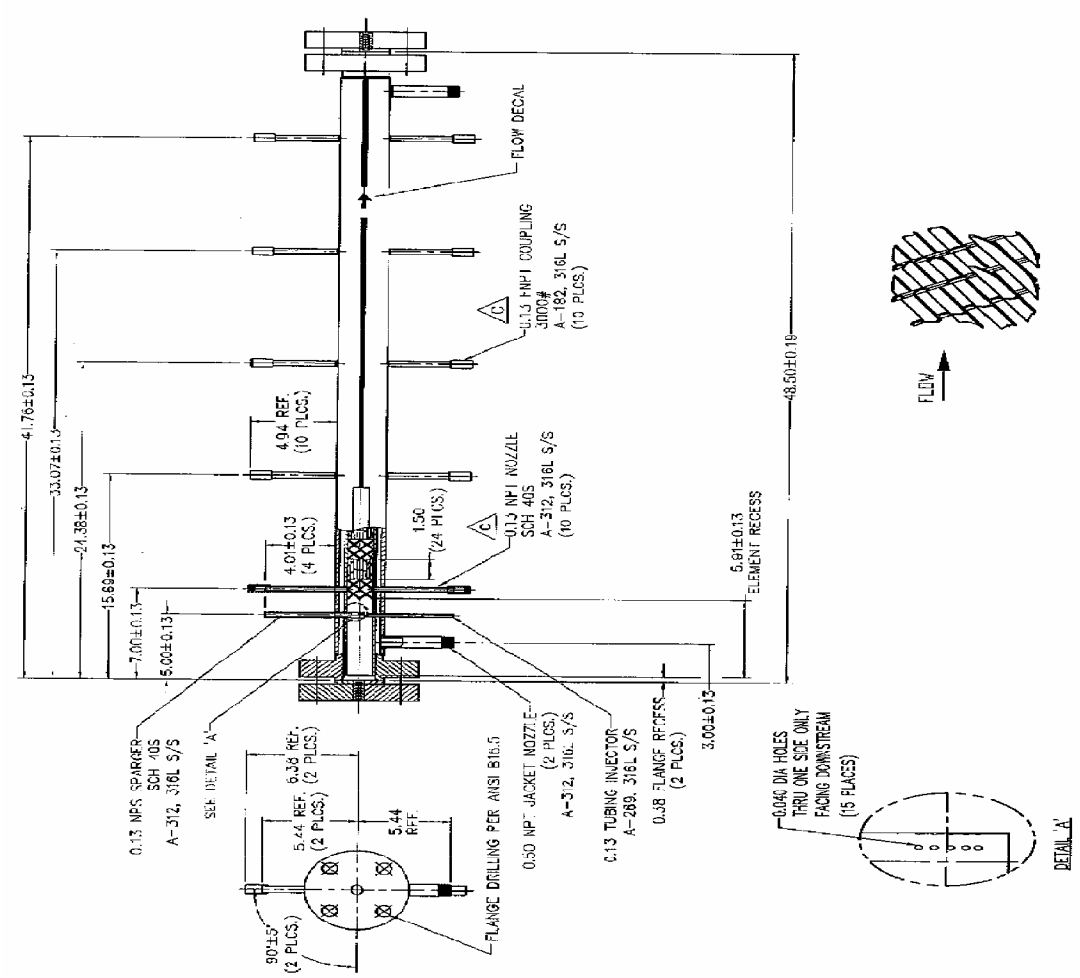

Figure 6.2 Specifications of the reactor and the internal element (drawing from Chemineer, Inc.,)

From Figure C.1, the optimum temperatures at which the inlet polymer and steam should be are T_S = 413 K for T_0 = 413 K, such that the change in the reactor temperature along the length of the reactor is minimal. Like wise, for different inlet temperature of the polymer solution, there lies an optimum steam temperature that would keep the reactor temperature almost constant. Simulations were conducted by varying the Peclet number, mean residence time to study the temperature drop along the length of the reactor. It seems that the temperature drop is not high for the range of Peclet number (Pe

= 10 to 100) and mean residence time (τ = 20 to 60 min) considered. Further, the actual temperature drop obtained in the SM reactor is discussed in Chapter 7. The product from the reactor is cooled to room temperature by sending through a double pipe heat exchanger, the design details of which are discussed in the next section.

6.1.2 Double Pipe Heat Exchanger

The product from the SM reactor enters the heat exchanger through the inner pipe while cold water flows in the annulus. The heat exchanger is operated in a counter current fashion and the cold water flow rate is adjusted using a needle valve based on the heat load. Since, the product enters at a very high temperature and high pressure, a 1 inch ID, 80S is chosen as the inner pipe while the outer pipe is 2 inch ID, 40S (since water at ambient conditions flows through the annulus). The detailed calculations for the design of the double pipe heat exchanger are given in Appendix C. The optimum length would be 1 m and the heat exchanger would be versatile for different operating conditions.

6.1.3 Metering Pump Calibration

Two reciprocating pumps (supplied by Milton Roy) were used to separately pump the polymer and the catalyst solution. Both the pumps were primed before calibrating them. The pumps were designed for pumping the unsaturated polymer solution up to 750 psig. The flow rate of the pumps was determined by measuring the volume collected over a specific time interval. The pump was set to the desired setting and allowed to operate for at least one minute. The flow rate for a specific pump setting was obtained by repeating the measurement three times. The polymer pump was calibrated with 2.5% (w/w) and 5.0% (w/w) polymer solutions separately at different operating pressures. Figure 6.3 shows the resulting measurements obtained with 2.5% (w/w) unsaturated polymer solution at atmospheric pressure, 350 psig and 500 psig. The data thus obtained was fitted using linear regression and is expressed using the following expression:

$$\text{Solution Flow Rate (ml/min)} = a \cdot (\text{Pump Setting}) + b \qquad \textbf{(6.1)}$$

Since the catalyst pump is used to pump the catalyst solution which is a homogeneous mixture of catalyst and pure solvent, it is calibrated with the solvent (monochlorobenzene (MCB)) alone. With 95% confidence interval, the constants a and b and the corresponding standard errors for the parameters, the error for the solution flow rate predicted using equation (6.1), corresponding R^2, for the two pumps with different solutions at different operating pressures is reported in the Table 6.1.

Table 6.1 Parameters obtained from linear regression for the pump settings and flow rate

	Solution % (w/w)	Pressure (psig)	a ml/min	Error Estimate for a (ml/min)	b ml/min	Error Estimate for b (ml/min)	Error for the predicted flow rate (ml/min)	R^2
	2.5	14.7	1.60	0.02	12.24	1.19	2.41	0.99
Polymer	2.5	350	1.50	0.01	-9.89	0.58	0.77	0.99
Pump	2.5	500	1.56	0.02	-14.21	1.52	1.79	0.99
	5.0	500	1.49	0.007	-18.10	0.29	0.22	0.99
Catalyst	MCB	350	0.298	0.0352	-5.3	2.51	1.11	0.96
Pump	MCB	500	0.285	0.0333	-4.058	1.36	0.47	0.99

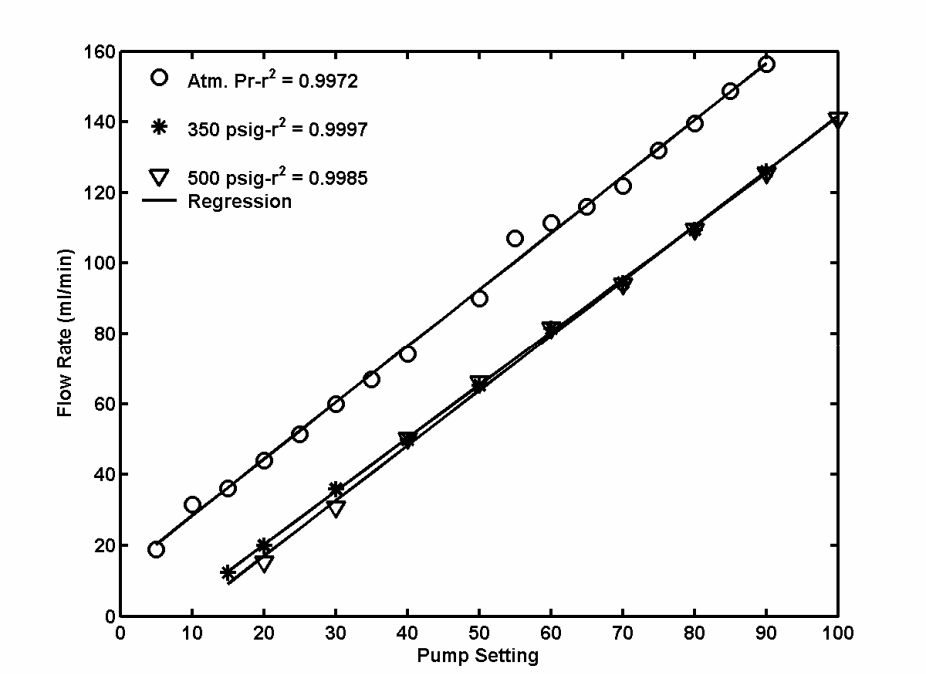

Figure 6.3 Calibration of the polymer side pump with 2.5% (w/w) unsaturated polymer at atmospheric pressure, 350 psig and 500 psig.

6.2 Experimental Procedure

6.2.1 Unsaturated Polymer Solution Preparation

The unsaturated polymer/rubber solution is prepared by dissolving the pre-weighed rubber in the solvent (MCB). The concentration of the starting solution is adjusted such that the dilution due to the catalyst stream is compensated. Based on the polymer to catalyst flow ratio, higher concentration of rubber is used in the starting solution. The NBR used was Krynac 38.50 with an acrylonitrile content of approximately 38%, supplied by Lanxess Inc. The rubber to be dissolved in the solvent is cut into small pieces and transferred to a 20 L polyethylene carboy. The rubber is completely dissolved in the solvent by agitating with a mixer that has multi agitators (Rushton turbines) along the length of the rotating shaft. In order to overcome the problem of dissolved oxygen, the solution is degassed simultaneously with oxygen free nitrogen. Since, each experiment consumes 8 L of polymer solution, degassing and mixing of the rubber solution is performed overnight. The solution was then transferred into a 12 L polyethylene carboy which is shown in Figure 6.1 (designated by '1'). After that, again the solution is bubbled with oxygen free nitrogen through a dip tube for approximately three to four hours before the actual experimental run. Thus, at most care is taken to ensure that the solution will be almost free of oxygen/air.

6.2.2 Catalyst Synthesis and Preparation

The catalyst used in the present study is $OsHCl(CO)(O_2)(PCy_3)_2$. The catalyst is synthesized using the techniques described by Parent (1996). Since, each experiment in the continuous set up requires more catalyst, a large amount of catalyst is synthesized. The activity of every new batch of catalyst thus synthesized, is evaluated by conducting hydrogenation in a batch reactor and compared with the previously reported catalyst activity. Since the osmium catalyst is not air sensitive, it did not require any special storage. Figure 6.4 shows the hydrogenation degree obtained in the batch reactor which was used to evaluate the catalyst activity. The operating conditions used are 275 mM [C=C], 80 μM $OsHCl(CO)(O_2)(PCy_3)_2$ catalyst, 350 psig for all experiments. In Figure 6.4 (a) and (b) refer to the experiments conducted at T = 130 C and Figure 6.4 (c) and (d) refer to T = 140 C. The corresponding activities evaluated from these experiments are shown in Table 6.2. These values are in good agreement with the catalyst activity reported by Parent (1996) with identical operating conditions.

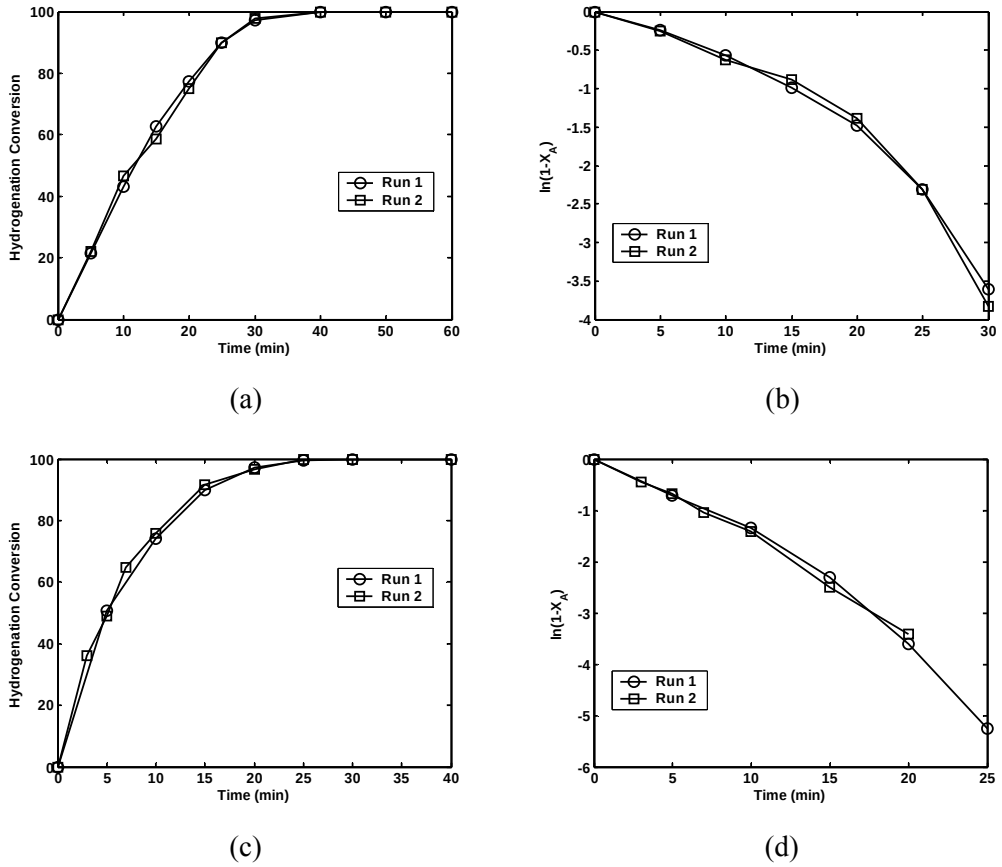

Figure 6.4 Estimation of catalyst activity through batch experiments – operating conditions: 275 mM [C=C], 80 μM $OsHCl(CO)(O_2)(PCy_3)_2$ catalyst, 350 psig. For (a) and (b) T = 130 C;for (c) and (d) = T = 140 C.

Table 6.2 Rate constants obtained at different temperatures from batch experiments

Temperature (C)	**Run 1 (s^{-1})**	**Run 2 (s^{-1})**
130	3.78×10^{-3}	3.82×10^{-3}
140	4.34×10^{-3}	4.23×10^{-3}

The catalyst thus synthesized is used to prepare catalyst solution using the apparatus shown in Figure 6.5. The experimental set up consists of two 2 L round bottom flasks: one for degassing the solvent while the other for mixing the catalyst and degassed solvent, a 1 L stainless steel bomb for storing the catalyst solution. All the three pieces of equipment are connected to vacuum and nitrogen lines that are controlled by using the corresponding valves. The solvent (monochlorobenzene) to be

dissolved is taken in the round bottom flask (A) and is degassed with oxygen free nitrogen through a dip tube.

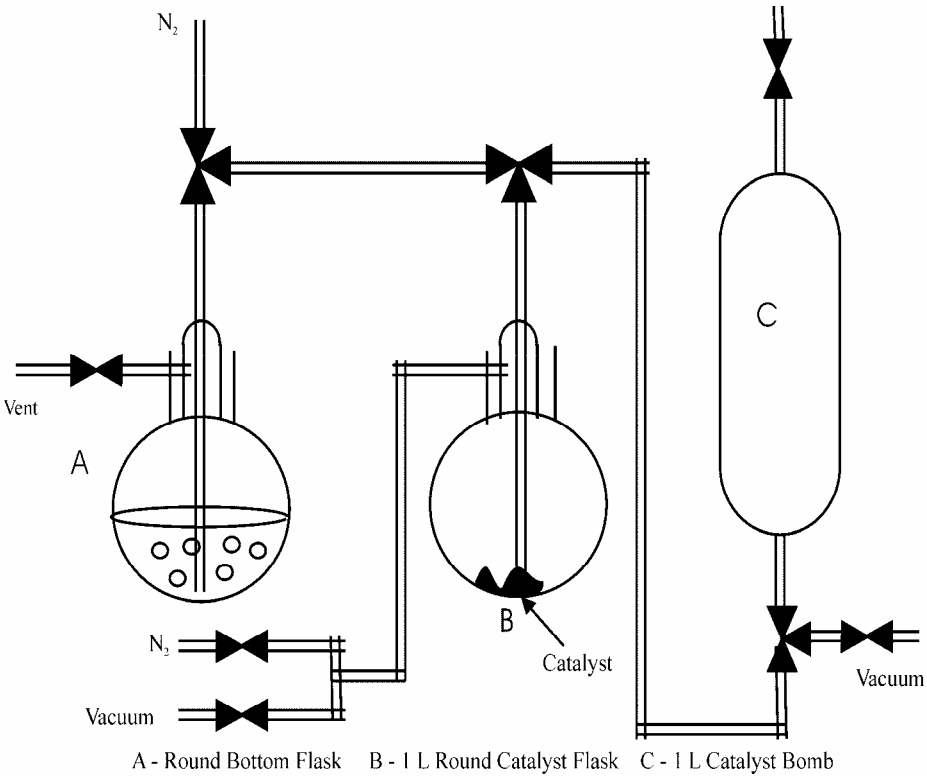

Figure 6.5 Experimental set up used to make catalyst solution.

A 1 cm stirrer bar is used to enhance the degassing. Based on the polymer to catalyst ratio, the catalyst solution concentration (before mixing with the polymer solution in the reactor) is determined first and the corresponding weight of osmium catalyst to be dissolved is estimated. The weighed osmium catalyst is transferred to the 1 L round catalyst flask – B, and the valve on the vacuum line is slowly opened. At most care should be taken when the valve is opened as otherwise part of the osmium catalyst will be lost because of sudden vacuum. With positive pressure due to nitrogen in flask A and vacuum in flask B, the thoroughly degassed solvent from flask A is transferred to flask B (with the vacuum valve in closed position) through a transfer line. Mean while, the 1 L stainless steel bomb is thoroughly washed with pure solvent and dried by passing air. Then, the bomb is connected to the vacuum line such that it is easy to draw the catalyst solution from the flask – B. Now, the nitrogen valve on flask B is opened so that the catalyst solution from flask – B is transferred to the 1 L stainless steel catalyst bomb through the transfer line. Once all the solution is transferred, the bomb

is sealed and disconnected. Finally, the bomb is pressurized with oxygen-free hydrogen and attached to the bench scale reactor set up.

6.2.3 Reactor Operating Procedure

Figure 6.6 Bench scale set up constructed for conducting continuous hydrogenation of NBR

Figure 6.6 shows the bench scale experimental set up constructed for conducting the hydrogenation of diene based polymers. The desired pressure is obtained by pressurizing the system through the preheater/premixer and the SM reactor simultaneously adjusting the back pressure regulator. The whole set up is always left under pressure to avoid oxygen contamination. The set up is purged off oxygen with hydrogen at 100 psig if for any reason it is depressurized. After priming the catalyst pump and the polymer pump, unsaturated polymer solution is pumped into the preheater/premixer. The reaction temperature is attained by turning on the heater in the preheater and opening the steam flow through the jacket of the static mixer reactor. Since the preheater/premixer is away from the SM

reactor, the temperature in the preheater/premixer is set to 30 C above the desired reaction temperature. Simultaneously, the water supply to the double pipe heat exchanger is turned on. The desired hydrogen flow rate is set and the system is run till the flow and temperature along the length of the SM reactor are steady. Then, the pumps are operated at the desired settings. The samples are collected from top to bottom of the reactor such that the flow equilibrium is not disturbed. Two three-way valves connected after the exit of the heat exchanger distribute the gas/liquid mixture to the gas/liquid separators. The solution is slowly drained into a collection tank and then repressurized using the gas return line (controlled by the needle valve). The repressurizing phenomenon should be done very slowly as otherwise there will be process upset due to sudden pressure variations.

Once the experiment is completed, the pumps and the gas flow are turned off. Then, the steam and heater in the premixer/preheater are turned off. The set up is sealed and allowed to cool by natural convection. The liquid hold up is measured by draining the polymer solution using the three way valve present at the bottom of the reactor after it is cooled. Appendix C shows the list of components used in the continuous set up and corresponding specifications obtained from different suppliers.

6.3 FTIR Analysis of NBR Saturation

The hydrogenation degree or the degree of saturation in the hydrogenated NBR samples was defined as:

$$\text{Hydrogenation Degree (\%)} = \frac{[C=C]_o - [C=C]}{[C=C]_o} \times 100 \qquad \textbf{(6.2)}$$

where, $[C=C]_o$ is the initial olefin concentration and [C=C] is the remaining olefin concentration. Fourier Transform Infrared Spectroscopy (FTIR) is used to determine the exact concentration of the different olefin concentrations. The 2270 cm^{-1} peak resulting from the cyano group, the 970 cm^{-1} peak characteristic of the level of unsaturated trans-olefin by the proton vibration on the C=C-H and a modified peak at 730 cm^{-1} which resulted from the oscillating H attached to the saturated backbone -CH_2-CH_2- are used to estimate the degree of hydrogenation according to the expression (equation 6.11) developed by Brück (1989).

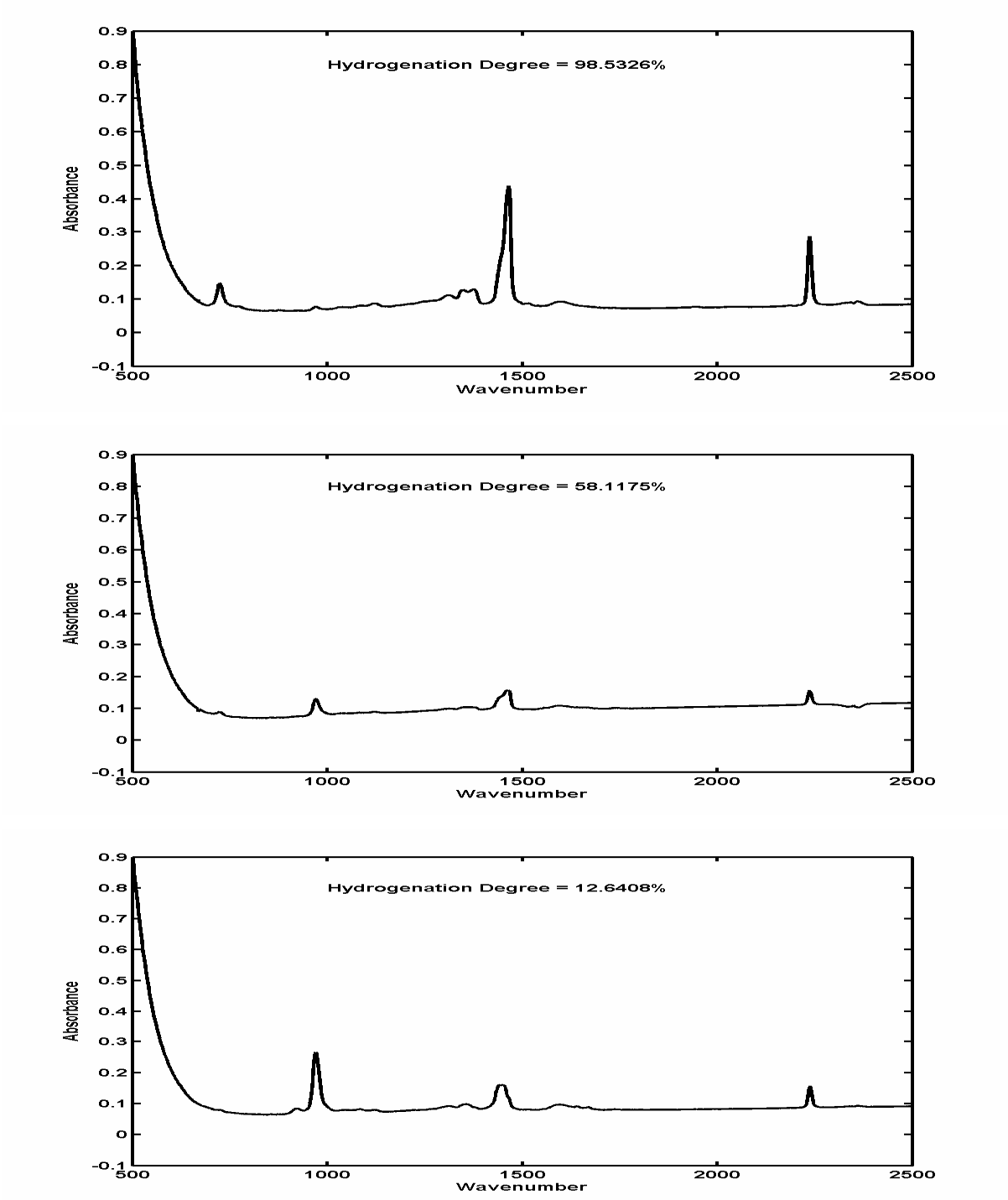

Figure 6.7 Typical FTIR spectra obtained for rubber with different hydrogenation degree

$$\text{Hydrogenation Degree (\%)} = \frac{\dfrac{A(730)}{k(730)}}{\left[A(2230) + \dfrac{A(970)}{A(970)} + \dfrac{A(730)}{k(730)}\right](1 - ACN)} \qquad \textbf{(6.3)}$$

where A(x) is the absorbance height at wavelength, x cm^{-1}, and ACN is the acrylonitrile content in the rubber. The constants, k(x), are determined by plotting the ratio A(730)/A(2230) versus A(970)/A(2230). More information is detailed in Parent's work (1996). Figure 6.7 shows the FTIR spectra obtained for the different samples representing different hydrogenation degree (98.5326%, 58.1175%, and 12.6408%).

Chapter 7
Hydrogenation in Static Mixer Reactor

7.1 Results and Discussion

Hydrogenation experiments were conducted in the bench scale continuous set up with different operating conditions to evaluate the performance of the static mixer reactor. The catalyst used in the experiments is $OsHCl(CO)(O_2)(PCy_3)_2$, which is stable in chlorinated solvents. This catalyst is more active compared to its five-coordinate form and doesn't require a cocatalyst which is necessary for the rhodium analog. The desired catalyst concentration is achieved by adjusting the catalyst to polymer flow ratio. The preparation of the polymer solution and the catalyst solution was discussed in section 6.2.1 and section 6.2.2 respectively. The reactor operating procedure was discussed in section 6.2.3. Preliminary experiments were carried out with 2.5% (w/w) polymer solution at 350 psig and 138 C.

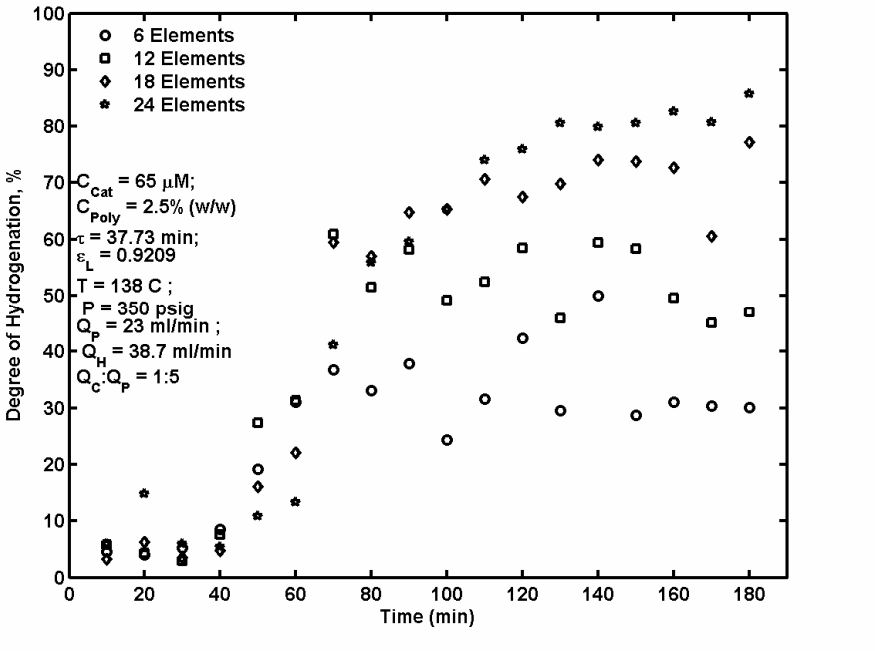

Figure 7.1 Dynamic degree of hydrogenation vs. reaction time with 2.5% (w/w) polymer, 65 μM $OsHCl(CO)(O_2)(PCy_3)_2$, 350 psig, 138 C (other operating conditions as mentioned on the figure)

In those experiments, the effect of gas flow rate on the conversion is studied by keeping the polymer flow rate constant. It is observed that the gas flow rate has a significant effect on the performance of the SM reactor. One of the most important design parameters that has a strong impact on the performance of the SM reactor is the gas hold up which in turn depends on the gas liquid flow rates. Though at low gas hold up, the turn over of the hydrogenated polymer is greater, yet the degree of hydrogenation would be low because of low availability of hydrogen in the liquid phase. On the other hand, high gas hold up would reduce the turn over. Hence, there lies an optimal liquid hold up for achieving higher turn over with a good degree of hydrogenation. From the cold experimental results discussed in Chapter 5, 90% liquid hold up can be obtained when the superficial gas flow rate is 4 to 6 times of the superficial polymer flow rate. Figure 7.1 shows the dynamic experimental degree of hydrogenation results obtained when the superficial gas flow rate is approximately 1.7 times of the superficial polymer flow rate. The other operating conditions are mentioned on the figure. The maximum conversion obtained is this experiment was 82% approximately. Two important aspects seemed to affect the final conversion or the degree of hydrogenation. One of them is the high liquid hold up (low gas hold up) which is due to low gas flow rate. The other fact is that, since the gas/liquid separators were repressurized using the gas return line, there was always a process upset because of low gas flow rate. The dynamic conversions from Figure 7.1 at different ports (after 6, 12, 18 and 24 elements) along the length of the reactor shows the scattered experimental data that was due to this upset. To overcome this problem, higher gas flow rates were used in the successive experiments. Another way to overcome this problem is discussed in the recommendations section of the chapter 9.

Further, experiments were designed such that the pressure is maintained at 500 psig and the temperature was targeted to be 140 C. From the batch experimental results conducted by Parent (Parent, 1996), it is evident that the catalyst activity increases with the increase in the reaction temperature while an increase in pressure also had a proportional effect on the degree of hydrogenation. Hence, keeping the pressure and the temperature constant, other operating parameters such as, the polymer concentration, the catalyst concentration and the mean residence time are varied to study the performance of the SM reactor. 2^3 factorial experiments were designed and performed with the factors being polymer concentration, catalyst concentration and mean residence time at two levels. The two levels in the polymer concentration are 2.5% (w/w) and 5% (w/w) while for the mean residence time they are 16 min and 36 min. The two levels of the catalyst concentration were fixed based on the degree of hydrogenation obtained with the low level catalyst and taking the catalyst

deactivation into consideration. The effect of catalyst deactivation is discussed in the later part of this chapter.

Table 7.1 List of the 2^3 experiments conducted at 500 psig and 138 C

Experiment #	Mean Residence Time (min)	Polymer Conc. (w/w)	Catalyst Conc. (μM)	Liquid Flow Rate ml/min	Hydrogen Flow Rate ml/min	Liquid hold up ε_L
1	35.16	2.5	35	23	144	0.89
2	35.16	2.5	80	23	144	0.89
3	16.7	2.5	80	50	200	0.89
4	16.7	2.5	120	50	200	0.89
5	35.18	5.0	100	23	144	0.90
6	35.18	5.0	130	23	144	0.90
7	17.0	5.0	85	50	200	0.90
8	17.0	5.0	140	50	200	0.90

Table 7.1 shows the factorial experiments performed in the SM reactor to study the effect of different operating parameters. The corresponding liquid hold up for each experimental run is also tabulated which was obtained by measuring the polymer drained after the experiment was completed. In the 35 min mean residence time experiments the hydrogen flow rate was six times of the polymer flow rate while it was four times the polymer flow rate for the 16 min residence time experiments. Before conducting the designed factorial experiments, the reproducibility of the experiments is evaluated by repeating an experiment. The concentration of the polymer is 2.5% (w/w), 80 μM catalyst with a 35.16 min mean residence time.

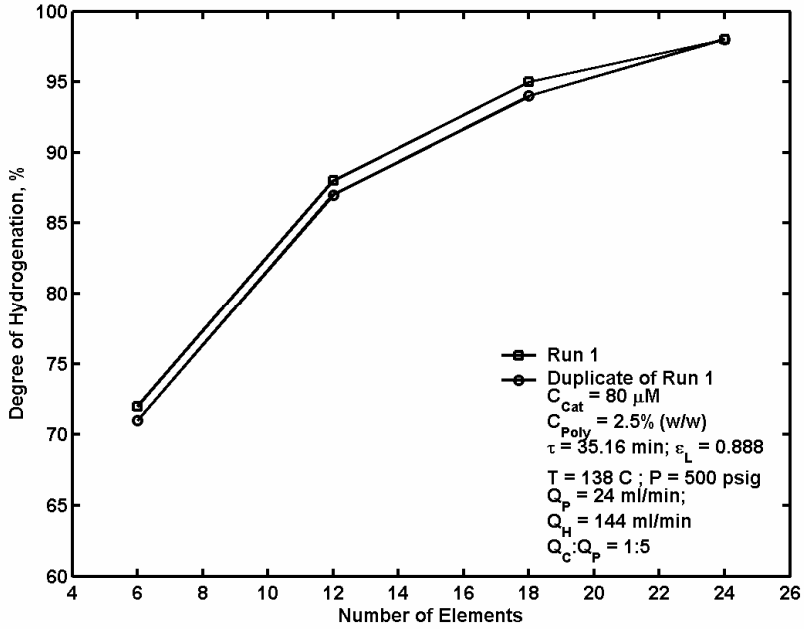

Figure 7.2 Comparison of steady state conversions obtained in the SM reactor for two experiments with identical operating conditions (mentioned on the figure).

Figure 7.2 shows the comparison of the steady state degree of hydrogenation obtained for the two replicate runs performed in the continuous process with the operating conditions mentioned on the figure. The most important factors that would affect of the reproducibility of experiments in the present process are the fluctuations in the process when the gas/liquid separators are repressurized resulting in fluctuations in the fluid hydrodynamics during sampling and changes in temperature profiles. All of these factors would affect the reproducibility and reactor performance also. Figure 7.2, clearly shows that the process assures good reproducibility. From statistical analysis, the mean square error in the degree of hydrogenation from these replicate runs is found to be +/- 0.866%. The dynamic hydrogenation degrees vs. time data for these two replicate runs are shown in Appendix B. The small deviation in the dynamic data can be due to any of the factors discussed earlier. Since repeating all experiments in the continuous process is tedious, the error for all experimental runs is considered to be +/- 0.866%.

7.1.1 Optimum Catalyst Concentration for Hydrogenating 2.5% (w/w) Polymer

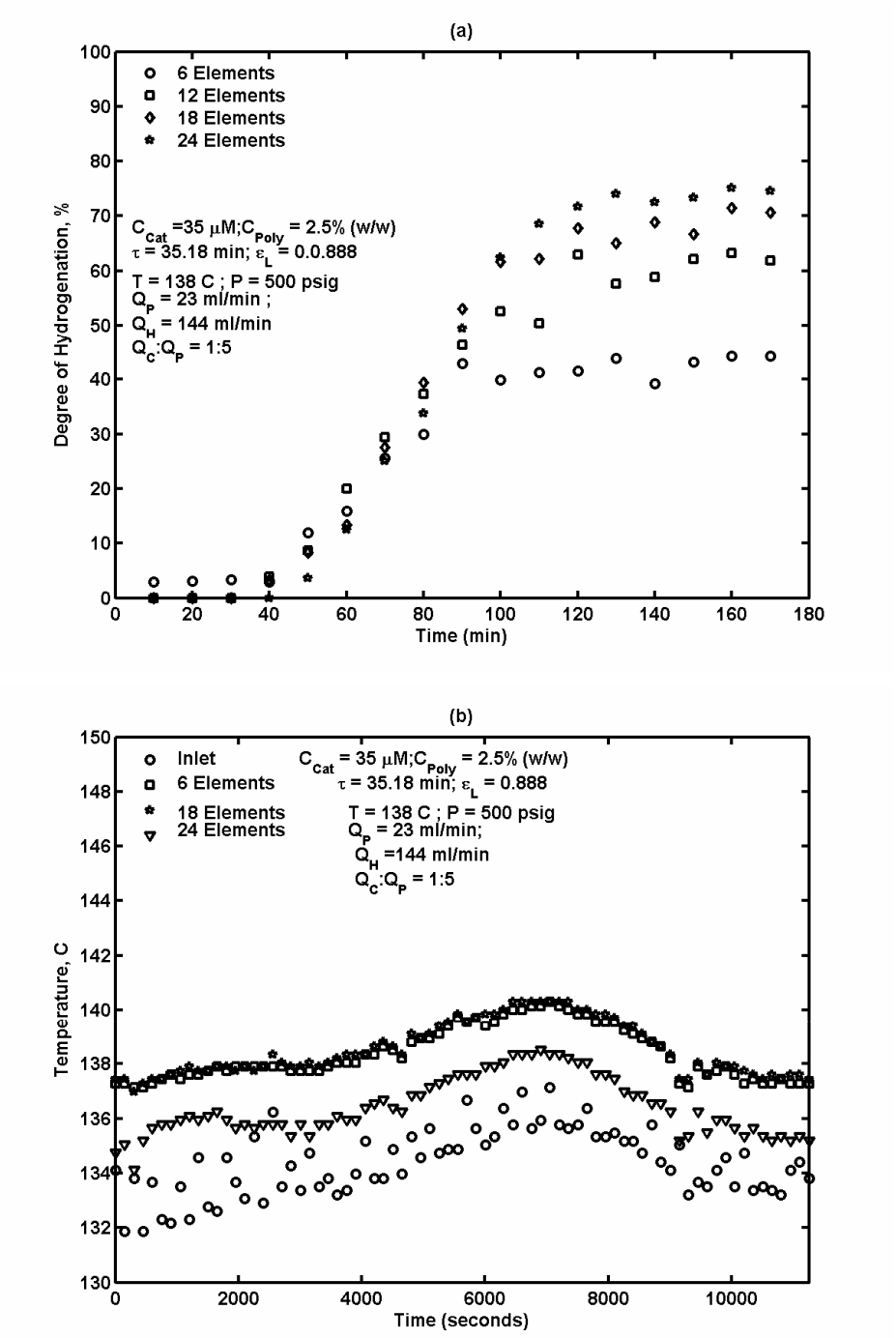

Figure 7.3 (a) Degree of hydrogenation vs. time (b) Reaction temperature vs. time 35 μM $OsHCl(CO)(O_2)(PCy_3)_2$, 2.5% (w/w) polymer, τ = 35.18 min (other conditions mentioned on figure)

The hydrogenation experiments were performed such that the catalyst concentration level is initially at a low level.Based on the degree of hydrogenation, the catalyst concentration is increased in steps of 50% to 100%. The optimum catalyst concentration corresponds to the minimum catalyst concentration required to obtain at least a 95% degree of hydrogenation. Figure 7.3 (a) shows the dynamic profiles of degree of hydrogenation vs. time for the experiment with 35 μM catalyst and 35.18 min mean residence time (other operating conditions as mentioned on the figure). Figure 7.3 (b) shows the corresponding reaction temperature profiles vs. time. In this experiment, the maximum conversion achieved at the end of 24 elements is approximately 74%. The profiles are fairly smooth and steady state is reached after 108 minutes which is approximately three times of the mean residence time (τ = 35.18 min). The steady state conversions along the length of the reactor follow a first order profile. For a first order system, it takes approximately three times of the residence time to reach the steady state which is also evident from the experimental results. More discussion on the first order profile and reaction rate constants is presented in the later part of this chapter. The temperature profile shows a hump which was due to an upset in the steam pressure upstream. Though a control valve maintains the steam pressure at a particular level, upsets in the steam pressure used to occur some times. This can be avoided by proper design of the control system. Nevertheless, in most of the other experimental results the temperature profiles were almost flat. In Figure 7.3 (b), the temperature at the entrance (inlet) of the reactor is 6C to 8 C less than the design temperature. This phenomenon is observed in all experimental results. This is a result of two possible reasons: one is due to the polymer entering the reactor from preheater at a lower temperature compared to the reaction temperature and the other is due to the cold catalyst solution entering the reactor. Though the polymer solution is heated to 160 C to 170 C, because of the heat loss that occurs when the polymer is pumped from the preheater to the reactor, it may enter the reactor at lower temperature than the design temperature. Since the catalyst to polymer flow ratio is either 1:4 or 1:5, the cold catalyst solution entering at inlet of the reactor would cause a temperature drop. The temperature at the exit of the reactor i.e. after the 24 elements was also observed to be 2 C to 4 C less than the desired reaction temperature. This is due to the fact that most of the reaction occurs with in 50% of the reactor length where the cis and vinyl groups are preferentially hydrogenated before converting the trans olefin. Since the maximum conversion achieved in this experiment was 74%, the next experiment was conducted with the catalyst concentration maintained at 80 μM and all other operating conditions being same.

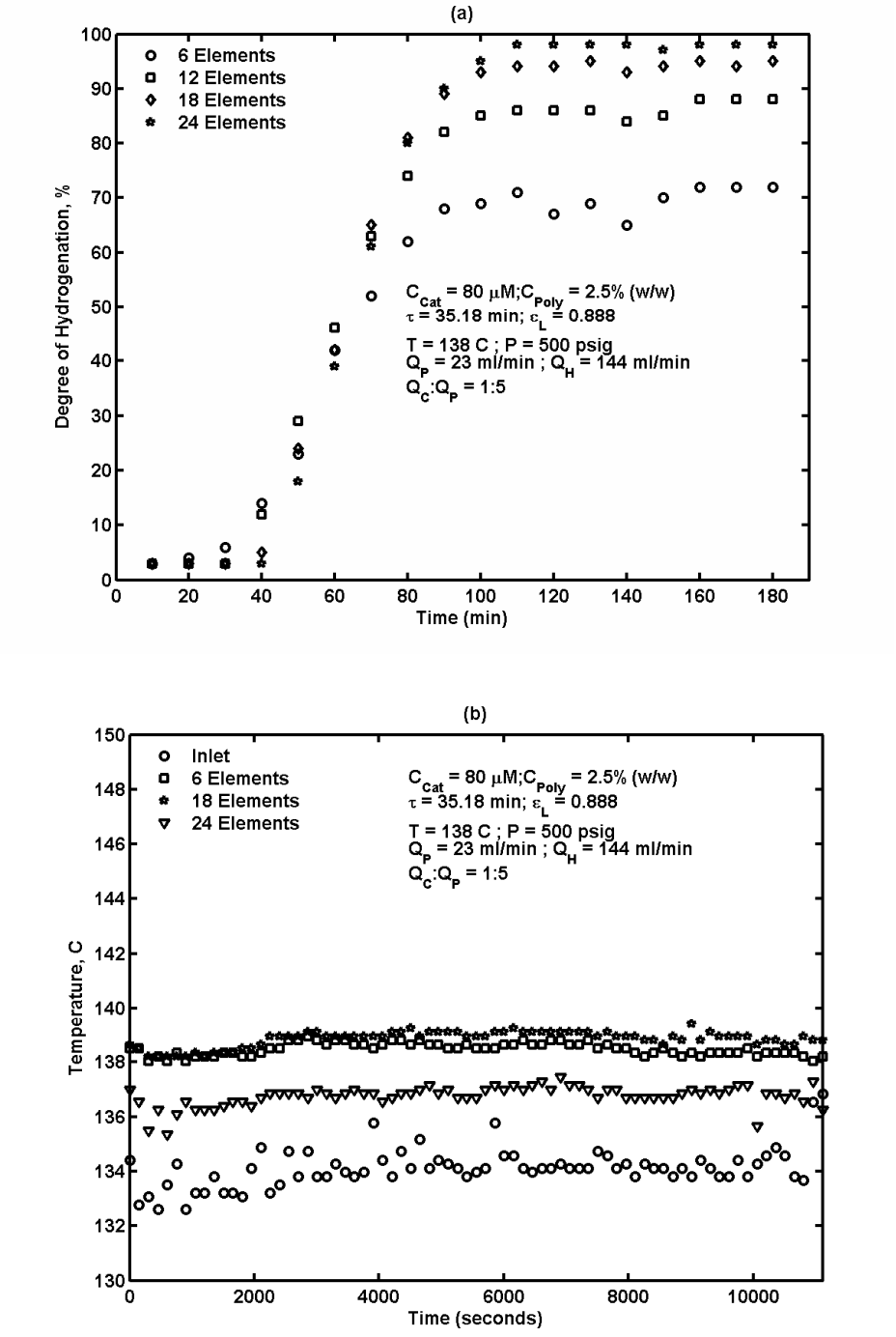

Figure 7.4 (a) Degree of hydrogenation vs. time (b) Reaction temperature vs. time 80 μM $OsHCl(CO)(O_2)(PCy_3)_2$, 2.5% (w/w) polymer, τ = 35.18 min (other conditions mentioned on figure)

As shown in Figure 7.4(a), with 80 μM catalyst, the conversion at the outlet was over 98%. In Figure 7.4(b), it is evident that the temperature profiles are almost flat with out any humps. Similar trends as discussed for the experiment with 35 μM catalyst were found for the degree of hydrogenation profiles. From these two experiments, it can be concluded that the minimum catalyst concentration required to achieve a degree of hydrogenation over 95% with 2.5% (w/w) polymer and 35.18 min mean residence time is 80 μM. Similarly, hydrogenation experiments were performed with 2.5% (w/w) polymer and a 16.7 min mean residence time. The lower level catalyst concentration used in this experiment was 80 μM with which the maximum final conversion obtained at the exit of the reactor was 84.97%. The higher level catalyst concentration was designed at 120 μM which gave a final conversion of 97.0%. The dynamic degree of hydrogenation profiles and corresponding temperature profiles for all other experiments are shown in Appendix B.

From the hydrogenation experiments conducted with 2.5% (w/w) polymer at 500 psig, 138 C, the minimum catalyst required to achieve a degree of hydrogenation over 95% is:

- 80 μM $OsHCl(CO)(O_2)(PCy_3)_2$ for 35. 18 min mean residence time
- 120 μM $OsHCl(CO)(O_2)(PCy_3)_2$ for 16.7 min mean residence time

7.1.2 Optimum Catalyst Concentration for Hydrogenating 5.0% (w/w) Polymer

Hydrogenation experiments with 5.0% (w/w) polymer were conducted with different catalyst concentrations. Before conducting the experiments 5, 6, 7 and 8 (refer Table 7.1), two experiments were performed with very low catalyst concentration for both low level and high level mean residence time. Severe catalyst deactivation was witnessed in both the experiments. There are three possible reasons to explain the catalyst deactivation phenomenon. One of them is, when the polymer concentration is increased the concentration of the impurities in the polymer also increases which reduces the reaction rate. The next reason could be inefficient degassing and susceptibility of air to come in contact with the reactor mixture. The last but most important reason is, though the double bond concentration ([C=C]) doesn't have an effect on the reaction rate constant, the nitrile concentration has a significant impact. This is because of the tendency of the catalyst to coordinate to the cyano group (Parent, 1996). The nitrile group competes with the double bond to occupy the catalyst site and there by hinders the reaction rate. Figure 7.5(a) and (b) shows the degree of hydrogenation vs. time for the hydrogenation experiments conducted with 5.0% (w/w) polymer with τ = 35.18 min, 60 μM catalyst and τ = 35.18 min, 85 μM catalyst respectively.

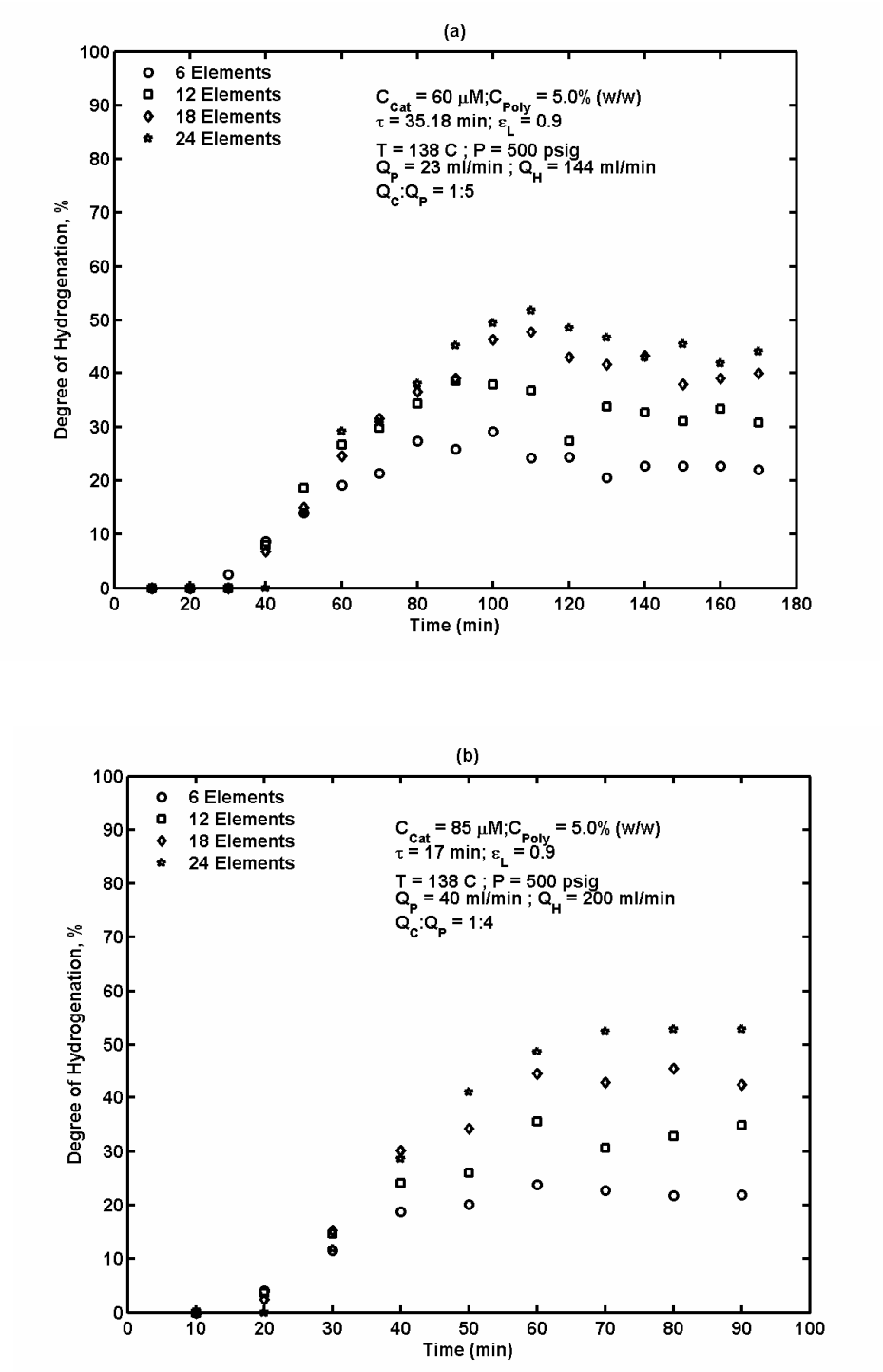

Figure 7.5 Degree of hydrogenation vs. time (a) τ = 35.18 min, 60 μM $OsHCl(CO)(O_2)(PCy_3)_2$ (b) τ = 17.0 min, 85 μM $OsHCl(CO)(O_2)(PCy_3)_2$ (other conditions as mentioned on the figure).

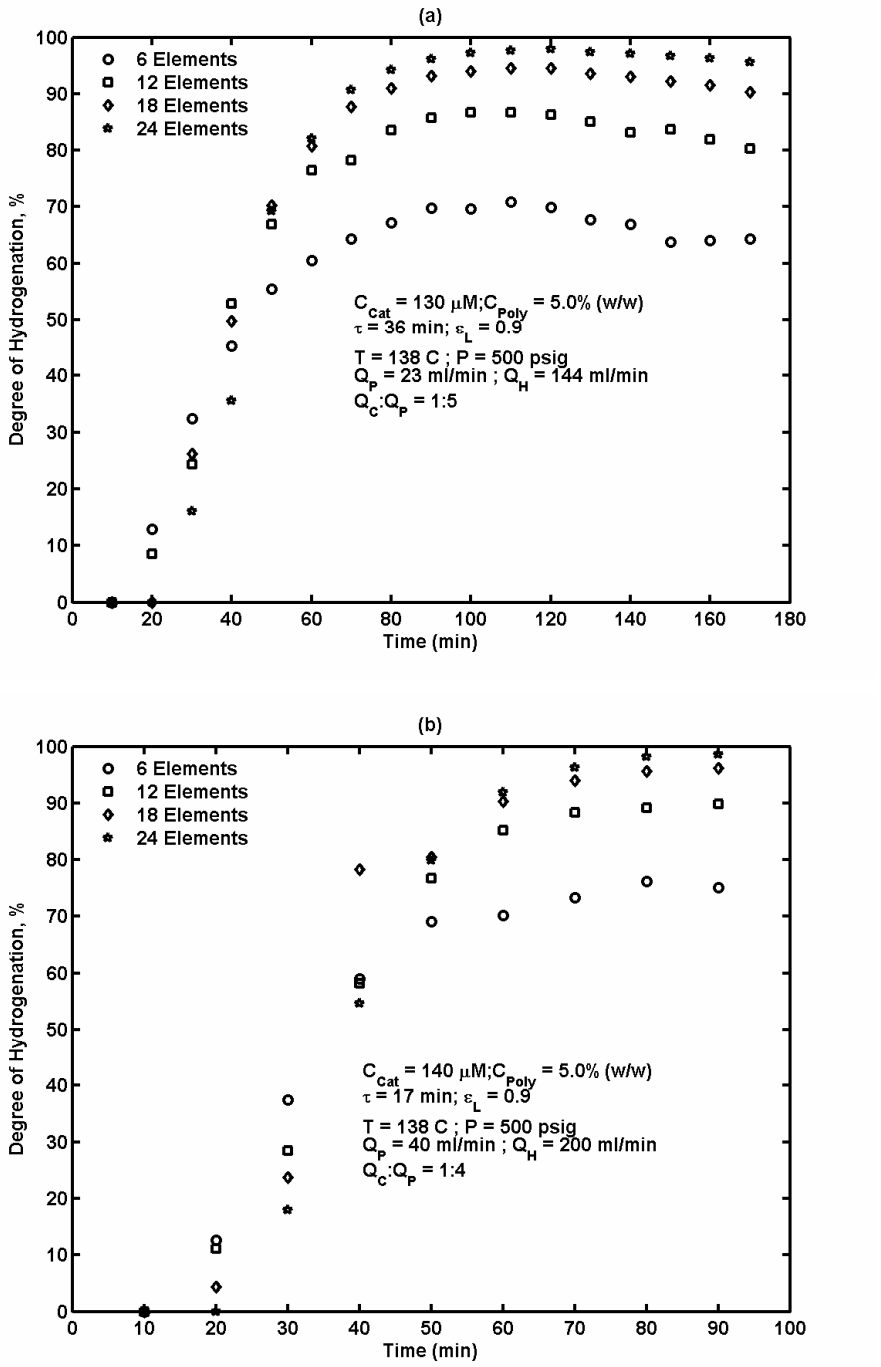

Figure 7.6 Degree of hydrogenation vs. time (a) τ = 36 min,130 μM $OsHCl(CO)(O_2)(PCy_3)_2$ (b) τ = 17.0 min, 140 μM $OsHCl(CO)(O_2)(PCy_3)_2$ (other conditions as mentioned on the figure).

From the experimental results, it is clearly seen that the catalyst suffers deactivation as the maximum conversion obtained at the exit of the reactor is 43.5% and 52.7% for (a) and (b) respectively. A further experiment was performed with the catalyst concentration maintained at 100 μM for τ = 36 min and the maximum steady state conversion achieved at the exit of the SM reactor is 82.63%. Hence, experiments 7 and 8 (refer Table 7.1) were designed and performed to achieve degree of hydrogenation over 95% despite catalyst deactivation. Figure 7.6 (a) and (b) show the degree of hydrogenation profiles obtained for experiments 7 and 8 carried out with 5.0% (w/w). A degree of hydrogenation over 97% was achieved in both cases.

From the hydrogenation experiments conducted with 5.0% (w/w) polymer at 500 psig, 138 C, the minimum catalyst required to achieve a degree of hydrogenation over 95% is:

- 130 μM $OsHCl(CO)(O_2)(PCy_3)_2$ for 36 min mean residence time
- 140 μM $OsHCl(CO)(O_2)(PCy_3)_2$ for 17 min mean residence time

7.1.3 Statistical Analysis

From the experimental results obtained from the designed 2^3 factorial experiments, statistical analysis is performed to evaluate the effect of different factors.

Table 7.2 Coded variables and corresponding conversions for the 2^3 experiments

Factor-level combination			Conversion	
			1	2
A	B	C		
1	1	1	84.97	85.84
2	1	1	97.65	98.52
1	2	1	73.88	74.75
2	2	1	82.63	83.50
1	1	2	97.06	97.93
2	1	2	99.95	99.08
1	2	2	98.00	98.87
2	2	2	96.40	97.27

1 – represents the lower level and 2 - represents the higher level of the factor. As mentioned in the section 7.1, the error from the replicated runs is used for analysis of the variance.

Table 7.2 shows the coded variables corresponding to the experiments listed in Table 7.1. In

Table 7.2, A, B and C are the coded variables for catalyst concentration, mean residence time and polymer concentration respectively.

Table 7.3 Analysis of Variance (ANOVA) for the experiments listed in

Table 7.2

V	SS	df	MS	F	P	Conclusion
Model	1247.2381	7				
A	119.3993	1	119.3993	318.4169	0.0000	S
B	193.9613	1	193.9613	517.2606	0.0000	S
C	660.8498	1	660.8498	1762.3697	0.0000	S
AB	14.2657	1	14.2657	38.0442	0.0003	S
AC	110.3130	1	110.3130	294.1853	0.0000	S
BC	148.4255	1	148.4255	395.8245	0.0000	S
ABC	0.0234	1	0.0234	0.0624	0.8090	NS
Error	2.9998	8	0.3750			
Total	1250.2380	15				

Number of replicates on each factor-level are: 2

With a given significance level of α: 0.05

The results are significant (S) and/or not significant (NS).

Table 7.3 shows the analysis of variance for the 2^3 experiments listed in

Table 7.2. The analysis is carried out with a significance level of $\alpha = 0.05$. The analysis clearly shows that the factors chosen to study the degree of hydrogenation have a strong impact. The first order effects and second order interactions are found to be significant while the third order interactions

were not significant. Instead of modeling the conversion as a function of these factors, an empirical model is derived which is a function of the Peclet number ($\boldsymbol{Pe} = \frac{\overline{\boldsymbol{U}}\boldsymbol{L}}{\boldsymbol{D_a}}$), θ_τ (τ/τ_R), q ($[C=C]_0/H^*$), and R (reaction resistance over mass transfer resistance). All these factors are indirect functions of the factors considered and the relationships were given in Chapter 4. The details of this model are discussed at the end of this chapter.

7.2 Reaction Rate Constant

The conversions obtained from the hydrogenation experiments tended to follow the expected first order profiles. The rate constants were determined by plotting ln(1-conversion) versus reaction time and calculating the slope. Some deviations between the first order model and experimental results were observed. Figure 7.7 (a) and (b) shows the first order profiles for the hydrogenation experiments conducted with τ = 36 min and τ = 17 min respectively. From the figure it clear that the deviation is more at the first port where the polymer temperature was always 6 to 8 C less than that of the other ports. In the case of experiments that suffered catalyst deactivation, almost perfect first order profiles were observed as can be seen in Figure 7.8 (a). The corresponding rate constants were 0.0003 s^{-1} and 0.0008 s^{-1} for 60 μM catalyst and 85 μM catalyst respectively. Figure 7.8 (b) shows the plot of reaction rate constants versus the catalyst concentration obtained by first order regression (corresponding to experiments shown in Figure 7.7. There are many reasons to justify the deviations. Since there were fluctuations in the temperature profile along the length of the reactor, this might have influence on the rate constant because the rate constant is a strong function of reaction temperature. Though the temperature difference between the different ports is within 8 to 10 C, the rate constant is highly sensitive at high temperatures (above 130 C where the reaction is usually conducted). Another reason might be the disturbance in the hydrodynamic flow because of sampling frequently. Samples were usually collected every 10 min along the length of the reactor. The process upset due to repressurizing of the gas/liquid separator also causes hydrodynamic disturbance. The effect of dispersion may not be far from negligible. The dispersion is mostly a function of the gas/liquid flow rates, with dispersion being decreased with an increase in liquid flow rate and vice versa with the gas flow rate. Experiments with different gas/liquid velocities would help clarify this issue. As shown in Figure 7.8 (b), the reaction rate constant is in the range of 0.0007 to 0.008 s^{-1}. These rate constants are far away from those obtained in the batch system (refer to Table 6.2) and this is an usual phenomenon that occurs with continuous systems.

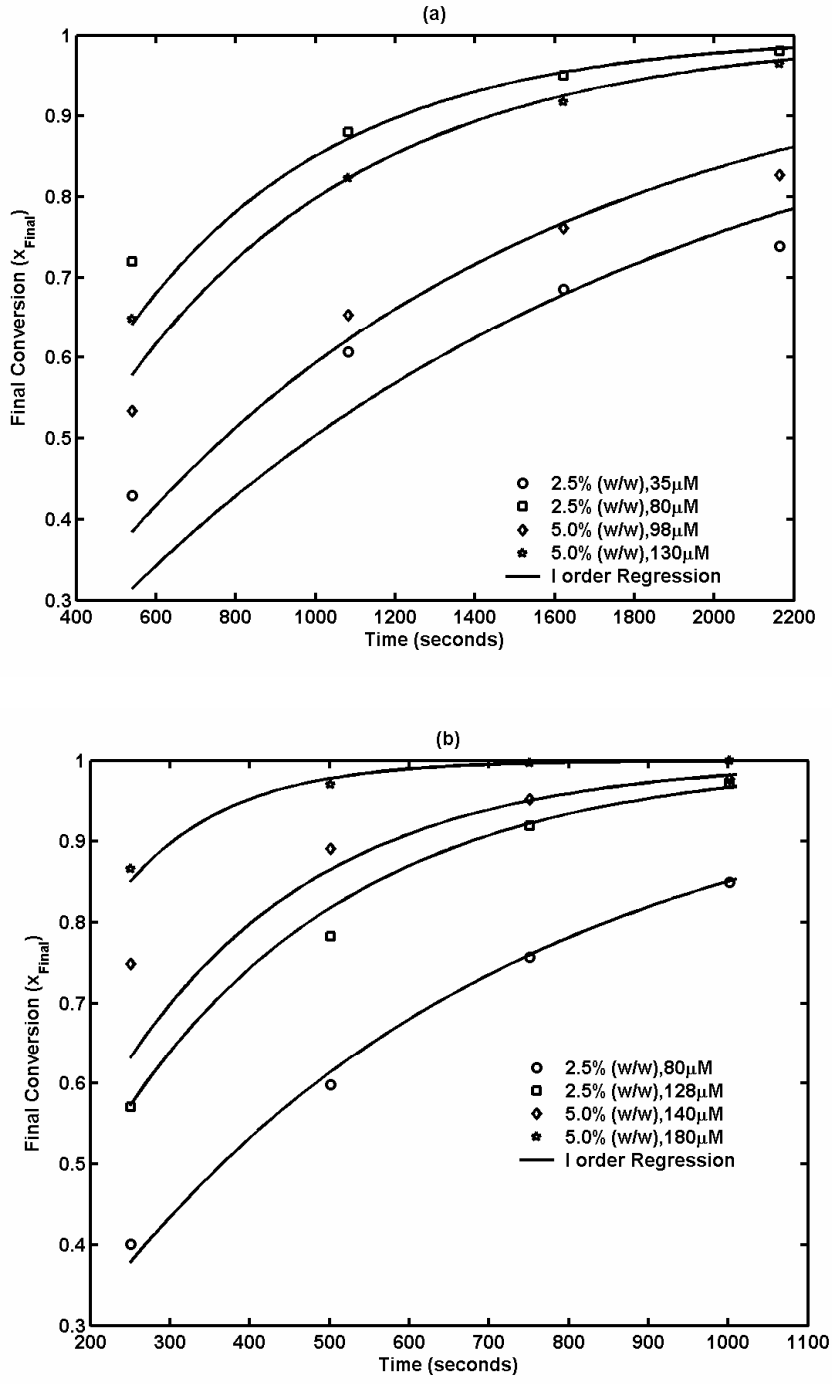

Figure 7.7 Typical first order conversion profiles versus reaction time for (a) τ = 36 min and (b) τ = 17 min (other conditions as mentioned on the figures)

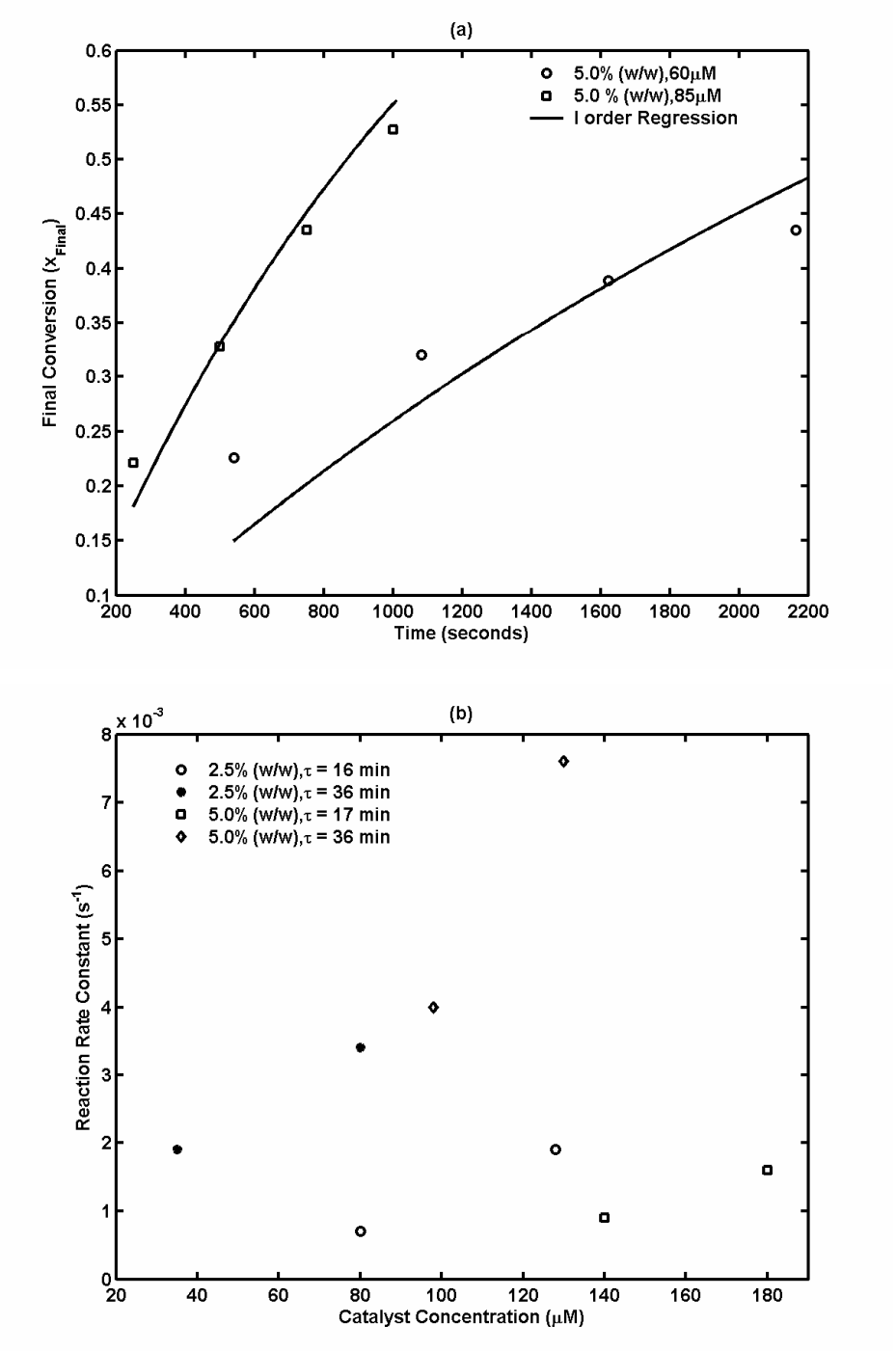

Figure 7.8 (a) First order conversion profile for the experiments with catalyst deactivation. (b) plot of reaction rate constant versus catalyst concentration (other conditions as mentioned on the figure).

7.3 Empirical Model

From the hydrogenation experimental results, it was found that the mean residence time, catalyst and polymer concentration have a strong effect on the degree of hydrogenation. The final conversion or the degree of hydrogenation is modeled using the corresponding dimensionless parameters which functions of these factors. The dimensionless parameters used in this model consists of the Peclet number ($\boldsymbol{Pe} = \frac{\overline{\boldsymbol{U}}\boldsymbol{L}}{\boldsymbol{D_a}}$), θ_τ (τ/τ_R), q ($[C{=}C]_0/H^*$), and R (reaction resistance over mass transfer resistance). All parameters are the same as defined earlier in the chapter 4 except τ_R and R which are defined by equations (8.6) and (8.7) respectively. The empirical model is given by linear regression of the above said parameters. The corresponding mode is given by equation (7.1)

$$\boldsymbol{y} = \boldsymbol{\beta}_1 + \boldsymbol{\beta}_2\boldsymbol{X}_1 + \boldsymbol{\beta}_3\boldsymbol{X}_2 + \boldsymbol{\beta}_4\boldsymbol{X}_3 + \boldsymbol{\beta}_5\boldsymbol{X}_1\boldsymbol{X}_2 + \boldsymbol{\beta}_6\boldsymbol{X}_2\boldsymbol{X}_3 + \boldsymbol{\beta}_7\boldsymbol{X}_3\boldsymbol{X}_1 \qquad \textbf{(7.1)}$$

where y = final conversion (after 24 elements), X_1 = Peclet number, $X_2 = \theta_\tau$, X_3 = q/R and β_1 through β_7 are the parameters. The R^2 was found to be 0.9938. The parameters and the corresponding confidence intervals are shown in Table 7.4.

Table 7.4 Parameter values and confidence intervals corresponding to equation (7.1)

Parameter	Value	Confidence Interval (x 10^{-3})	
β_1	320.9455	-0.4249	1.0668
β_2	-47.2309	-0.2113	0.1168
β_3	-28.8234	-0.1208	0.0632
β_4	-54.1589	-0.1955	0.0872
β_5	6.294	-0.015	0.0276
β_6	5.1383	-0.0095	0.0198
β_7	4.0937	-0.0046	0.0128

In addition to the above empirical model, simulation results from the dynamic model for studying the experimental conversion along the length of the SM reactor are presented in Chapter 8. The hydrogenation data obtained in the continuous process is tabulated in Appendix D.

Chapter 8
Model Prediction of Hydrogenation Performance and Scale up of Pilot Plant Process

8.1 Model Prediction of Hydrogenation Performance in the SM Reactor

The results obtained from the hydrogenation experiments performed in the continuous process with SM reactor using osmium catalyst is modeled using the design equations discussed in Chapter 4. Modification of the model is made according to the reality of the process. In the current process, the catalyst solution is pumped into the reactor separately and the catalyst flow also experiences dispersion along the length of the reactor before the flow becomes steady. Based on the previous work done on the continuous process using a packed bed, where the catalyst solution and the polymer solution enter simultaneously at the same point before the reactor inlet (where the size of the inlet is restricted and plug flow is assumed), closed-closed boundary conditions were used to numerically assess the performance of the reactor. In the current process, catalyst solution and polymer solution enter separately and open-open boundary conditions are more close to reality compared to the closed-closed boundary conditions. These are the most important aspects taken into account for modifying the model. Since, the osmium concentration is not uniform throughout the reactor before it reaches steady state, the source term or the reaction term in equation (4.3) has to account for this. Also, at moderate pressures, the reaction order with respect to hydrogen was reported to be two (Parent, 1996). Hence, the reaction term is given by equation (8.1).

$$\phi(c) = R_H = k'[Os][C = C][H_2]^2 \qquad \textbf{(8.1)}$$

where, [Os] is the concentration of osmium. A mole balance on the osmium inside the reactor would lead to equation (8.2).

$$\frac{\partial[Os]}{\partial t} = D_a \frac{\partial^2[Os]}{\partial z^2} - \bar{U}\frac{\partial[Os]}{\partial z} \qquad \textbf{(8.2)}$$

Equation (8.2) combined with equations (4.4) and (4.5) would form the proposed model for predicting the degree of hydrogenation of NBR in the SM reactor.

The dimensionless design equations of the proposed model for prediction of hydrogenation performance are obtained by combining equations (4.4), (4.5), (8.2) and (8.3). The simplified model is given by the following equations:

$$\frac{\partial \boldsymbol{x}}{\partial \boldsymbol{\theta}} = \frac{1}{\boldsymbol{Pe}} \cdot \frac{1}{\boldsymbol{\theta_\tau}} \frac{\partial^2 \boldsymbol{x}}{\partial \boldsymbol{\lambda}^2} - \frac{1}{\boldsymbol{\theta_\tau}} \frac{\partial \boldsymbol{x}}{\partial \boldsymbol{\lambda}} + (1-\boldsymbol{x}) \cdot \boldsymbol{\zeta} \cdot \boldsymbol{h}^2 \qquad \textbf{(8.3)}$$

$$\frac{\partial \boldsymbol{h}}{\partial \boldsymbol{\theta}} = \frac{1}{\boldsymbol{Pe}} \cdot \frac{1}{\boldsymbol{\theta_\tau}} \frac{\partial^2 \boldsymbol{h}}{\partial \boldsymbol{\lambda}^2} - \frac{1}{\boldsymbol{\theta_\tau}} \frac{\partial \boldsymbol{h}}{\partial \boldsymbol{\lambda}} - \boldsymbol{q} \cdot (1-\boldsymbol{x}) \cdot \boldsymbol{\zeta} \cdot \boldsymbol{h}^2 + \frac{\boldsymbol{q}}{\boldsymbol{R}}(1-\boldsymbol{h}) \qquad \textbf{(8.4)}$$

$$\frac{\partial \boldsymbol{\zeta}}{\partial \boldsymbol{\theta}} = \frac{1}{\boldsymbol{Pe}} \frac{1}{\boldsymbol{\theta_\tau}} \frac{\partial^2 \boldsymbol{\zeta}}{\partial \boldsymbol{\lambda}^2} - \frac{1}{\boldsymbol{\theta_\tau}} \frac{\partial \boldsymbol{\zeta}}{\partial \boldsymbol{\lambda}} \qquad \textbf{(8.5)}$$

where, ζ is the normalized catalyst concentration, $[Os]/[Os]_o$. The parameters Pe ,θ_τ, and q are the same as defined in Chapter 4 while τ_R and R are given by the equation (8.6) and (8.7) respectively:

$$\boldsymbol{\tau_R} = \frac{1}{\boldsymbol{k}'[\boldsymbol{Os}]_o [\boldsymbol{H}_2^*]^2} \qquad \textbf{(8.6)}$$

$$\boldsymbol{R} = \frac{\boldsymbol{k}[\boldsymbol{C}=\boldsymbol{C}]_o [\boldsymbol{Os}]_o [\boldsymbol{H}_2^*]^2}{\boldsymbol{K_L a}[\boldsymbol{H}_2^*]} \qquad \textbf{(8.7)}$$

The open-open boundary conditions for equations (8.3) through (8.5) are given by the following equations:

Initial Condition : At $\boldsymbol{\theta} = 0; \forall \boldsymbol{\lambda}$ $\boldsymbol{x} = 0, \quad \boldsymbol{h} = \boldsymbol{h_o}, \quad \boldsymbol{\zeta} = 0$

Boundary Condition 1 :

At $\boldsymbol{\lambda} = 0;$ $\quad \boldsymbol{\upsilon}(0^-, \boldsymbol{\theta}) + \frac{1}{\boldsymbol{Pe}} \frac{\partial \boldsymbol{\upsilon}}{\partial \boldsymbol{\lambda}}\Big|_{(0^-, \boldsymbol{\theta})} = \boldsymbol{\upsilon}(0^+, \boldsymbol{\theta}) + \frac{1}{\boldsymbol{Pe}} \frac{\partial \boldsymbol{\upsilon}}{\partial \boldsymbol{\lambda}}\Big|_{(0^+, \boldsymbol{\theta})}$

$$\boldsymbol{\upsilon}(0^-, \boldsymbol{\theta}) = \boldsymbol{\upsilon}(0^+, \boldsymbol{\theta})$$

Boundary Condition 2 :

At $\boldsymbol{\lambda} = 1;$ $\quad \boldsymbol{\upsilon}(1^-, \boldsymbol{\theta}) + \frac{1}{\boldsymbol{Pe}} \frac{\partial \boldsymbol{\upsilon}}{\partial \boldsymbol{\lambda}}\Big|_{(1^-, \boldsymbol{\theta})} = \boldsymbol{\upsilon}(1^+, \boldsymbol{\theta}) + \frac{1}{\boldsymbol{Pe}} \frac{\partial \boldsymbol{\upsilon}}{\partial \boldsymbol{\lambda}}\Big|_{(1^+, \boldsymbol{\theta})}$

$$\boldsymbol{\upsilon}(1^-, \boldsymbol{\theta}) = \boldsymbol{\upsilon}(1^+, \boldsymbol{\theta})$$

where, $\boldsymbol{\upsilon} = \boldsymbol{x}, \boldsymbol{h}, \boldsymbol{\zeta}$

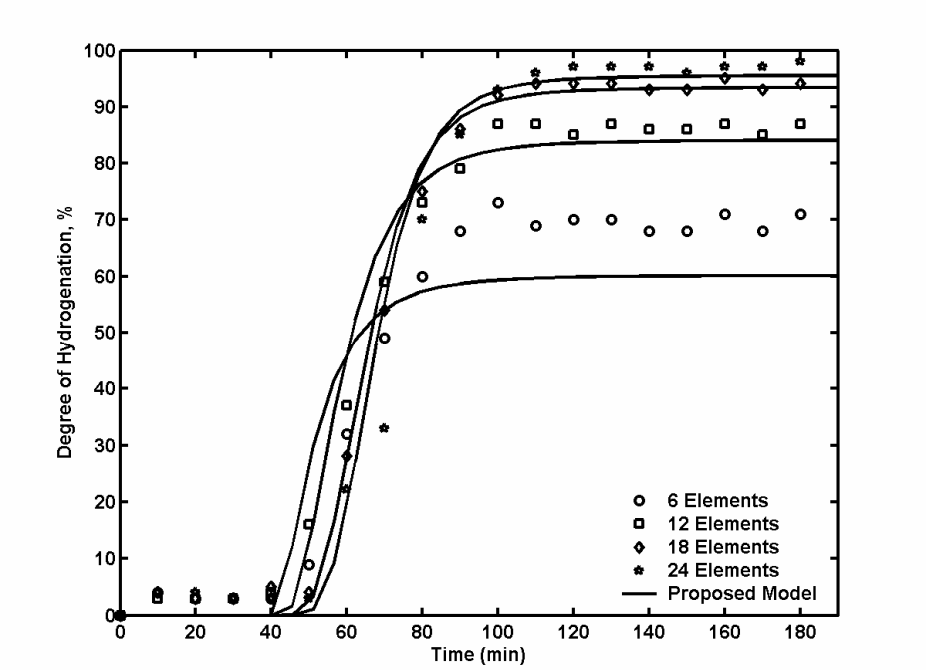

Figure 8.1 Model prediction vs. experimental degree of hydrogenation. Operating conditions: 2.5% (w/w) polymer solution, τ = 35.16 min, 80 μM $OsHCl(CO)(O_2)(PCy_3)_2$.

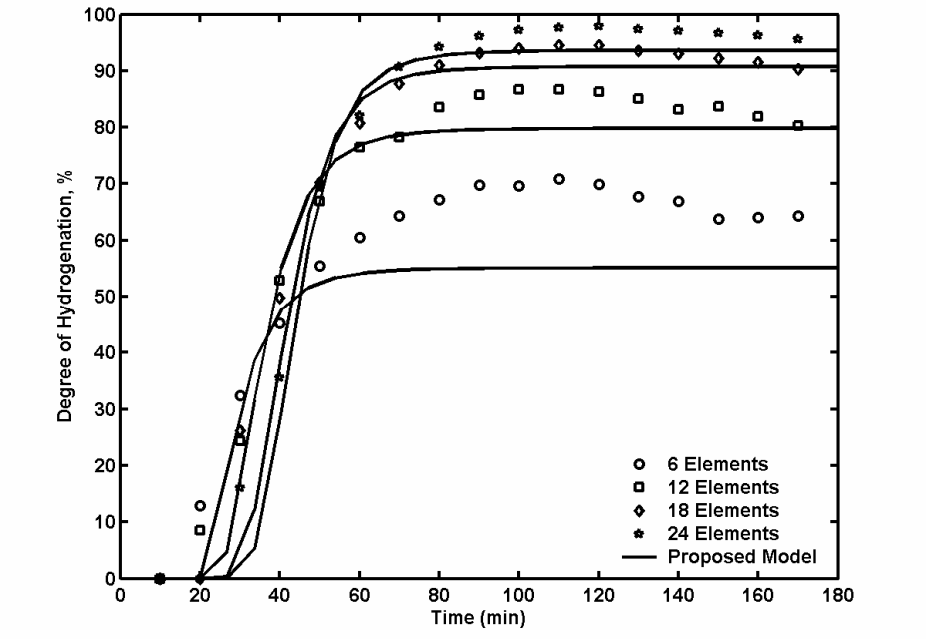

Figure 8.2 Model prediction vs. experimental degree of hydrogenation. Operating conditions: 5.0% (w/w) polymer solution, τ = 35.18 min, 130 μM $OsHCl(CO)(O_2)(PCy_3)_2$.

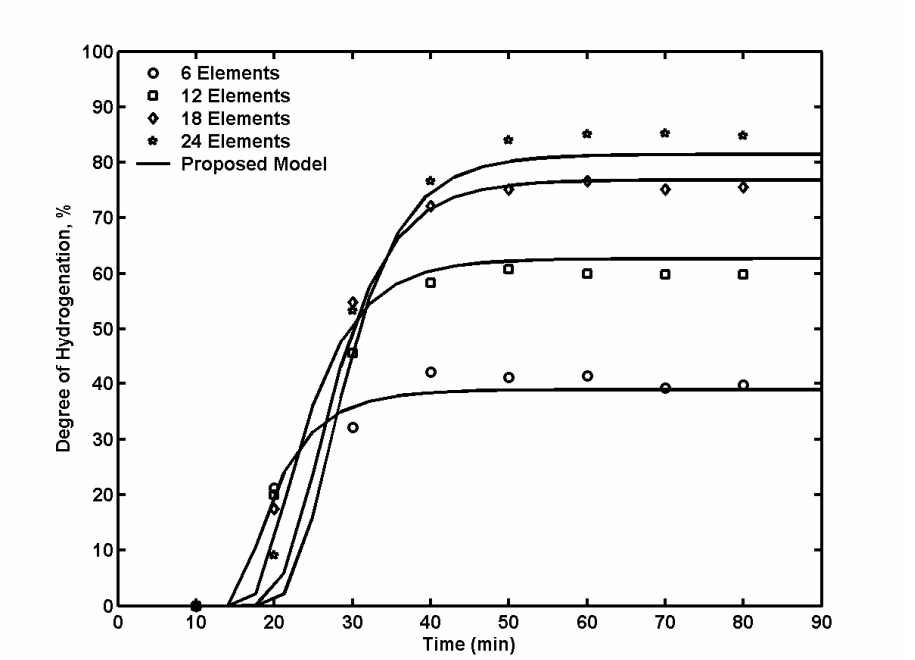

Figure 8.3 Model prediction vs. experimental degree of hydrogenation. Operating conditions: 2.5% (w/w) polymer solution, τ = 16.7 min, 80 μM $OsHCl(CO)(O_2)(PCy_3)_2$.

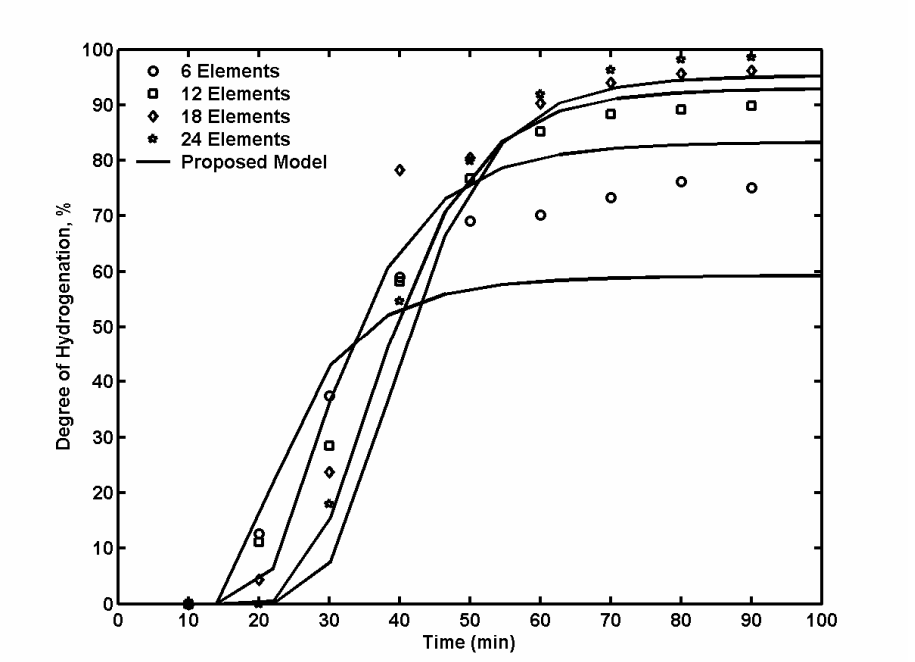

Figure 8.4 Model prediction vs. experimental degree of hydrogenation. Operating conditions: 5.0% (w/w) polymer solution, τ = 17 min, 140 μM $OsHCl(CO)(O_2)(PCy_3)_2$.

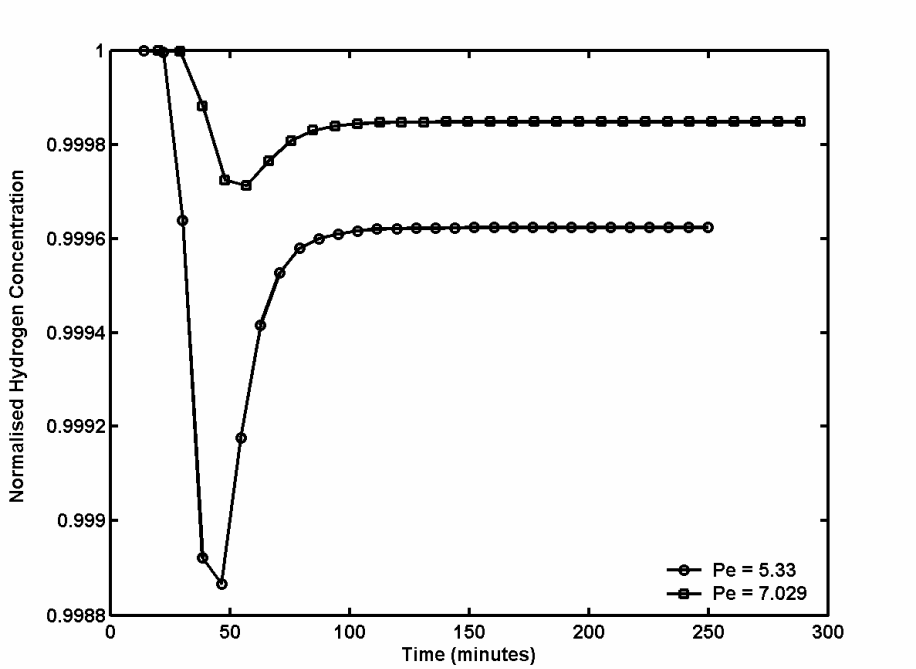

Figure 8.5 Normalized hydrogen concentration profiles (model) Operating conditions: ○ – 2.5% (w/w) polymer solution, τ = 35.16 min, 80 μM catalyst; □ – 5.0% (w/w) polymer solution, τ = 17 min, 140 μM catalyst.

The proposed model along with the boundary conditions is numerically solved by using method of lines (described in section 4.2). The model parameters are obtained from the various hydrodynamic results discussed in the previous chapter. For example, the Peclet number is estimated by using equation (5.6), the K_La data required for estimating R is calculated from equation (3.11), and rate of the reaction from section 7.2.

Figure 8.1 through

Figure 8.4 show a comparison of the experimental degree of hydrogenation with the proposed model prediction for various hydrogenation experiments conducted in the continuous process with the SM reactor. Figure 8.5 and Figure 8.6 show, the corresponding normalized hydrogen concentration profiles and normalized osmium concentration profiles predicted by the model for the experiment #2 & #8 (refer Table 7.1) respectively. It is evident from the results that the proposed model satisfactorily predicts the degree of hydrogenation obtained from experimental results. The model could not predict correctly for the degree of hydrogenation at 6 elements in all the cases. Also, the

prediction at the exit of the reactor was always lower than the experimental value though not far from negligible.

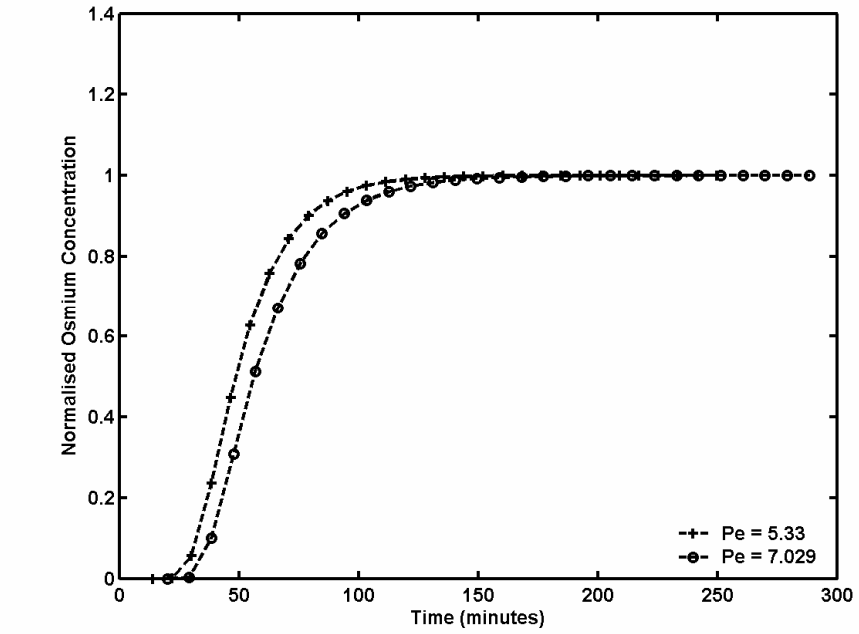

Figure 8.6 Normalized osmium concentration profiles (model) Operating conditions: ○ – 2.5% (w/w) polymer solution, τ = 35.16 min, 80 μM catalyst; + - 5.0% (w/w) polymer solution, τ = 17 min, 140 μM catalyst

There are many possible reasons for the deviation of the model prediction with the experimental values. The first and foremost reason is the parameters used in the model are all obtained from the hydrodynamic data obtained at ambient conditions rather than at the operating condition (high pressure and high temperature). This can have a very strong impact on the prediction of the model. The mass transfer coefficient, liquid hold up, Peclet number can always be different at high temperature and pressure compared to that at ambient conditions. Secondly, the reaction rate constant used in the model did not account for the temperature change along the reactor. The proposed model assumes constant temperature along the length of the reactor. However, the temperature at the inlet and outlet were always found to be less than the temperature at other ports. Since, the reaction rate constant is a strong function of temperature, variations along of the reactor can cause the reaction rate to vary. Thirdly, the model did not take the catalyst deactivation phenomenon into account. According to Parent (1996), 25 μM catalyst is lost for the 80 μM catalyst level when hydrogenating

2.5% (w/w) NBR solution at 350 psig and 130 C in the batch reactor. It means that the active catalyst is 55 μM. In the present continuous reactor, owing to the hydrodynamic constraints such as dispersion, the loss of catalyst would me more and the active catalyst concentration taking part in the hydrogenation has to be used in the model to predict the degree of hydrogenation. Overall, the proposed model could predict the trend and approximate degree of hydrogenation in the SM reactor for various operating conditions. The improvement of the continuous process for better performance is discussed in the last chapter.

8.2 Scale up of the Continuous Process - Pilot Plant Design

The design of a pilot plant is usually done based on the conversion and yield data obtained from the laboratory reactors (bench scale reactors). A pilot plant is hardly designed using only the fundamental rate constants from the literature because of possible changes in the catalyst activity, effects of heat transfer, mass transfer and mixing phenomenon. On the other hand process equipment used for unit operations such as distillation columns, heat exchangers and other separation equipment can be designed to a higher scale from the physical properties of the system and empirical correlations for the transport rates.

The normal procedure for scale up of the continuous hydrogenation process is to carry out laboratory experiments over a wide range of operating conditions (by varying gas/liquid flow rates, catalyst concentration, temperature, pressure, polymer concentration) to determine the catalyst activity and catalyst deactivation phenomenon. Upon arriving at favorable conditions, there are two approaches one can use for scale up. The first method involves scale up in stages using the same type of reactor and operating conditions. Though this is a time consuming method the data obtained from the different stages of scale up can be used to design an efficient large scale reactor. Some times, it would become difficult to predict the performance of the scaled up reactor from results obtained in different stages. A second method involves finding the intrinsic kinetics from the laboratory scale experiments which is finding the conditions where kinetic parameters influence the conversion or yield. The advantage with the second method is that it can be used to compare performance of different types of reactors for the same objective. If it difficult to get this data, then the data obtained should be corrected for the effects of heat transfer, diffusion and mixing. Further, this data is used to estimate the reaction order, rate constant and activation energy of the main reaction.

For the scale up to pilot plant design of the continuous hydrogenation of NBR using the SM reactor, the computations were based on a throughput of 50 tons of HNBR per year. The utilization of the first method of scale up is made as the prediction of the hydrogenation results using the proposed model is good. In this method the reactor geometric similarity is maintained and so are the inlet/outlet conditions, and the physical and chemical properties of the working fluids. Also, in this method, dimensionless groups are formed using the Buckingham Pi theorem and some of them are maintained at a constant level when scaling up to pilot design. More information on dimensional analysis and Buckingham Pi theorem can be obtained from the work of Bridgman (1951). Since, hydrogenation of NBR is a homogeneous, irreversible reaction the conversion is influenced by both mass and heat transfer processes. The flow condition inside the reactor is described by the following variables:

$$\{\boldsymbol{U}, \boldsymbol{d}, \boldsymbol{L}, \boldsymbol{\rho}, \boldsymbol{\mu}\} \qquad \textbf{(8.8)}$$

where U is the velocity, d and L are diameter and length of the SM reactor respectively, ρ is the fluid density and μ is the fluid viscosity. All physical properties are related to known inlet temperature, T_o. The conversion or degree of hydrogenation is related to the inlet and outlet carbon-carbon double bond concentration as shown in equation (4.13) as well as the reaction rate constant k'. The reaction rate constant is a function of temperature and can be represented by using the Arhenius law (refer equation (6.3)). The mass transfer coefficient, K_La can be related to the diffusion coefficient by using Fick's law. Hence, the variables that would describe heat and mass transfer are shown below:

$$\{\boldsymbol{D}, \boldsymbol{C_P}, \boldsymbol{K}, [\boldsymbol{C}=\boldsymbol{C}]_o \Delta \boldsymbol{H_R}, \boldsymbol{T_o}, \Delta \boldsymbol{T}\} \qquad \textbf{(8.9)}$$

where, D is the diffusion coefficient (which can represent the dispersion also in addition to the diffusion), C_P is the heat capacity, K is the thermal conductivity, $[C=C]_o\Delta H_R$ is the heat of reaction per unit time and volume, ΔT is the temperature difference between the polymer solution and the reactor wall. Hence, the complete list of those variables that have a direct impact on the performance of the SM reactor with respect to hydrogenation are:

$$\{\boldsymbol{U}, \boldsymbol{d}, \boldsymbol{L}, \boldsymbol{\rho}, \boldsymbol{\mu}, [\boldsymbol{C}=\boldsymbol{C}]_o, [\boldsymbol{C}=\boldsymbol{C}], \boldsymbol{k_o}, \boldsymbol{E}/\boldsymbol{R}, \boldsymbol{D}, \boldsymbol{C_P}, \boldsymbol{K}, [\boldsymbol{C}=\boldsymbol{C}]_o \Delta \boldsymbol{H_R}, \boldsymbol{T_o}, \Delta \boldsymbol{T}\} \qquad \textbf{(8.10)}$$

From the above 15 dimensional parameters, 9 numbers can be formed as the primary quantities are 6 (mass, length, time, temperature, mol, amount of heat). After performing dimensional analysis and grouping the pi terms, the nine numbers thus obtained are shown below:

$$\{\frac{\boldsymbol{L}}{\boldsymbol{d}}, \frac{[\boldsymbol{C}=\boldsymbol{C}]}{[\boldsymbol{C}=\boldsymbol{C}]_{\boldsymbol{o}}}, \frac{\boldsymbol{E}}{\boldsymbol{RT_o}}, \boldsymbol{k_o\tau}, \frac{\Delta \boldsymbol{T}}{\boldsymbol{T_o}}, \frac{\boldsymbol{\rho C_P T_o}}{[\boldsymbol{C}=\boldsymbol{C}]_{\boldsymbol{in}} \Delta \boldsymbol{H_R}}, \mathrm{Re}, \boldsymbol{Sc}, \mathrm{Pr}\} \qquad \textbf{(8.11)}$$

The above nine numbers form the complete pi-set. The inlet reaction temperature has to be kept constant even in the scaled up reactor (as it can effect k_o), and so are the physical and chemical properties of the reactants. If the SM reactor scale up for a given geometry (L/d = identical) is performed at T_o and $\Delta T/T_o$ = identical, then all other numbers in the equation remain unchanged except $k_o\tau$ and Re. To attain a specified degree of hydrogenation $[C=C]_{out}/[C=C]_{in}$, it would be enough if we can adjust $Re = Ud\rho/\mu$ and $k_o\tau = k_oL/U$ such that they are identical. This is not at all possible as it will be difficult to maintain L/d = identical. Because keeping Ud = identical, is the same as keeping UL = identical. When Re is changed i.e., UL is changed however, at the same time $k_o\tau$ (= k_oL/U) will not be constant and hence this would contradict the geometric similarity. This is an inherent problem that occurs in the scale up of tubular reactors such as static mixer reactors; packed bed reactors, bubble columns etc. In these type of situations, Damköhler (1936), proposes to abandon the geometric similarity and fluid dynamic similarity (Re = identical) but to try to satisfy chemical similarity.

Table 8.1 Dimensions of the SM reactor for pilot scale

SM Reactor Dimensions	Corresponding Dimensionless Parameters
Volume = 30.504 L	Pe = 5.19
Inside Diameter = 9.588 cm	θ_τ = 7.31
Length = 4.21 m	τ = 5.076 hours
Number of Elements = 44	τ_R = 0.6944 hours

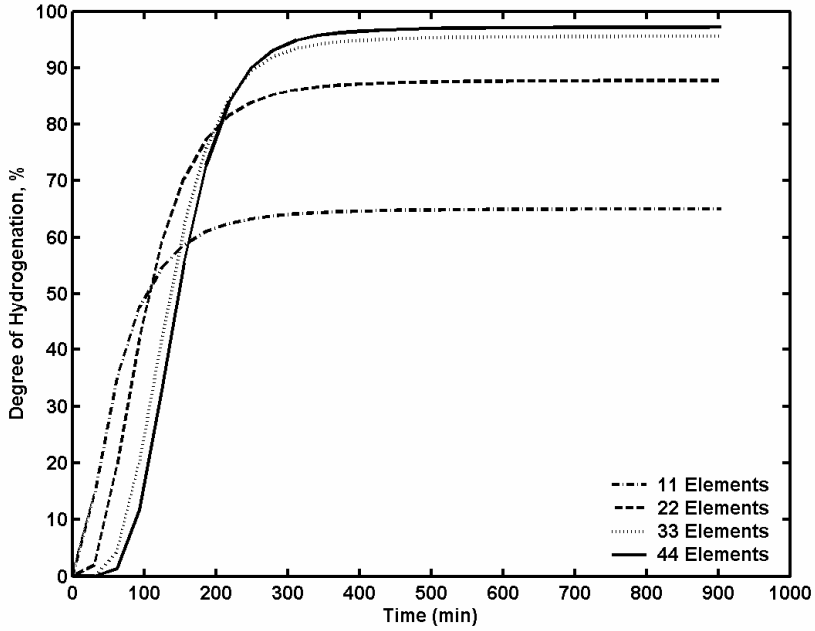

Figure 8.7 Estimation of the conversion in the pilot plant using the proposed model. Operating conditions 5.0% (w/w) polymer, 140 μM $OsHCl(CO)(O_2)(PCy_3)_2$, 500 psig, 138 C (other dimensions and parameters refer to Table 8.1)

Hence, preliminary analysis based on the chemical similarity is done and the scale up to pilot plant is done accordingly. The pilot plant is designed to process the 5.0% (w/w) polymer at 138 C, 500 psig, with catalyst concentration of 140 μM and a throughput of 50 ton per year. By keeping the $k_o\tau$ = identical, the scale up is performed and the dimensions of the reactor are estimated accordingly and are shown in Table 8.1. Figure 8.7 shows the hydrogenation degree profiles predicted using the proposed model (equation (8.3) to (8.5)) along the length of the pilot scale reactor for 5.0% (w/w) polymer, 140 μM $OsHCl(CO)(O_2)(PCy_3)_2$, 500 psig, 138 C. From the figure it is promising that a degree of hydrogenation over 98% can be achieved in the designed pilot SM reactor. Although, this is a preliminary analysis, evaluation on scale up of pilot plant could be carried out with a further investigation made where other phenomenon such as heat transfer are also taken into consideration.

8.3 Comparison of the Performances of Static Mixer Reactor with Multistage Agitated Column Reactor

Zhang (2007) studied the feasibility of conducting hydrogenation of NBR using a six stage agitated column reactor. The performance of the SM reactor is compared to that of a multistage-agitated column (MAC) reactor with respect to hydrogenation of NBR using osmium catalyst. The reactor dimensions used in Zhang's study are: stage diameter – 2.5", stage height – 2.5", impeller diameter – 1.25" and central opening – 0.6". The volume of the MAC reactor is 1150 cc and a Rushton turbine is used as impeller in each stage. The experimental conditions used in his study are similar to those used in the continuous process, except that the mean residence time is different because of the different reactor volumes.

Table 8.2 Operating conditions used in SM and MAC reactors

Operating Variable	SM Reactor		MAC reactor (Zhang 2007)	
Catalyst Concentration (μM)	80	140	80	140
Polymer Concentration (% w/w)	2.5	5.0	2.5	5.0
Mean Residence Time (min)	35	35	40	40
Speed of the Agitator (rps)	0	0	750	750
Liquid Hold up (ε_L)	0.88	0.9	0.85	0.92
Degree of Hydrogenation (%)	98	98	98	98

Table 8.2 shows the operating conditions used in the SM and MAC reactors and the corresponding degree of hydrogenation obtained in continuous process with SM reactor and MAC reactor. It shows that both processes give the same degree of hydrogenation under identical operating conditions. But, the continuous process with SM reactor would be economical compared to MAC reactor if HNBR has to be commercially produced. The reasons are: (a) there are no moving parts in the SM reactor while in the MAC the agitator has to be operated by using heavy duty motors (because the plant would be operated in a continuous fashion), hence the operation cost is much lower in SM compared to the MAC. (b) The investment cost of the MAC reactor could be very high (Zhang 2007) compared to that of the SM reactor; hence the plant cost with SM reactor would be much lower compared to the MAC reactor. The only probable disadvantage with SM reactor could be when high polymer concentrations are used (which has to be further confirmed). However, when the reaction rate is different at different lengths of the reactor, then a MAC is efficient because temperature could be operated at different

levels since the temperature in the jackets of the different stages could be independently controlled. Further experiments with increased polymer concentration would enable us to comment on the performance of both reactors. For hydrogenating NBR up to 5.0% (w/w) concentration, the total cost per pound of HNBR produced would be less in SM reactor compared to that of MAC.

8.4 Concluding Remarks

The hydrogenation data obtained in the SM reactor is modeled by using the coupled model for conversion, hydrogen and catalyst concentration. The proposed model satisfactorily predicts the degree of hydrogenation obtained from experimental results. At the exit of the sixth element, the deviation of the model from the experimental results is far from negligible. The possible reasons for this deviation and other issues related to the parameters used in the model were discussed.

The successful hydrogenation of NBR using the osmium catalyst in the continuous process using the SM reactor and corresponding successful modeling of the degree of hydrogenation paved the way to go for a scale up of pilot plant design. Various variables affecting the scale up and the procedure used for scale up were discussed. A pilot plant with 30.504 L volume, 44 mixing elements, 9.588 cm ID and with length of 4.21 m is designed to process a throughput of 50 tons HNBR per year. The performance of the pilot plant is numerically predicted by using the proposed model.

Chapter 9
Conclusions and Recommendations for Future Research

9.1 Conclusions

9.1.1 Hydrodynamics in Air-Water System

The RTD experiments in the static mixer reactor with open-flat blade internal structure showed that plug flow behavior can be achieved under various operating conditions. RTD experimental results showed that for a constant mean residence time, the Peclet number (same as Peclet number) varies 4.7 times of the number of mixing elements in the SM reactor. The gas hold up (ε_G) experiments showed that the superficial gas and liquid velocities govern the extent of gas hold up. The gas hold up data is conveniently modeled using an empirical correlation in terms of gas side and liquid side Reynolds numbers and the number of mixing elements inside the reactors. The preliminary mass transfer experiments showed that high mass transfer coefficients (K_La) can be achieved in the SM reactor compared to other conventional reactors (for the same amount of energy dissipation). An empirical correlation for K_La as a function of gas side and liquid side Reynolds numbers was derived. All the hydrodynamic experimental results showed that the SM reactor is promising in giving plug flow behavior and good mass transfer.

9.1.2 Numerical Investigation of SM Reactor for Hydrogenation

The experimental results in the SM reactor paved the way to model the flow behavior using a plug flow with axial dispersion model (PFAD). With the mass transfer also taken into account, coupled PFAD model for [C=C] double bond and hydrogen are designed. The designed model was converted to dimensionless form using the different dimensionless parameters (related to the operating conditions and physical/chemical properties of the working fluid). From the simulations, it was found that the θ_τ (the ratio of mean residence time to reaction time only) has a strong influence on the degree of hydrogenation compared to other parameters (such as Peclet number, q, R, α) at identical operating conditions. From the simulation results, a static mixer reactor with 20 elements would assure high degree of hydrogenation while maintaining θ_τ greater than 4. This enabled to design the actual SM reactor with 24 elements by considering a safety factor of 20%.

9.1.3 Hydrodynamics in Hydrogen/Polymer Solution System

The hydrodynamic parameters (Peclet number and liquid hold up) in the actual system where hydrogen gas and polymer solution are used as working fluids are evaluated by performing experiments in the actual reactor. The Peclet numbers for 2.5% (w/w) polymer solution and 5.0% (w/w) polymer solution with and without gas phase are obtained from the RTD experiments where n-butylacetate is used as tracer. It was found that the gas velocity had an adverse affect on the Peclet number for a given polymer velocity. Also, the viscosity of the polymer solution had a marginal negative effect on the Peclet number. An empirical correlation for the Peclet number as a function of gas side and liquid side hydraulic Reynolds numbers was developed. Liquid hold up (ε_L) experiments with the solvent (MCB), 2.5% (w/w) polymer, 5.0% (w/w) polymer and hydrogen gas were conducted. An interesting phenomenon observed in the liquid hold up experiments was that the liquid hold up in 2.5% (w/w) polymer system was lower than the liquid hold up in 5.0% (w/w) polymer system and solvent systems. This might be because of the physical properties of the working fluids. An empirical correlation was developed for liquid hold up as a function of superficial gas-liquid velocities and physical properties (viscosity, density, surface tension) of the working fluids.

9.1.4 Hydrogenation in the SM Reactor

Hydrogenation of NBR using osmium catalyst was conducted in the SM reactor for various operating conditions. The experiments were carried out at a constant temperature of 138 C. The different operating conditions used consisted of varying the mean residence time, pressure, catalyst and polymer concentrations. Optimum catalyst concentrations required for achieving a degree of hydrogenation over 97% were estimated from these experiments. It was found that the optimum catalyst concentration required with the 2.5% (w/w) polymer system for a 35 min mean residence time is 80 μM and for a 17 min mean residence time it is 120 μM. With the 5.0% (w/w) polymer hydrogenation, severe catalyst deactivation was observed when very low catalyst concentration is used. This was taken into consideration to design further experiments and was found that with the 5.0% (w/w) system for a 35 min mean residence time is 120 μM and for a 17 min mean residence time it is 140 μM. An empirical correlation for the final conversion (obtained from the 2^3 hydrogenation experiments) as a function of Peclet number ($\boldsymbol{Pe} = \frac{\bar{U}L}{D_a}$), θ_τ (τ/τ_R), q ($[C{=}C]_0/H^*$), and R (reaction resistance over mass transfer resistance) was derived.

9.1.5 Hydrogenation Modeling and Scale Up

The degree of hydrogenation obtained in the SM reactor was modeled by proposing a dynamic model. The modeling involved developing equations obtained from the mass balance for carbon-carbon double bonds, the hydrogen concentration and the catalyst concentration. Further, the equations were made dimensionless by using dimensionless groups. The ultimate model involved coupled, non-linear partial differential equations. The resulting model was solved numerically by using the method of lines. The values for the design parameters in the resulting model were obtained from the hydrodynamic data and hydrogenation data. The proposed model has satisfactorily predicted the degree of hydrogenation obtained from the experimental results in the SM reactor (for different operating conditions). This showed that the proposed model could be used to scale up the process. Preliminary analysis for scale up of the SM reactor to a pilot scale was done for a basis of 50 ton per year. Reaction similarity was used in the scale up of the continuous process. The design shows that a 30.504 L SM reactor with 9.59 cm ID, 4.21 m length and 44 elements could give degree of hydrogenation over 97% when 5.0% (w/w) polymer solution is hydrogenated using 140 μM $OsHCl(CO)(O_2)(PCy_3)_2$ at 500 psig and 138 C.

9.2 Recommendations for Future Work

9.2.1 Hydrodynamic Study

More details of the hydrodynamic parameters at the process conditions with different concentrations of the polymer would help to realize the transport properties of the SM reactor. For example, information on the Peclet number, the liquid hold up, the mass transfer coefficient, heat transfer coefficient at elevated pressure and temperature varying the concentration of polymer (2.5% (w/w) to 10.0% (w/w)) should be obtained so that the operating flow conditions could be optimized.

9.2.2 Process Improvement

The only drawback of the designed continuous process is the way the gas-liquid separators are repressurized using the gas line before the back pressure regulator. Though the purpose of this method is to utilize the outgoing hydrogen, frequent removal of the product from the gas-liquid separators and repressurizing causes sudden decreases in the system pressure. The consequence of this would range from a simple disturbance to high degree flow instability. This could be avoided by connecting a separate hydrogen gas line to the gas-liquid separators for repressurizing them.

Otherwise, the product line could be connected to a large tank that has automatic level controller. By either of these two ways, the pressure inside the SM reactor and hence the continuous system can be maintained at a constant level.

9.2.3 Catalyst Deactivation

Extensive study on the amount of catalyst lost in the bench scale continuous set up with different polymer concentrations, catalyst concentrations, operating conditions is recommended for successful design and optimization of the continuous process at a large scale. In addition to this, the effect of the impurities in the high concentration polymers, on the reaction rate can be studied which would also help to design the operating conditions of the continuous set up.

9.2.4 Hydrogenation with Rhodium and Ruthenium Catalysts

The hydrogenation of NBR in the continuous process with other catalyst systems such as rhodium and ruthenium systems could be an interesting future work to study the effect of the type of catalyst. Consequently, the product quality obtained by using different catalysts can be analyzed and the most economic and efficient catalyst could be used in the continuous process.

Notation

A, B, a_1, a_2, α, β	constants
A_P	projected area (m^2)
a	Specific surface area (m^2/m^3)
a	heat transfer area per unit volume (m^2/m^3)
C, C'	constants
C_1, C_2	constants
C	Concentration (mol L^{-1})
C_P	heat capacity (J $Kg^{-1}K^{-1}$)
d	diameter of the particle (m)
d_s	Sauter mean diameter (m)
d_h or D_h	hydraulic mean diameter (m)
D	Diameter of the mixer (m)
D_o	outside diameter (m)
d_i or D_i	inside diameter (m)
D_L or $\overline{D_L}$	logarithmic mean of Do and Di (m)
D_a	Axial dispersion coefficient (m^2/s)
D_F	Diffusion coefficient (m^2/s)
E	exit age distribution (s^{-1}), Activation energy (J/mol)
f	friction factor
F_T or F	total molal flow rate (mol per unit time)
h	dimensionless variable (normalized hydrogen concentration)
h_q	specific enthalpy of the q^{th} phase
h_o	outside heat transfer coefficient ($W/m^2\,^oC$)
h_i	inside heat transfer coefficient ($W/m^2\,^oC$)
H	reaction heat (J)
k_m	thermal conductivity of wall ($W/m\,^oC$)
K_m,K_L,K_T	static mixer constants
K_{pq}	interphase momentum exchange coefficient

k, k',K',K_1,K_2,K_5	reaction rate constants
k_L	Mass transfer coefficient (m/s)
K_La	over all mass transfer coefficient (s^{-1})
L	total length of the mixer (m)
$\dot{m}$ or G	mass flow rate (Kg s^{-1})
M	molarity
n or n_e	number of mixing elements
N_c	Number of CSTRs
Ne	Newtonian Number (friction factor/2)
Nu	Nusselt Number
O	order of
Os	osmium
P	power (J s^{-1})
P	pressure (N m^{-2})
P_{tot}	total energy consumption (w)
P_o	power number
Pe	Peclet Numeber
Δp	Pressure drop (N/m^2)
Pr	Prandtl Number
q	dimensionless variable
$\dot{q}$	heat flux (J $m^{-2}K^{-1}$)
Q_i	flow rate (i = 1,2…) (m^3 s^{-1})
Re	Reynolds Number
R_{in}	inside radius (m)
R	dimensionless variable , universal gas constant (J/mol.K)
R_H	hydrogenation reaction rate (mol s^{-1})
Sc	Schmidt number ($\mu/\rho D_F$)
St	Stanton Number ($K_La.\tau$)
t	time (s)
T	Temperature (K)
U	Superficial velocity (m/s)

U_{in}	Overall heat transfer coefficient based on inside area (W $m^{-2}K^{-1}$)
$\overline{U}$	average velocity
V	mixer volume (m^3), variable
$\dot{V}$	Volumetric flow rate (m^3/s)
Vi	Viscosity Number
v_s	superficial velocity (m/s)
v	velocity (m/s)
w_p	concentration of the polymer (%)
We	Weber Number
We_c	Critical Weber Number
x	conversion w.r.t double bond concentration
x_w	thickness of the wall of the reactor (m)
X	pressure ratio for gas-liquid pressure drop estimation, variable
y	arbitrary dependent variable
z	variable representing reactor length (m)
[Os]	concentration of osmium
$[PPh_3]$	concentration of Tri-Phenyl Phosphine
$[H_2]$	concentration of hydrogen
[C=C]	concentration of double bond

Greek Letters

α	constant, reaction order
β	constant
γ	constant
Δ	change
∇	divergence operator
ρ	density (Kg/m^3)
ε_L	liquid hold up
ε_G	gas hold up
ε_v	void fraction
μ	viscocity (Pa s), micro

ϕ_L and ϕ_G	correction factors for pressure drop
$\boldsymbol{\phi}$	function (of concentration etc)
ε or $\dot{\varepsilon}$	Mass specific energy dissipation (W/Kg)
φ_d	Dispersed phase hold up
σ	Interfacial tension (N/m) or standard deviation
σ^2	variance
τ	space time (s)
θ	dimensionless time (can be t/t_m or t/τ_R)
λ	dimensionless reactor length (z/L)
ζ	normalized catalyst concentration
υ	variable (representing x, h or ζ)
ψ	normalized concentration (C/C_{TO})
ξ	normalized oxygen concentration

Subscripts

a	axial
c	Continuous phase, clear
C	catalyst
cat	catlayst
critical	critical value
d	Dispersed phase, dirt
final	final value
G/L	Gas-Liquid
G	Gas
G-h	Gas side hydraulic
h or H	Hydraulic, hydrogen
i	component, node, initial
L	Liquid
L-h	liquid side hydraulic
m	mean
o	inlet
O_2	oxygen

p	Particle
P, poly	polymer
TO	initial tracer
r	radial
R	based on reaction only
s	superficial, steam
w	Wall

Superscripts

*	equilibrium value
-	left neighborhood
+	right neighborhood

Abbreviations

CSTR	Continuously Stirred Tank Reactor
PFR	Plug Flow Reactor
SM	Static Mixer
RTD	Residence Time Distribution
MCB	monochlorobenzene
erf	error function
w/w	weight/weight
ID	inside diameter
OD	outside diameter

Appendix A

Hydrodynamic Data in Air/Water System

Table 0.1 Residence time distribution data in SM reactor with 18 elements

Liquid Side Reynolds Number	Gas Side Reynolds Number	Peclet Number
10.8	0	5.9
12.3	0	11.1
20.4	0	18.9
32.2	0	28.6
5.1	29.7	4.44
5.1	37.5	4.5
5.1	47.2	4.76
5.1	55.9	5
9.7	29.7	4.97
9.7	37.5	5.07
9.7	47.2	4.9
9.7	55.9	5.05
16.5	29.7	5.5
16.5	37.5	5.68
16.5	47.2	6.25
16.5	55.9	5.49
25.0	29.7	6.21
25.0	37.5	5.52
25.0	47.2	5.92
25.0	55.9	6.21

Table 0.2 Gas hold up data in the SM reactor

Liquid Side Reynolds Number	Gas Side Reynolds Number	Number of Internal Elements	Gas Hold up
37.8	410.8	18	0.027

37.8	632.6	18	0.043
37.8	883.0	18	0.06
37.8	1129.9	18	0.078
37.8	1369.7	18	0.1
37.8	1599.8	18	0.123
37.8	1844.9	18	0.144
95.1	410.8	18	0.023
95.1	632.6	18	0.04
95.1	883.0	18	0.055
95.1	1129.9	18	0.071
95.1	1369.7	18	0.096
95.1	1599.8	18	0.115
95.1	1844.9	18	0.142
175.0	410.8	18	0.022
175.0	632.6	18	0.037
175.0	883.0	18	0.056
175.0	1129.9	18	0.074
175.0	1369.7	18	0.094
175.0	1599.8	18	0.115
175.0	1844.9	18	0.135
212.5	410.8	18	0.023
212.5	632.6	18	0.038
212.5	883.0	18	0.055
212.5	1129.9	18	0.073
212.5	1369.7	18	0.093
212.5	1599.8	18	0.115
212.5	1844.9	18	0.136
371.0	410.8	18	0.021
371.0	632.6	18	0.038
371.0	883.0	18	0.051
371.0	1129.9	18	0.066
371.0	1369.7	18	0.087

371.0913	1599.8	18	0.105
371.0913	1844.9	18	0.125
554.8356	410.8	18	0.017
554.8356	632.6	18	0.034
554.8356	883.0	18	0.05
554.8356	1129.9	18	0.063
554.8356	1369.7	18	0.081
554.8356	1599.8	18	0.098
554.8356	1844.9	18	0.116
37.8297	632.6	12	0.04
37.8297	883.0	12	0.055
37.8297	1129.9	12	0.076
37.8297	1369.7	12	0.098
37.8297	1599.8	12	0.12
37.8297	1844.9	12	0.143
95.11467	632.6	12	0.038
95.11467	883.0	12	0.053
95.11467	1129.9	12	0.075
95.11467	1369.7	12	0.096
95.11467	1599.8	12	0.118
95.11467	1844.9	12	0.138
175.0975	632.6	12	0.036
175.0975	883.0	12	0.051
175.0975	1129.9	12	0.071
175.0975	1369.7	12	0.091
175.0975	1599.8	12	0.108
175.0975	1844.9	12	0.133
212.5669	632.6	12	0.031
212.5669	883.03	12	0.046
212.5669	1129.9	12	0.068
212.5669	1369.7	12	0.085
212.5669	1599.8	12	0.103

212.5669	1844.984	12	0.13
371.0913	632.629	12	0.03
371.0913	883.0354	12	0.043
371.0913	1129.915	12	0.06
371.0913	1369.741	12	0.081
371.0913	1599.868	12	0.1
371.0913	1844.984	12	0.121
554.8356	632.629	12	0.026
554.8356	883.0354	12	0.041
554.8356	1129.915	12	0.056
554.8356	1369.741	12	0.078
554.8356	1599.868	12	0.085
554.8356	1844.984	12	0.106
37.8297	1129.915	6	0.073
37.8297	1369.741	6	0.09
37.8297	1599.868	6	0.11
37.8297	1844.984	6	0.133
95.11467	1129.915	6	0.07
95.11467	1369.741	6	0.086
95.11467	1599.868	6	0.106
95.11467	1844.984	6	0.123
175.0975	1129.915	6	0.066
175.0975	1369.741	6	0.083
175.0975	1599.868	6	0.106
175.0975	1844.984	6	0.126
212.5669	1129.915	6	0.063
212.5669	1369.741	6	0.08
212.5669	1599.868	6	0.096
212.5669	1844.984	6	0.12
371.0913	1129.915	6	0.06
371.0913	1369.741	6	0.07
371.0913	1599.868	6	0.083

371.0913	1844.984	6	0.103
554.8356	1129.915	6	0.053
554.8356	1369.741	6	0.056
554.8356	1599.868	6	0.063
554.8356	1844.984	6	0.086

Table 0.3 Mass transfer data in SM reactor

Liquid Side Reynolds Number	Gas Side Reynolds Number	Number of Internal Elements	Mass Transfer Coefficient (K_La)
44	440.9	18	0.027
44	555.5	18	0.031
44	698.8	18	0.033
44	828.8	18	0.035
82.9	440.9	18	0.022
82.9	555.5	18	0.027
82.9	698.8	18	0.03
82.9	828.8	18	0.032
140.5	440.9	18	0.028
140.5	555.5	18	0.018
140.5	698.8	18	0.02
140.5	828.8	18	0.027
212.6	440.9	18	0.017
212.6	555.5	18	0.018
212.6	698.8	18	0.031
212.6	828.8	18	0.029
44	440.9	12	0.016
44	555.5	12	0.017
44	698.8	12	0.019
44	828.8	12	0.021
82.9	440.9	12	0.013
82.9	555.5	12	0.014

82.9	698.8	12	0.012
82.9	828.8	12	0.017
140.5	440.9	12	0.011
140.5	555.5	12	0.012
140.5	698.8	12	0.011
140.5	828.8	12	0.012
212.6	440.9	12	0.012
212.6	555.5	12	0.013
212.6	698.8	12	0.013
212.6	828.8	12	0.015
44	440.9	6	0.019
44	555.5	6	0.019
44	698.8	6	0.02
44	828.8	6	0.024
82.9	440.9	6	0.018
82.9	555.5	6	0.018
82.9	698.8	6	0.019
82.9	828.8	6	0.02
140.5	440.9	6	0.018
140.5	555.5	6	0.019
140.5	698.8	6	0.019
140.5	828.8	6	0.02
212.6	440.9	6	0.016
212.6	555.5	6	0.017
212.6	698.8	6	0.018
212.6	828.8	6	0.018
44	440.9	18	0.027

Appendix B

Hydrodynamic Data in Hydrogen/Polymer System

Table 0.4 Peclet number in SM reactor with open-curve blade geometry

Polymer Flow Rate (cc/min)	Hydrogen Flow Rate (cc/min)	Peclet Number in 2.5% (w/w) system	Peclet Number in 5.0% (w/w) system
23.86	0	26.2	19.7
35.14	0	35.4	26.4
50.715	0	45.6	29.4
98.43	0	56.3	34.2
28.86	57.72	20.1	13.2
28.86	86.58	12.7	10.9
28.86	115.44	9.85	5.7
28.86	173.16	6.4	4.2
35.14	70.28	24.3	19.3
35.14	105.42	20.2	14.1
35.14	140.56	13.7	8.4
35.14	210.84	8.2	5.9
50.72	101.43	18.5	13.9
50.72	152.12	9.62	12.6
50.72	202.86	4.1	7.7
98.43	105.42	21.05	16.7
98.43	196.86	14.2	9.4
98.43	295.29	5.7	4.1

Table 0.5 Liquid hold up data in SM reactor with open-curve blade geometry

Liquid Velocity ($cm\ s^{-1}$)	Hydrogen Velocity ($cm\ s^{-1}$)	ε_L MCB	ε_L 2.5 % (w/w)	ε_L 5.0% (w/w)
3.3099	3.3099	0.9679	0.9572	0.9411
3.3099	6.6197	0.9679	0.9251	0.9251

3.3099	13.2394	0.9679	0.9143	0.9197
3.3099	19.8592	0.9572	0.7216	0.8876
3.3099	26.4789	0.9465	0.6627	0.8608
3.3099	33.0986	0.9411	0.6092	0.8126
3.3099	49.6479	0.8983	-	-
3.3099	66.1972	0.8501	-	-
3.3099	99.2958	0.7002	-	-
4.4122	4.4122	0.9679	0.9465	0.9465
4.4122	8.8244	0.9679	0.727	0.909
4.4122	17.6488	0.9679	0.7056	0.9036
4.4122	26.4732	0.9465	0.6788	0.8555
4.4122	35.2976	0.9358	0.636	0.8233
4.4122	44.122	0.9251	0.5824	0.7805
4.4122	66.1831	0.8983	-	-
4.4122	88.2441	0.8769	-	-
4.4122	132.3661	0.818	-	-
4.4122	176.4881	0.7805	-	-
6.6197	6.6197	0.9679	0.9411	0.9358
6.6197	13.2394	0.9679	0.818	0.8876
6.6197	26.4789	0.9518	0.7002	0.8608
6.6197	39.7183	0.9304	0.6467	0.834
6.6197	52.9578	0.9143	0.5931	0.7966
6.6197	66.1972	0.8983	0.5236	0.727
6.6197	99.2958	0.7912	-	-
6.6197	132.3944	0.7109	-	-
6.6197	198.5917	0.6627	-	-
13.238	13.238	0.9679	0.9358	0.9465
13.238	26.4761	0.9679	0.9143	0.9143
13.238	39.7141	0.9358	0.6734	0.8233
13.238	52.9521	0.9251	0.6467	0.8287
13.238	79.4282	0.8929	0.5878	0.743
13.238	105.9042	0.8715	0.5343	0.7537

13.238	132.3803	0.8448	-	-
13.238	198.5704	0.7859	-	-
13.238	264.7606	0.7216	-	-
13.238	397.1408	0.6039	-	-
26.47	52.9521	0.9358	-	-
26.47	105.9042	0.8822	-	-
26.47	158.8563	0.8233	-	-
26.47	211.8084	0.7805	-	-
26.47	264.7606	0.7109	-	-
26.47	397.1408	0.4754	-	-

Appendix C

Double Pipe Heat Exchanger and Reactor Jacket Calculations

C.1 Reactor Jacket – Temperature Profile Simulations

With the similar approach described in Chapter 4, the continuity equation and the energy balance equation are solved numerically to estimate the temperature profile along the length of the reactor for different inlet polymer temperature and steam temperatures. The continuity equation for the carbon-carbon double bond ([C=C]) is given by the following equation:

$$\frac{1}{\boldsymbol{Pe}}\frac{\boldsymbol{d}^2\boldsymbol{x}}{\boldsymbol{d}\lambda^2}-\frac{\boldsymbol{dx}}{\boldsymbol{d}\lambda}+\frac{\boldsymbol{kL}}{\overline{\boldsymbol{U}}}(1-\boldsymbol{x})=0 \qquad \textbf{(C.1)}$$

where Pe is the Peclet number, k is the reaction rate constant, x is the [C=C] conversion, λ is the dimensionless length of the reactor, L is the length of the reactor and $\overline{\boldsymbol{U}}$ is the superfacial liquid velocity. The energy balance on the inner side of the reactor leads to the following equation:

$$\frac{1}{\boldsymbol{\tau}}\sum_i \boldsymbol{\rho_i C_{pi}}\frac{\boldsymbol{dT}}{\boldsymbol{d}\lambda}=\frac{2\boldsymbol{U_{in}}}{\boldsymbol{R_{in}}}(\boldsymbol{T_s}-\boldsymbol{T})+(-\Delta\boldsymbol{H_R})\boldsymbol{k}[\boldsymbol{C}=\boldsymbol{C}]_{\boldsymbol{o}}(1-\boldsymbol{x}) \qquad \textbf{(C.2)}$$

where ρ_i and C_{pi} are the density and specific heat capacity of component i (here components are hydrogen, NBR and HNBR) respectively. U_{in} is the overall heat transfer coefficient, R_{in} is the inner radius of the reactor, T is the temperature inside the reactor, T_s is the saturation temperature of steam, $-\Delta H_R$ is the enthalpy of reaction. The reaction rate constant k (in equations (C.1) and (C.2)) can be conveniently represented as a function of temperature using the Arhenius equation.

$$k = k_o \exp(-E/RT) \qquad \textbf{(C.3)}$$

In equation (C.3), R is the universal gas constant (8.314 J mol^{-1} K^{-1}) the frequency factor k_o (69747.1 s^{-1}) and the activation energy E (57979.2 J/mol) for hydrogenation of NBR in the presence of the $OsHCl(CO)(PCy_3)_2$ catalysyt are taken from Parent's thesis (Parent, 1996). The enthalpy of the reaction, $-\Delta H_R$, and the specific heat capacity of components, C_{pi}, are also functions of temperature as described by equation (C.4) and equation (C.5) respectively.

$$\Delta H_R = \Delta H^0 + \Delta a \cdot T + \frac{\Delta b}{2} \cdot T^2 + \frac{\Delta c}{3} \cdot T^3 \qquad \textbf{(C.4)}$$

$$C_{pi} = a + bT + cT^2 \qquad \textbf{(C.5)}$$

The coefficients a, b, and c for different reaction components are taken from the work of Bhattacharjee et al. (1989). In equation (C.4), Δ refers to sum of products minus sum of reactants, for example, $\Delta a = a_3-(a_1+a_2)$.

Table 0.6 Thermodynamic parameters for reaction components at 298 K (Bhattacharjee et al. 1989)

Component (i)	ΔH^0 (kJ/mol)	a cal/mol K	10^2b cal/mol K^2	10^4c cal/mol K^3
NBR	-36657	578.90	13593.	-818.03
H_2	8.46	6.42	0.1	$-781x10^{-4}$
HNBR	-96993	2055.53	14653	-858.16

The overall heat transfer coefficient U_{in} in equation (C.2) is calculated by using equation (C.6).

$$U_{in} = \frac{1}{\frac{1}{h_i} + \frac{x_w}{K_m}\left(\frac{D_i}{\overline{D_L}}\right) + \frac{1}{h_o}\left(\frac{D_i}{D_o}\right)} \qquad \textbf{(C.6)}$$

where, h_i and h_o are the individual heat transfer coefficients defined based on inside and outside films at the wall. $\overline{D_L}$ is the logarithmic mean of inside diameter of the reactor, D_i and outside diameter, D_o. While, K_m is the thermal conductivity of the material of the reactor and x_w is the thickness of the reactor wall. The individual heat transfer coefficients h_i and h_o are evaluated using equation (C.7) (Bayer et al. 2003) and equation (C.8) respectively.

$$\frac{h_i D_H}{K} = 2.6(\mathrm{Re}_h\,\mathrm{Pr})^{0.35}(\mathrm{Pr}/\mathrm{Pr}_w)^{0.14} \qquad \textbf{(C.7)}$$

$$\frac{h_o D_H}{K} = 0.023\,\mathrm{Re}_h^{0.8}\,\mathrm{Pr}^{1/3} \qquad \textbf{(C.8)}$$

where, D_H is the hydraulic diameter of the reactor defined as $D_H = \frac{4 \cdot \varepsilon \cdot V}{A_P}$ for the SM reactor and $D_H = \frac{D_o^2 - D_i^2}{4D_i}$ for the jacket, K is the thermal conductivity of the corresponding fluid, V is the volume of the reactor, A_P is the wetted perimeter, Re_h is the Reynolds number based on the hydraulic diameter and Pr is the Prandtl number (subscript w refers to Pr evaluated at wall temperature). For initial estimation the $(Pr/Pr_w)^{0.14}$ term is neglected. Equations (C.1) and (C.2) are numerically solved by incorporating equations (C.3) through (C.5) for different steam and polymer solution temperatures. The boundary conditions for equations (C.1) and (C.2) are given as follows:

At x = 0, T = T_0 K;

At $\lambda = 0^+$, $x = \frac{1}{Pe}\frac{\partial x}{\partial \lambda}\Big|_{\lambda=0^+}$ and

At $\lambda = 1$, $\frac{\partial x}{\partial \lambda} = 0$

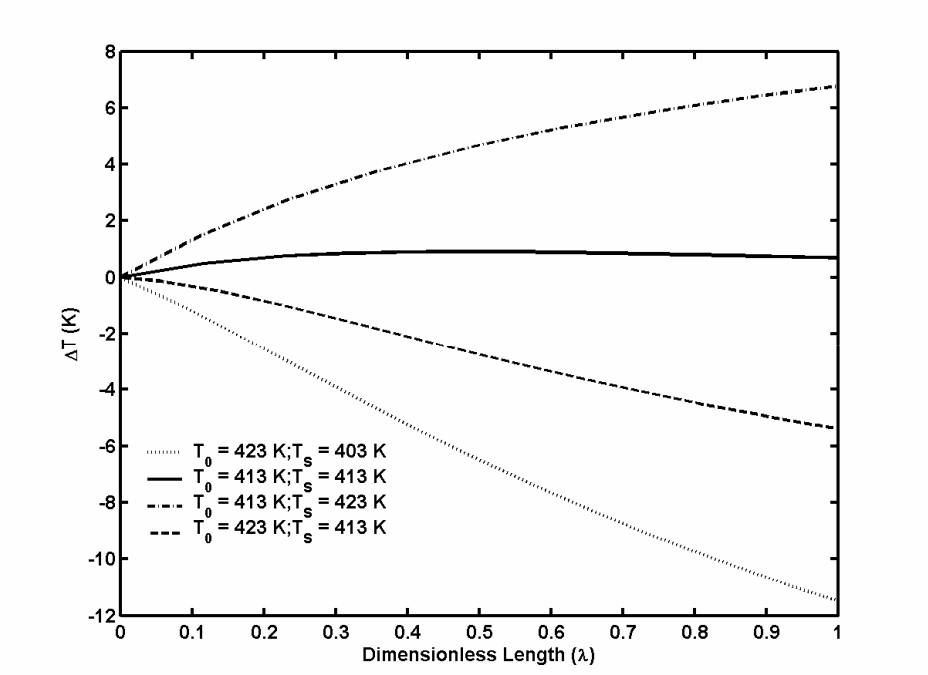

Figure C.1 Temperature drop vs. dimensionless length of the reactor for Pe = 100, τ = 20 min, [C=C] = 275 mM with various steam and inlet polymer temperatures.

C.2 Double Pipe Heat Exchanger Calculations

1. Heat Load

$$\dot{m}_w C_P \Delta T\Big|_{water} = \dot{m}_{HNBR} C_P \Delta T\Big|_{HNBR\ solution}$$

The properties of HNBR solution and water are evaluated at mean temperature.

$$\dot{m}_w \text{x} 4.178\text{x}10^3\ (40-25) = 2.7665\text{x}10^3\ \text{x} 2.912\text{x}10^3\ (150-40)$$

$$\dot{m}_w = 0.014\,\text{kg/s} \quad ; \quad Q = \frac{\dot{m}_w}{\rho} = 848\ \text{cc/min}$$

$$\text{Heat Load} = \dot{q} = 886.16\,\text{J}$$

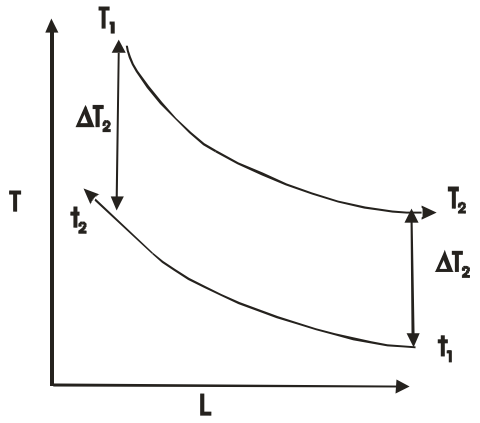

2. LMTD (Logarithmic Mean Temperature Difference)

$\Delta T_1 = T_1 - t_2 = 150 - 40 = 110^oC$

$\Delta T_2 = T_2 - t_1 = 40 - 25 = 15^oC$

$LMTD = (\Delta T_1 - \Delta T_2)/\ln(\Delta T_1/\Delta T_2) = 47.68^o\ C$

3. Hot fluid (Inner pipe)

Flow area $a_p = \pi D^2/4 = \pi(0.957 \text{ x } 0.0254)^2/4 = 4.6407 \text{ x } 10^{-4}\ m^2$

Mass velocity $G = \dot{m}_{HNBR}/a_p$ 5.76 Kg / m^2 s

$$N_{Re} = \frac{DG}{\mu} = 35$$

Since the flow is in laminar regime, the corresponding correlation for heat transfer coefficient is:

$$\frac{h_i D}{k} = 1.86\left(\frac{4}{\pi}\frac{mC_P}{kL}\right)^{1/3}$$

Table 0.7 The properties are evaluated at mean temperatures of the working fluids.

	Water	**Hydrogen**	**NBR**
Mean Temperature (^oC)	32.5	95	95
Density ρ (Kg/m^3)	997	0.06691	1106.6
Heat Capacity C_P (kJ/Kg K)	4.178	14.482	1.699
Thermal Conductivity k (W/m K)	616.7e-03	219.81e-03	0.116
Viscosity μ (Pa.s)	7.8563e-04	10.3e-06	0.004

Since length of the heat exchanger is unknown, h_i in terms of length is obtained as

$$h_i = \frac{33.043}{L^{1/3}} \quad \text{and } h_{io} = h_i\,(ID/OD) = 24.047/L^{1/3}$$

For water

$$N_{\mathrm{Re}} = \frac{D_H G}{\mu} = 265.228; \quad D_H = D_o - D_i = 0.019m$$

since this is also in laminar flow, same equation for heat transfer coefficient is used as in the case of HNBR solution. In this case also, the heat transfer coefficient is expressed in terms of the unknown variable length (L).

$$h_o = \frac{298.41}{L^{1/3}}$$

The clean overall heat transfer coefficient U_C is given as

$$U_C = \frac{h_{io} + h_o}{h_{io} h_o}$$

plugging in the h_i and h_{io} values in terms of L we get,

$$U_C = \frac{22.2537}{L^{1/3}}$$

When water is used for cooling, the clean overall coefficient usually will be in the range of 20 – 30 W/m^2k.

For $U_C = 20$; L = 1.3 m

$U_C = 25$; L = 0.71m

$U_C = 30$; L = 0.4 m

The optimum design of the heat exchanger are inner pipe – 1 in ID 80S, outer pipe – 2 in ID 40S with the length being 1 m.

Appendix D

Hydrogenation Data in SM Reactor

Table 0.8 Conversion and Steady state Temperature data Experiment # 1 (Table 7.1)

Time (minutes)	6 Elements	12 Elements	18 Elements	24 Elements
10	3	0	0	0
20	3.12	0	0	0
30	3.34	0	0	0
40	2.91	3.87	3.16	0
50	11.87	8.73	8.2	3.55
60	15.87	20.03	13.34	12.55
70	25.56	29.39	27.48	25.04
80	29.95	37.3	39.3	33.8
90	42.91	46.32	52.99	49.47
100	39.87	52.58	61.61	62.42
110	41.21	50.37	62.12	68.57
120	41.5	62.99	67.75	71.63
130	43.83	57.65	65	74.01
140	39.18	58.85	68.82	72.46
150	43.14	62.12	66.71	73.29
160	44.22	63.24	71.47	75.04
170	44.31	61.81	70.57	74.6
Temperature (^{o}C)				
0,6,18,24 elements	135	137	137	134

Table 0.9 Conversion and Steady state Temperature data Experiment # 2 (Table 7.1)

Time (minutes)	6 Elements	12 Elements	18 Elements	24 Elements
10	3	3	3	3
20	4	3	3	3

30	6	3	3	3
40	14	12	5	3
50	23	29	24	18
60	42	46	42	39
70	52	63	65	61
80	62	74	81	80
90	68	82	89	90
100	69	85	93	95
110	71	86	94	98
120	67	86	94	98
130	69	86	95	98
140	65	84	93	98
150	70	85	94	97
160	72	88	95	98
170	72	88	94	98
180	72	88	95	98
Temperature (^{o}C)				
0,6,18,24 elements	136.2	138.2	138.8	136.8

Table 0.10 Conversion and Steady state Temperature data Experiment # 3 (Table 7.1)

Time (minutes)	6 Elements	12 Elements	18 Elements	24 Elements
10	0	0	0	0
20	21.24	20.03	17.34	9.12
30	32.19	45.55	54.81	53.24
40	42.09	58.26	72.14	76.63
50	41.17	60.73	75.04	83.93
60	41.4	60	76.55	85.03
70	39.18	59.76	75.04	85.16
80	39.7	59.79	75.56	84.73
10	0	0	0	0

Temperature (^{o}C)				
0,6,18,24 elements	136.1	140.3	139.8	136.5

Table 0.11 Conversion and Steady state Temperature data Experiment # 4 (Table 7.1)

Time (minutes)	6 Elements	12 Elements	18 Elements	24 Elements
10	4.06	0	0	0
20	33.74	29.39	25.65	15.15
30	63.58	75.59	75.72	65.11
40	64.57	85.96	92.72	94.75
50	68.36	87.72	95.63	98.25
60	63.05	85.74	95.3	98.38
70	55.77	80.31	92.52	97.57
80	55.5	75.04	90.81	96.57
90	60.5	82.19	92.6	97.34
100	56.5	75.5	91.94	96.74
Temperature (^{o}C)				
0,6,18,24 elements	136.1	140.3	139.8	136.5

Table 0.12 Conversion and Steady state Temperature data Experiment # 5 (Table 7.1)

Time (minutes)	6 Elements	12 Elements	18 Elements	24 Elements
10	0	0	0	0
20	0	0	0	0
30	17.27	27.01	10.75	4.98
40	29.63	26.67	28.08	22.34
50	21.64	39.97	46.28	41.03
60	44.97	47.88	46.64	58.72
70	48.27	63.26	67.88	68.97
80	51.41	63.21	72.64	76.01
90	56.58	66.64	75.7	76.31
100	54.38	65.97	75.86	82.72

110	53.05	65.56	78.41	84.56
120	53.6	64.66	75.24	82.15
130	52.35	64.84	74.73	81.09
Temperature (^{o}C)				
0,6,18,24 elements	135.9	137.7	137.9	133.2

Table 0.13 Conversion and Steady state Temperature data Experiment # 6 (Table 7.1)

Time (minutes)	6 Elements	12 Elements	18 Elements	24 Elements
10	0	0	0	0
20	12.94	8.55	0	0
30	32.46	24.36	26.13	16.05
40	45.27	52.85	49.76	35.58
50	55.42	66.89	70.19	69.28
60	60.48	76.42	80.75	82.03
70	64.34	78.3	87.67	90.67
80	67.13	83.57	90.88	94.2
90	69.74	85.74	93.06	96.12
100	69.68	86.72	93.99	97.19
110	70.83	86.65	94.49	97.68
120	69.98	86.28	94.44	97.83
130	67.68	85.07	93.57	97.34
140	66.94	83.17	93.02	97.06
150	63.83	83.67	92.17	96.67
160	64.08	81.97	91.5	96.23
170	64.33	80.3	90.19	95.63
Temperature (^{o}C)				
0,6,18,24 elements	141.0	141.8	142.6	138.3

Table 0.14 Conversion and Steady state Temperature data Experiment # 7 (Table 7.1)

Time (minutes)	6 Elements	12 Elements	18 Elements	24 Elements

10	0	0	0	0
20	4.09	3.56	2.34	0
30	11.51	14.72	15.15	11.74
40	18.81	24.08	30.04	28.6
50	20.18	25.94	34.23	40.96
60	23.82	35.5	44.44	48.7
70	22.74	30.63	42.74	52.48
80	21.72	32.84	45.4	52.87
90	21.85	34.88	42.41	52.88
Temperature (^{o}C)				
0,6,18,24 elements	135.6	138.9	138.2	134.7

Table 0.15 Conversion and Steady state Temperature data Experiment # 8 (Table 7.1)

Time (minutes)	6 Elements	12 Elements	18 Elements	24 Elements
10	0	0	0	0
20	12.64	11.07	4.27	0
30	37.47	28.47	23.72	17.91
40	59.05	58.12	78.19	54.67
50	69.04	76.71	80.48	79.87
60	70.25	85.15	90.18	91.94
70	73.33	88.33	93.97	96.19
80	76.16	89.13	95.58	98.22
90	75.04	89.78	96.07	98.53
Temperature (^{o}C)				
0,6,18,24 elements	135.6	136.2	137.1	132.6

Appendix E

Continuous Reactor set up components

Component	Supplier	Specifications
A. 12 liter carboy	Nalgene	Polyethylene
B. High pressure metering pump	Milton Roy	Model# RT1115A1SEM2NN
		1.09 gph, 2000 psi max
		Model# RT1177A1SEM2NN
		0.21 gph, 2000 psi max
C. Mass flow control valve	Brooks	Model#5850E, 1250 psi max
Mass flow controller	Brooks	Model# 5896
D. Check Valves	Whitey	Kal-rez sealing seat
E. Preheater/premixer	Parr	Model# 4532
		2 L capacity, 1900 psi max
F. Catalyst Bomb	Whitey	1 liter stainless steel bomb
G. Double pipe heat exchanger	Kenics	custom design 316SS
		ID 1” 80S, OD 2” 40S
H. Separators	Penberthy	Model# IRM8-316SS
		500 cm^3, 2300 psi max
	Parr	Model# 4642, 2 L, 2000 psi max
I. Bourdon guage	Weksler	0 – 3000 psi range
J. Back-pressure regulator	Tescom	Model# 26-1725-24
		0 – 1500 psi range
K. Gas rotameter	Brooks	Model# R-25-B-MM
L. Steam pressure regulator	Watts	Model# 141M1
		30 – 140 psi range
M. Steam trap	Spirax Sarco	Model# T-250, 250 psi max
N. Valves and tubing	Niagara valves	

Bibliography

1. Bayer, T., K. Himmler. and V.Hessel, *Don't be baffled by static mixers*, Chemical Engineering, May, **50**, 50 -57, 2003.

2. Behkish, A , R. Lemoine., R. Oukaci. and B.I Morsi, *Novel correlations for gas holdup in large-scale slurry bubble column reactors operating under elevated pressures and temperatures*, Chemical Engineering Journal,**115**, 157-171, 2006.

3. Bhattacharjee, S, K.A. Bhowmick. and B.N. Avasthi, *High pressure hydrogenation of nitrile rubber: Thermodynamics and Kinetics,*Industrial and Engineering Chemistry Research, **30**, 1086-1092, 1991.

4. Bridgman, P.W., *Dimensional analysis*, Yale University Press, New Haven, 1882.

5. Brück, D., *IR-Spectrometric determination of the proportions of acrylonitril, butadiene and hydrogenated butadiene in hydrogenated acrylonitrile-butadiene rubbers*: Part1. Principles, Kautschuk+Gummi Kunststoffe 42, Jahrgang, Nr.2, 107-110, 1989.

6. Chandra, K.G., and D.D. Kale, *Pressure drop for two-phase air-non-newtonian liquid flow in static mixers*, The Chemical Engineering Journal, **59**, 277 – 280, 1995.

7. Couvert, A., M. Peculier. and A. Laplanche, *Pressure Drop and Mass Transfer Study in Static Mixers with Gas Continuous Phase*, Canadian Journal of Chemical Engineering, **80**, 727-733, 2002.

8. Cybulski, A., and K. Werner, *Static mixers – criteria for applications and selection*, International Chemical Engineering, **26**, 171-180, 1986.

9. Danckwerts, P.V., *Continuous Flow Systems – Distribution of Residence Time*, Chemical Engineering Science, **2**, 1-3, 1953.

10. Damköhler, G., Z.f. Elektrochemie 42, *Einflüsse der Strömung, Diffusion und des Wärmeüberganges auf die Leistung von Reaktionsöfen,* 846-862, 1936.

11. Fogler, H.S., *Elements of chemical reaction engineering*, second edition, Prentice Hall, New Jersy, 1992.

12. Froment, G. F. and K.B. Bischoff, *Chemical Reactor Analysis and Design*, 2nd edition, Wiley Publisher, 529-533, 1990.

13. Harriott, P, *Chemical reactor design*, Marcel Dekker, Inc.,New York, 2003.

14. Heniche, M., P. A. Tanguy., M. F.Reeder. and J. B. Fasano, *Numerical Investigation of Blade Shape in Static Mixing*, American Institute of Chemical Engineers Journal, **51**, 44-58, January, 2005.

15. Heyouni, A., M. Roustan. and Z. Do-Quang, *Hydrodynamics and mass transfer in gas-liquid flow through static mixers*, Chemical Engineering Science, **57**, 3325-3333, 2002.

16. Hobbs, D.M., and F.J. Muzzio, *The Kenics Static Mixer: a three dimensional chaotic flow*, Chemical Engineering Journal, **67**, 153-166, 1997.

17. Huai, Z.L, C. Fasol. and L. Choplin, *Residence time distribution of rheologically complex fluids passing through a Sulzer SMX static mixer*, Chemical Engineering Communications, **165**, 1-15, 1998.

18. Kehl, S., *Catalytic hydrogenation of nitrile butadiene rubber in a packed bed*, Masters thesis, Department of Chemical Engineering, University of Waterloo (1998).

19. Lakota, A., M. Jazbec. and J. Levec, *Impact of Structured Packing on Bubble Column Mass Transfer Characteristics. Part 2. Analysis of Gas-Liquid Mass Transfer Measurements*, Acta Chimca Slovinica, **49**, 587-604, 2002.

20. Lockhart, R.W. and R.C. Martinelli, *Proposed correlation of data for two-phase two component flow in pipes*, Chemical Engineering Progress, **45**, 39-48, 1949.

21. Martin, P., N.T. McManus. and G.L. Rempel, , *A detailed study of the hydrogenation of nitrile-butadiene rubber and other substrates catalyzed by Ru(II) complexes*, J.Mol.Cat.A: Chemical **126** 115-131, 1997.

22. McManus, N.T., and G.L. Rempel, *Chemical modification of polymers: Catalystic hydrogenation and related reactions,* J.M.S. – Rev. Macromoleculas-Chemical Physics. **C35**, 239-285, 1995.

23. Middleman, S., *Drop size distributions produced by turbulent pipe flow of immiscible fluids through a static mixer*, Industrial and Engineering Chemistry Process Design and Development, **13**, 78–83, 1974.

24. Moucha, T., V. Linek. and E. Prokopova, *Gas hold-up, mixing time and gas-liquid volumetric mass transfer coefficient of various multiple-impeller configurations: Rushton turbine, pitched blade and techmix impeller and their combinations*, Chemical Engineering Science, **58**, 1839 – 1846, 2003.

25. Nagel, O., H. Kurten. and B. Hegner, *Criteria for the selection and design of gas liquid reactors*, Int. Chem. Eng., **21**, 161-172, 1981.

26. Nigam, K.D.P. and K.Vasudeva, *Residence time distribution in static mixer*, Canadian Journal of Chemical Engineering, **58**, 543-544, 1980.

27. Nigam, K.D.P. and E.B. Naumann, *Residence time distribution of power law fluids in motionless mixers*, Canadian Journal of Chemical Engineering, **63**, 519-521, 1985.

28. Nguyen, K.T., E. Flaschel. and A. Renken, *Bulk polymerization of styrene in a static mixer*, Chemical Engineering Communications, **36**, 251-267, 1985.

29. Naumann, E.B., *Reactions and residence time distributions in motionless mixers*, Canadian Journal of Chemical Engineering, **60**, 136-140, 1982.

30. Pan, Q, G.L. Rempel. and F.T.T.Ng, *Numerical investigation of continuous processes for catalytic hydrogenation of nitrile butadience rubber*, Polymer Engineering and Science, **42**, 899-910, 2002.

31. Pan, Q and G.L. Rempel, *Investigation of fundamental data for nitrile butadiene rubber in monochlorobenzene and 0-dichlorobenzene,* Polymer Engineering and Science, **44**, 88-95, 2004.

32. Parent, J.S., *Catalytic hydrogenation of butadiene copolymers*, Ph.D thesis. Department of Chemical Engineering, University of Waterloo, 1996.

33. Parent, J.S., and G.L. Rempel, *Solubility of hydrogen in chlorobenzene*, Journal of Chemical and Engineering Data, **41**, 192-194, 1996.

34. Parent, J.S., N.T. McManus. and G.L. Rempel, *OsHCl(CO)(O2)(PCy3)2-Catalyzed Hydrogenation of Acrylonitrile-Butadiene Copolymers*, Industrial and Engineering Chemistry Research, **37**, 4253-4261, 1998.

35. Pustelnik, P., , *Investigation of Residence Time Distribution in Kenics Static Mixers*, Chemical Engineering and Processing, **20**, 147-154, 1986.

36. Rader, R.G., M. Mutsakis, F. Grosz-Roell. and W. Maugweiler, *Better absorption? Try a static mixer*, Chemical Engineering, July: 137–142. 1989.

37.Raines, G.E., and R.E. Corrigan, *The use of axial dispersion model to predict conversion of first and second order reactions*, Chem. Eng.Progress Syposium Series, **72**, 90-96, 1967.

38. Schneider, G., *Static mixers as gas/liquid reactors*, I.Chem.E. Symposium series, No.121, 1988.

39. Shah, N.F., and D.D. Kale, *Two-phase, gas-liquid flows in static mixers*, American Institute of Chemical Engineers Journal, **38**, 302-310, 1992.

40. Steigal, G.J., and Y.T. Shah, *Axial dispersion in a rectangular bubble column*, Canadian Journal of Chemical Engineering, **55**,3-8, 1977.

41. Streiff, F.A., S. Jaffer. and G. Schneider, *The design and application of static mixer technology*,Sulzer technical reviews (from Sulzer company).

42. Streiff, F.A., P. Mathys. and T.U. Fischer, *New fundamentals for liquid-liquid dispersion using static mixers*, Proceeding /9th European conference on mixing, March 1997.

43. Streiff, F.A., and J.A.Rogers, *Don't Overlook Static Mixer Reactors*, Chemical Engineering, June, 76-82, 1994.

44. Thakur, R.K., Ch. Vial, K.D.P. Nigam, E.B. Naumann. and G. Djelveh, *Static mixers in the process industries – a review*, Institution of Chemical Engineers, **81**, 787-826, 2003.

45. Thanos, A. M., P. A. Galtier. and N. G. Papyannakos, *Liquid Flow Non-Idealities and Hold-up in a Pilot Scale Packed Bed Reactor with Cocurrent Gas-Liquid Upflow,* Chemical Engineering Science, **51**, 2709-2714, 1996.

46. Veera, U.P, A.W. Patwardhan. and J.B. Joshi., *Measurement of gas hold-up profiles in stirred tank reactors by gamma ray attenuation technique,* Trans IChemE, **79**, 684-688, 2001.

47. Weterterp, K.R., W.P.M. van Swaaij. and A.A.C.M. Beenackers., *Chemical reactor design and operation*, John Wiley & Sons, New York, 1984.

48. Zhang, L.F., *Development of novel continuous process for hydrogenation of unsaturated polymers,*, Ph.D thesis, Department of Chemical Engineering, University of Waterloo 2007.